Inaugural-Dissertation

zur
Erlangung der Doktorwürde
der
Naturwissenschaftlich-Mathematischen Gesamtfakultät
der
Ruprecht-Karls-Universität
Heidelberg

vorgelegt von
Diplom-Mathematiker Jevgeni Vihharev
aus Sillamäe in Estland

Tag der mündlichen Prüfung:

Adaptive methods for modeling chemical transport in the Earth's atmosphere

Betreuer: Prof. Dr. Dr. h.c. Rolf Rannacher
PD. Dr. Cristoph S. Garbe

Abstract

This work is devoted to analysis and development of efficient adaptive algorithms for problems related to the transport of chemical species in the Earth's atmosphere from data of remote-sensing instruments.

Processes describing the transport of chemical species are given by nonlinear systems of partial differential equations. For the determination of the concentrations in a domain of interest so-called inverse problems must be solved. The observations obtained by remote-sensing instruments and used as overspecification for the inverse problems must be often calculated from radiative transfer models. The form of the radiative transfer models depends strongly on cloudiness. This makes necessary the analysis of available cloud maps, which can be carried out by the means of image processing techniques.

For the numerical treatment, we discretize these infinite dimensional problems by a Galerkin finite element method. For the solution of the resulting algebraic systems iterative methods should be employed. This discretization process and subsequent iterative solution cause errors which should be taken into account in order to obtain reliable results.

Focal point of the thesis is the assessment of different types of errors by a posteriori error analysis. On the basis of these a posteriori error estimates the algebraic iteration can be adjusted to discretization within a succesive mesh adaptation process. For the solution of the resulting algebraic systems any fixed-point iteration can be used. We pay a special attention to the Newton-type methods. Since the considered problems describing atmospheric transport are ill-posed, we consider different types of regularization particularly accounting for the perturbations of the model.

The presented adaptive algorithms are applicable for a wide range of problems. The efficiency and reliability of the proposed techniques are confirmed by several examples involving the cloud segmentation from satellite observations, the calculations of radiative transfer models and nonlinear parabolic systems of partial differential equations. Furthermore, the recovery of the concentrations of bromine oxide in a Polar region from integrated measurements is presented.

Zusammenfassung

Gegenstand dieser Arbeit ist die Analysis und die Entwicklung von adaptiven Algorithmen zur Lösung von Problemen, die den Transport von chemischen Stoffen in der Erdatmosphäre mit Hilfe von Daten aus der Satellitenfernerkundung beschreiben.

Prozesse, die den Transport von chemischen Spezien beschreiben, sind durch Systeme von nichtlinearen partiellen Differentialgleichungen gegeben. Um die Konzentrationen in einer bestimmten Region der Atmosphäre zu bestimmen, müssen inverse Probleme gelöst werden. Die Messungen, die aus der Satellitenfernerkundung erhalten und als zusätzliche Lösungsinformation verwendet werden, müssen oft aus den Strahlungstransfermodellen berechnet werden. Die Form der Strahlungstransfergleichungen hängt von der Bedeckung des Himmels ab. Das macht die Analyse der verfügbaren Himmelskarten notwendig. Diese Analyse kann mit Hilfe von Bildverarbeitungstechniken durchgeführt werden.

Für die numerische Behandlung diskretisieren wir diese unendlich dimensionale Probleme mit der Galerkin Finite Elemente Methode. Zur Lösung der resultierenden algebraischen Systeme müssen iterative Verfahren eingesetzt werden. Dieser Diskretisierungsprozess und die anschließende iterative Lösung verursachen Fehler, welche für das Erzielen zuverlässiger Resultate berücksichtigt werden müssen.

Schwerpunkt der vorliegenden Dissertation ist die Abschätzung verschiedener Fehlerquellen mit Hilfe von a posteriori Fehleranalyse. Auf der Basis dieser a posteriori Fehlerabschätzungen kann der algebraische Fehleranteil an den Diskretisierungsfehler im Rahnem eines sukzessiven Gitterverfeinerungsprozesses angepasst werden. Für die Lösung der algebraischen Systeme können beliebige Fixpunktiterationen verwendet werden. Insbesondere werden die Newton-artige Methoden betrachtet. Die Probleme, die den atmosphärischen Transport beschreiben, sind schlecht gestellt. Zu diesem Zweck betrachten wir verschiedene Regularisierungstechniken, die ebenfalls die Störungen des Modells berücksichtigen.

Die entwickelten adaptiven Methoden können auf eine breite Klasse von Problemen angewendet werden. Die präsentierten Ergebnisse und die entwickelten Konzepte werden durch verschiedene numerische Tests bestätigt. Im Rahmen dieser Tests werden die Segmentierung von Objekten anhand Satellitenmessungen, ein Strahlungstransfermodell und ein nichtlineares System von parabolischen Gleichungen betrachtet. Zusätzlich wird ein Problem zur Rekonstruktion der Bromoxid-Konzentration in einer Polarregion aus integrierten Messungen betrachtet.

Contents

CHAPTER 1

Introduction

This work is devoted to analysis and development of adaptive techniques for problems related to the transport of chemical species in the Earth's atmosphere. Such problems include nonlinear systems of partial differential equations for the species' concentration, hyperbolic equations given by radiative transfer models and Euler equations resulting from image segmentation techniques.

Equations describing the atmospheric transport of chemical species involve parameters that cannot be measured directly or whose parametrization involves uncertainties. The most uncertain factors in such systems constitute the sources in the free atmosphere and the near-surface processes. The exact knowledge of these parameters would contribute to the understanding of underlying mechanisms. Consequently, the identification or calibration of these imprecisely known or even unknown parameters is necessary in order to describe the corresponding processes. This results in formulation of inverse problems in which the additional information of the solution (so-called overspecification) is obtained by remote sensing techniques. However, the concentrations of atmospheric constituents very often cannot be measured directly. Rather, they are deduced from the radiative absorption properties of chemical species. To this end, related radiative transfer models must be solved. The form of the radiative transfer models depends strongly on meteorological parameters such as cloudiness. This makes necessary analysis of supplied cloud maps, which can be carried out by the means of image processing techniques.

Provided observations are contaminated by noise due to the instrumental accuracy and the approximative solution of radiative transfer models. Thus, it is important to know the stability properties of the resulting inverse problems in order to obtain reliable approximations. From numerical point of view solution algorithms for parameter identification governed by partial differential equations require a certain amount of forward and backward solves and, as a consequence, more computational effort than a direct simulation. Furthermore, the analysis of the satellite-based observations results in a large amount of information needed to be processed, which makes the solution process expensive. The main goal of this work is to provide the analysis and the systematic approach for adaptivity for problems related to the atmospheric transport. Our approach bases on a posteriori error analysis for Galerkin finite element methods. Thus, the goal is to construct meshes that are optimized with respect to a desired quantity leading to an automatic model reduction. Furthermore, we address the question how exact the discrete systems must be solved. The answer leads to the assessment of different types of errors and, thus, to reliable and efficient adaptive techniques.

The concepts of adaptivity based on a posteriori error estimation for finite element discretization are well accepted for numerical solution of partial differential equations. The underlying theoretical framework of the proposed adaptive techniques is the Dual Weighted Residual (DWR) method originally proposed by Becker & Rannacher [17]. The provided concept is rather general and can be applied to the direct simulation for computing certain quantities as well as to the parameter identification problems. We apply these methods to problems related to the atmospheric transport including stationary and nonstationary nonlinear systems, hyperbolic equations given by radiative transfer models, and Euler equations resulting from image segmentation techniques.

The thesis is organized as follows: In Chapter 2, we discuss equations modeling the change of the concentrations of chemical species in the atmosphere. These are given by system of semilinear weakly-coupled parabolic equations. We pay special attention to the sources in the free atmosphere and near the surface. Furthermore, we discuss the mass kinetics constituting couplings between the equations and, thus, nonlinearities in the system. Without any assumptions on the nonlinearity in general blow-up can occur in finite time. Thus, we pose necessary conditions in order to circumvent this phenomenon and state the regularity of solutions of the system. These conditions are verified at the end of the chapter for two chemical reaction chains used later in our numerical calculations.

In Chapter 3, we discuss the Galerkin finite element method for the discretization of resulting nonlinear species equations. The problem is convection-dominated and, as a consequence, the presented spatial discretization scheme may become unstable. To avoid the instability, we introduce two stabilization techniques and discuss the advantages and the drawbacks of both presented schemes.

The most uncertain factors in chemical transport models are the sources. Therefore, we formulate in Chapter 4 the calibration problem scaling the modeled source terms. We treat the initial concentrations as a further unknown parameter. The resulting atmospheric inverse problem is further reformulated as an operator equation. We show that also in the case of provided distributed measurements this problem is ill-posed in the sense of Hadamard. In this sense, small errors in given observations can be arbitrarily amplified. Finally, we show the differentiability properties of the forward operator. These are used, on the one hand, for the stability analysis of the regularized solutions and for the construction of numerical methods, on the other.

Chapter 5 treats regularization methods for the inverse problems. The presentation is quite general allowing the direct transfer of the results to the atmospheric inverse problem. Particular emphasis is put on the ordinary and iterated Tikhonov regularization methods. The accuracy of the obtained regularized solutions depends strongly on the choice of the regularization parameters. In this sense, we review a priori, a posteriori, and heuristic parameter choice rules. Stability estimates for a posteriori parameter choice rules are usually derived under the assumption that the nonlinear operator equation is given without perturbations. We consider the perturbed Tikhonov functional with a rather general error source

and derive optimal stability estimate for the Morozov's discrepancy principle. Then, we discuss algorithmic aspects for the numerical solution of the inverse problems. At the end of this chapter, we give the precise form of the discrete equations of the atmospheric inverse problem regularized by a Tikhonov-type method. The behavior of the regularization methods is demonstrated for a numerical example involving a chemical reaction chain describing the ozone loss in Polar regions.

Chapter 6 is devoted to a posteriori error analysis for stationary and nonstationary situations. Usually a posteriori error estimates are developed generally for the unknown exact discrete solutions. We derive error estimator which assesses the influences of the discretization and the inexact solution of the arising algebraic equations. This allows us to balance both sources of the error. The estimator derived for the discretization error is used as stopping criterion for the algebraic iteration and provides the necessary information for the construction of locally refined meshes in order to improve the accuracy of the discretization. The method is formulated for a general fixed-point iteration. The iteration error can be further refined exploiting the structure of the DWR method and the Newton algorithm. The efficiency and reliability of the developed approach are verified by the computations including a weakly nonlinear diffusion-reaction problem, Euler equations resulting from cloud segmentation, a hyperbolic inverse problem, and a nonstationary inverse problem governed by a system of nonlinear convection-diffusion-reaction equations.

In Chapter 7, we consider the problem of reconstruction of distributed concentrations of bromine oxide from integrated measurements. The species equations are rewritten in accordance with the given observations in units of mole fractions and further transformed into terrain-following spherical coordinates. Here, we are faced with the situation in which the mechanisms responsible for the release or the destruction of bromine oxide are not precisely known. Due to this reason, the space and time dependent source represents an unknown parameter in the system. The comparison of the obtained results with the assimilated concentrations verifies the calculations.

In the last chapter conclusions and an outlook on future work are given. Here, we summarize the results presented in this work and discuss the possible extensions.

ACKNOWLEDGMENTS

I would like to express my gratitude to Prof. Dr. Dr. h.c. Rolf Rannacher and PD. Dr. Christoph S. Garbe for suggesting this interesting subject and for continuous supporting this work. Furthermore, I would like to express special thank to Prof. Dr. Thomas Richter and Dipl. Math. Matthias Klinger for many fruitful discussions. Finally, I would like to thank my wife Olesja for her encouragement and support.

This work has been supported by the Heidelberg Graduate School of Mathematical and Computational Methods for Sciences (HGS) at the Interdisciplinary Center of Scientific Computing (IWR), University of Heidelberg.

CHAPTER 2

Equations

In this chapter, we present the equations that model the change of the concentration of chemical species in the Earth's atmosphere. The main factors affecting the transport of the chemical constituents are the wind, the temperature, the turbulent diffusion, and the chemical and nonchemical transformations. In the following a mathematical modeling of these processes is presented. The resulting equations are written in an Eulerian framework. For the formulation in the Lagrangian and semi-Lagrangian coordinates, we refer to Jacob [62] and Fisher & Lary [38], respectively.

The underlying mathematical model describing the transport of chemical species in the atmosphere is the full set of the Navier-Stokes equations for the wind field, the energy equations for the temperature accompanied by the balance equations for the chemical species. This system of equations is coupled: the wind field transports the species, the chemicals react and produce heat affecting the temperature, and, finally, the temperature affects the wind field through buoyancy effects. This approach makes it possible to consider all the quantities at once in a monolithic manner but leads to a high computational effort.

On the other side, the influence of the trace gases on the temperature and wind field is usually negligibly small. Consequently, it is justifiable to consider the mass balance equations independently from the Navier-Stokes and the energy equations and vice versa. This approach is widely accepted in the area of data assimilation concerned with the modeling of the transport of atmospheric chemical constituents. In this thesis, we pursue the latter approach and assume the wind field and the temperature to be given by a general circulation model. Thus, our aim is derivation and analysis of the balance equations describing the chemical transport in the atmosphere.

The outline of this chapter is as follows: First, we discuss the equations modeling the transport of atmospheric constituents. Then, we explain the choice of boundary conditions. A special attention is put on the modeling of chemical and nonchemical source and sink terms, which are treated in Section 2.2. In Section 2.3, we analyze the derived system of nonlinear weakly-coupled parabolic equations. Without any assumptions on the nonlinearity in general blow-up can occur in finite time. To this end, we make necessary assumptions in order to circumvent this phenomenon and state the regularity of solutions of the system. At the end of the chapter, we verify these conditions for two chemical reaction chains used later in our numerical computations.

2.1. Continuity equation

In this section, we describe the equations governing the change of the concentrations of chemical species in the Earth's atmosphere. The main factors affecting the transport are the convection by wind, turbulent diffusion, emissions, and chemical reactions. The species can be represented by their mass density, mass or molar fractions. We present here the formulation in which the concentration of species is expressed in units of so-called "number density", i.e., the number of molecules of species per unit volume of air.

If we consider a fixed volume of the atmosphere, then the transport is characterized by the diffusion behavior $\nabla \cdot \mathcal{F}$ of flux $\mathcal{F}$ and source and sink terms $\mathcal{S}(t, x, \Theta, u)$, where Θ stands for the temperature and $u := (u_1, \ldots, u_d)^T$ for the vector of the concentrations of all species involved in the chemical reactions. t denotes the time and x the spatial variable. Generally the source may depend on the concentration of the trace gas itself and of other constituents coupled through chemical reactions. Thus, for a mixture of d chemical species the corresponding mass balance equations are given by

$$\partial_t u + \nabla \cdot \mathcal{F} = \mathcal{S}(t, x, \Theta, u), \tag{2.1}$$

where $\partial_t u = \frac{\partial u}{\partial t}$. In addition to the requirement that the species u must fulfill the above equation, the wind field v and the temperature Θ must in turn satisfy the Navier-Stokes and the energy equations, which are coupled through v, u, and Θ with the species equation and the ideal gas law

$$p = \frac{\rho_a R \Theta}{M_a}, \tag{2.2}$$

where p is the pressure, R the universal gas constant, M_a the mean molar mass of air, and ρ_a the air density.

In general, it is necessary to solve the coupled equations of mass, momentum and energy conservation in order to describe the changes in u, Θ, and v and the effect of the changes of these quantities on each other. However, as already mentioned in dealing with atmospheric trace gases, it is justifiable to consider the wind field v and the temperature Θ independently from the species concentrations u. Thereupon, we assume in the following that the convection velocity and the temperature are supplied by carrying out separate simulations. Thus, we concentrate on the modeling aspects of the transport coefficients and the source terms of system (2.1).

2.1.1. Transport coefficients

The flux $\mathcal{F}$ can be separated into the convection and diffusion components:

$$\mathcal{F} = \mathcal{F}_{\text{conv}} + \mathcal{F}_{\text{diff}}. \tag{2.3}$$

The convective part of the flux depends on the wind field and is given by

$$\mathcal{F}_{\text{conv}} = v\, u. \tag{2.4}$$

The diffusion flux can be further separated in molecular and turbulent components

$$\mathcal{F}_{\text{diff}} = \mathcal{F}_{\text{turb}} + \mathcal{F}_{\text{mol}}. \tag{2.5}$$

The molecular diffusion $\mathcal{F}_{\text{mol}}$ is usually neglected since its contribution to the transport is not significant. In order to model the turbulent component of the diffusion, we consider the convective part of the flux. Due to the turbulent nature of the flux both v and u show large fluctuations in time and are random functions of space and time, see, e.g., Seinfeld & Pandis [107]. The turbulent behavior of the atmospheric motion is a distinctive feature especially of the boundary layer of the atmosphere, i.e., in the region between the Earth's surface and 500-3000 m height. Direct measurements of the turbulent fluxes usually are not performed.

The most common approach to treating turbulence consists in considering the mean value of diffusive flux $\bar{\mathcal{F}} = \overline{v \cdot u}$ over some time interval. Thus, we decompose the wind field v and the concentrations u as the sums of the mean and fluctuating components

$$\begin{aligned} v &= \bar{v} + v', \\ u &= \bar{u} + u', \end{aligned} \tag{2.6}$$

where v' and u' denote the turbulent fluctuating components. By the Reynolds assumption the average of all perturbation is zero, $\overline{u'} = 0$ and $\overline{v'} = 0$. Inserting quantities (2.6) into (2.3), we obtain the mean value of the flux

$$\begin{aligned} \bar{\mathcal{F}} &= \bar{u}\bar{v} + \bar{u}\overline{v'} + \overline{u'}\bar{v} + \overline{u'v'} \\ &= \bar{u}\bar{v} + \overline{u'v'}. \end{aligned} \tag{2.7}$$

Thus, the turbulent diffusion part of the flux is given by

$$\mathcal{F}_{\text{turb}} = \overline{u'v'}, \tag{2.8}$$

which corresponds to a new unknown variable. This effect is known as the closure problem. The closure problem can be overcome by using the Lagrangian coordinates. However, the Lagrangian approach cannot be directly applied to the problems involving nonlinear chemical reactions, see, e.g., Seinfeld & Pandis [107].

The usual approach to parametrization of the occurring turbulence is the use of the so-called mixing-length K-theory or the Monin-Obukhov similarity theory, see, e.g., Jacobson [63]. In particular, a linear relationship between the turbulent diffusion flux and the gradient of the species concentration is assumed. Thus, the diffusive contribution of the flux is given by

$$\mathcal{F}_{\text{turb}} = -D\nabla u, \tag{2.9}$$

where $D(t, x) = (D_{11}, D_{22}, D_{33})$ is a diagonal matrix whose entries are the turbulent eddy diffusivities in general in terms of time and position.

By adding all the contributions, we obtain the total mean flux

$$\bar{\mathcal{F}} = \bar{v} \cdot \bar{u} - D \nabla \bar{u}. \tag{2.10}$$

We insert quantity (2.10) into equation (2.1) and obtain the species continuity equation for the mean concentration

$$\partial_t \bar{u} - \nabla \cdot (D \nabla \bar{u}) + \nabla \cdot (\bar{v}\, \bar{u}) = \bar{\mathcal{S}}, \tag{2.11}$$

where we have suppressed the dependence of $\bar{\mathcal{S}}$ on the temperature Θ. In the following, we omit the overbars in order to simplify the notation and always mean the averaged quantities, that is $u \equiv \bar{u}$, $v \equiv \bar{v}$, and $\mathcal{S} \equiv \bar{\mathcal{S}}$.

Although the mixing-length approach is the most widely used method to modeling turbulences, it has several limitations. It is applicable if the chemical reaction processes are slow compared to the turbulent transport, see, e.g., Lamb [76]. The alternative approach consists in estimation of the unknown diffusivity coefficients by solving a corresponding inverse problem, see, e.g., Storch et al. [111] and Campos et al. [23] for more details.

2.1.2. Boundary and initial conditions

In order to specify the boundary conditions, we consider a domain $\Omega \subset \mathbb{R}^n, n = 2, 3$, covering a region of the atmosphere. Let n be the outward unit normal vector to the boundary Γ of the domain. The boundary of the domain Ω consists of three parts

$$\Gamma = \Gamma_I \cup \Gamma_O \cup \Gamma_G,$$

corresponding to inflow, outflow, and ground portions of the boundary. Let $T > 0$ be a fixed time and $I = [t_0, T]$ be a time interval. Without loss of the generality, we set $t_0 = 0$ and define

$$\Omega_T := I \times \Omega, \quad \Sigma_I := I \times \Gamma_I, \quad \Sigma_O := I \times \Gamma_O, \quad \text{and} \quad \Sigma_G := I \times \Gamma_G.$$

For the inflow boundary comprising of the set of lateral or top boundary points, we impose nonhomogeneous Dirichlet boundary conditions

$$\begin{aligned} u(t,x) &= u^{\text{in}}(t,x) \quad \text{on } \Sigma_I, \\ v \cdot n &< 0. \end{aligned} \tag{2.12}$$

On the outflow boundary Σ_O, we prescribe homogeneous Neumann boundary conditions

$$\begin{aligned} D\, \partial_n u &= 0 \quad \text{on } \Sigma_O, \\ v \cdot n &> 0, \end{aligned} \tag{2.13}$$

where $\partial_n u = n \cdot \frac{\partial u}{\partial x}$.

The boundary condition at the ground part of the boundary must account for uptake and emissions of atmospheric species on the Earth's surface. Thus, we obtain

$$\begin{aligned} D\,\partial_n u - w\,u &= E_s(u,t,x) \quad \text{on } \Sigma_G, \\ v \cdot n &= 0, \end{aligned} \tag{2.14}$$

where $E_s(u,t,x)$ represents the surface emission rate and $w(t,x)$ the deposition velocity. The emission rate $E_s(u,t,x)$ usually is provided by ground-based or satellite measurements. The deposition velocity w is calculated using the aerodynamic resistance r_a, the bulk resistance of the diffusion of surface elements r_b, and the bulk surface resistance r_c:

$$w = \frac{1}{r_a + r_b + r_c}. \tag{2.15}$$

The aerodynamical resistance can be computed using the Stokes assumption and depends on the drag coefficient and the wind speed. The resistance r_b depends on the Schmidt and Prandtl numbers and the air kinematic viscosity. The surface resistance r_c depends on the surface and the season. These parameters depend on the particular species. Thus, the deposition velocity depends on the surface, species under consideration, and stability conditions of the atmosphere. For more details on the latter issue, we refer to Chapter 7. A detailed description of the calculation of the deposition velocity is given in Gao & Wesely [41] and Seinfeld & Pandis [107].

Finally, equation (2.11) is supplemented at the initial time point $t_0 = 0$ with the initial condition

$$u(0) = u^0 \quad \text{in } \Omega, \tag{2.16}$$

with a nonnegative function $u^0 = (u_1^0, \ldots, u_d^0)^T$. The initial condition is either treated as an unknown parameter of the system or given by the available measurements.

2.2. Modeling source terms

In this section, we consider modeling of surface emissions and source and sink terms in the free atmosphere constituting the right-hand side of the ground part boundary (2.14) and the continuity equation (2.11), respectively. The source terms depend on the area of interest, and we distinguish between anthropogenic and biogenic sources. Anthropogenic emissions occur due to human activities such as fuel combustion and traffic. Biological emissions that influence the transport of atmospheric constituents include emissions from forest canopies, pasture, sea salt, and wind-blown dust. The rate of emitted species depends on the meteorological parameters such as temperature and radiation. In many cases the emission terms can be considered as surface or be treated as elevated sources.

Other source and sinks in the free atmosphere occur due to the chemical reactions between the species and the wet deposition processes. In order to model chemical transformation terms, we use the Arrhenius law. Additionally, as a special chemical reaction, we consider

the loss of the concentration due to the radiation corresponding the first-order sink. In the following, we decompose the source term on the right-hand side of (2.11) as follows:

$$\mathcal{S} = E + f,$$

where E corresponds to the non-chemical sources and sinks, and f describes chemical transformations. In general the nonchemical emission term has the form

$$E = e\,a, \tag{2.17}$$

where e is the emission factor per unit of activity and a the amount of activity.

2.2.1. Anthropogenic emissions

Anthropogenic emissions originate mostly from burning of different kinds of fuel. Pollutants emitted into the atmosphere over urban areas due to industrial complexes, power plants, and factories include such species as nitrogen oxides NO_x (NO and NO_2), sulfur dioxide (SO_2), and formaldehyde (CH_2O). These emissions can be considered as surface fluxes or be treated as elevated sources. In the latter case the most common approach to representing the vertical distribution is the Gaussian plum model. The concentrations from emitting source are then proportional to the emission rate and inversely proportional to the wind speed. The time averaged pollutant concentration is described by a Gaussian distribution. This is justified by the fact that the solution of problem (2.11) with Dirac right-hand side representing a point source is given by Gaussian puff formula, see, e.g., Ermak [34] or Hurley [60].

Emissions due to domestic heating are related to area sources and used to model ground level releases with no plume rise. Thus, in this case the source term constitutes the ground boundary condition (2.14). The pollutants emitted in this instance are SO_2, CO and CO_2.

Emissions due to road traffic include such species as carbon monoxide (CO), nitrogen oxides (NO_x), and carbon dioxide (CO_2). The main factors needed to model the emission rates are traffic intensity with its temporal variation and classification of vehicles. Road traffic emissions are commonly represented as the sum of hot emissions (thermally stabilized motors) and cold emissions, where each contribution is modeled accordingly to (2.17). In general the amount of activity a on the right-hand side of (2.17) is given by the number of vehicles multiplied by the length of the stretch. More involved obstacle resolving models account for the arising turbulences in the street canyons. For more details on this issue, we refer to Jourmard [66] and Eggleston et al. [28]. Vehicle emissions are related to line sources consisting of infinitely many point sources. However, they are commonly treated as volume sources. The vertical distribution is given by the Gaussian distribution multiplied by the line integral over the length of stretch.

2.2.2. Natural emissions

Natural emissions comprise emissions of volatile organic compounds (VOC), NO_x and NH_3 from vegetation and soils, sea salt aerosols, the emissions from wind blown dust, and the re-emission of mercury from soils, vegetation and water, biomass burning. We do not aim at the detailed description of all of these processes but rather give a short description of modeling aspects used for some of the emissions. As in the case of anthropogenic emissions some of the natural sources can be treated either as surface or volumetric fluxes. In the second case the vertical distribution depends on the underlying process.

Thus, in order to model the emissions due to the vegetation such as forest, the canopies are divided into a number of horizontal layers. Each layer has a specific temperature and radiation flux for a prescribed chemical species. Furthermore, the rate of emissions depends on the sun light. The total source term is then obtained by summing the emissions from all layers. A detailed description of the modeling procedure with the corresponding values of emission rates is given in Guenther et al. [48] or in Norman [90]. The vertical distribution of the emitted species usually is taken to follow a triangular distribution as described in Lamb et al. [75].

The VOC emissions from pasture and grasses are related to the area sources. The rate of emission in equation (2.17) shows strong radiation and temperature dependency. For a detailed description of pasture emission model, we refer to Kirstine et al. [72]. Estimation methods for wind blown dust emissions are based on the threshold friction velocity, particle size, and horizontal saltation flux. The vertical flux is modeled using the plastic flow pressure and soil bulk density, see, e.g., Lu & Shao [77].

Sources in the free atmosphere that are treated as volumetric include the processes such as wet deposition resulting from cloud and precipitation scavenging. Wet deposition can be split into in-cloud scavenging and below-cloud scavenging. In-cloud scavenging deposition results from pollutant mass transfer into cloud followed by transport to the Earth's surface by perspiration. The mass removed by the rain is modeled with the help of the scavenging coefficient depending on rain intensity and cloud liquid water content. Below-cloud scavenging represents effect of falling rain drops on the species. Here, a scavenging coefficient is again used for the determination of the deposition flux. The presence and the modeling of these deposition processes depend on the chemical constituent under consideration and precipitation intensity. Thus, this source term is modeled using the meteorological observations such as cloud and precipitation maps. For detailed description of the modeling of this process, we refer to Sportisse & Bois [110] and Binkowski & Roselle [19].

Furthermore, the chemical species such as radon (Rn) and caesium (Cs) can be removed from the atmosphere by radioactive decay. In this case the source term is given by

$$E(u, t, x) = -\lambda\, u(t, x), \tag{2.18}$$

where $\lambda \in \mathbb{R}$ denotes the decay rate. This process corresponds to the first-order sink in the bulk atmosphere.

2.2.3. Chemical transformations

Other sources in the free atmosphere are due to chemical reactions. In order to describe the chemical transformations, we consider an elementary reaction r represented by

$$\sum_{k=1}^{d} a_{kr}\chi_k \xrightarrow{k_r} \sum_{i=1}^{d} b_{kr}\chi_k,$$

where χ_k are the chemical species, a_{kr} and b_{kr} the stoichiometric coefficients of the elementary reaction, and k_r the rate of reaction, $r = 1, \ldots, n_r$. Usually for each reaction up to three species are involved, i.e., only up to three coefficients a_{kr} do not vanish for each r. Very often in these three-body reaction the third species is inert and only gives the kinetic energy to stabilize the exited product. Thus, for large reaction mechanisms the matrices $A = \{a_{kr}\}_{k,r=1}^{n_r}$ and $B = \{b_{kr}\}_{k,r=1}^{n_r}$ are sparse.

The production rate f_k for species k expressed in units of number density is obtained by adding all reactions involved

$$f_k(\Theta, u) = \sum_{r=1}^{n_r} \left\{ (a_{rk} - b_{rk}) k_r(\Theta) \prod_{j=1}^{n_s} u_j^{a_{rj}} \right\}. \tag{2.19}$$

The rate of reaction is given following the Arrhenius law

$$k_r(\Theta) = A(\Theta) \exp\left(-\frac{E_a}{R\Theta}\right), \tag{2.20}$$

with activation energy E_a and the universal gas constant R. The frequency factor $A(\Theta)$ is usually determined experimentally and can be assumed to be independent on the temperature.

The other chemical transformation in the free atmosphere is the photolysis. It occurs if molecules are drop down by the sun light. An example of such reaction is given by

$$O_3 + h\nu \to O + O_2,$$

which generates an excited oxygen. We treat this process as a chemical transformation with the corresponding source term given by

$$f(\Theta, u) = -\lambda(t)u(t, x), \tag{2.21}$$

with a time-dependent photolysis rate $\lambda(t)$. In the following, we suppress the dependency on temperature and use the notation $f(\Theta, u) = f(u)$.

2.3. Analysis of the state equation

In this section, we formulate the results concerning existence, uniqueness, and regularity of weak solutions of the derived equations. Thus, we first formulate the weak form of the chemical transport model. The obtained results are then used for the analysis of the corresponding parameter estimation problems and the formulation of numerical algorithms.

Putting all together, the model describing the transport of chemical species in the atmosphere is given by

$$\begin{aligned} \partial_t u - \nabla \cdot (D\,\nabla u) + \nabla \cdot (v\,u) &= f(u) + E(u,t,x) && \text{in } \Omega_T, \\ u &= u^{\text{in}} && \text{on } \Sigma_I, \\ D\,\partial_n u &= 0 && \text{on } \Sigma_O, \\ D\,\partial_n u - w\,u &= E_s(u,t,x) && \text{on } \Sigma_G, \\ u(t_0) &= u^0 && \text{in } \Omega, \end{aligned} \tag{2.22}$$

for $u = (u_1, \ldots, u_d)^T$ and $D = \text{diag}(D_i)$. Here, d denotes the number of chemical species involved in corresponding chemical reactions. System (2.22) is then referred to as the state equation.

Since the problem under consideration is later discretized by a Galerkin finite element method, we postulate its weak form. To this end, we introduce notations from theory of functional spaces, which we will use throughout. The properties of these spaces are given in Evans [37] and in Alt [2].

NOTATION FOR FUNCTION SPACES

In order to introduce the spaces of test and trial functions, we define the space

$$V := \{\psi \in H^1(\Omega)\ ;\ \psi = 0 \text{ on } \Gamma_I\}.$$

Together with $H := L^2(\Omega)$ the Hilbert space V and its dual V^* build a Gelfand triple

$$V \hookrightarrow H \hookrightarrow V^*.$$

We adopt standard notation for the L_2-scalar product $(\cdot,\cdot)$. We use the Bochner space $L^p(\Omega_T)$ comprising of all functions with

$$\|u\|_{L^p(\Omega_T)} := \left(\int_I \int_\Omega |u(t,x)|^p \, dx\, dt \right)^{1/p} < \infty,$$

for $1 \le p < \infty$ and

$$\|u\|_{L^\infty(\Omega_T)} := \text{ess sup}_{t\in I, x\in\Omega} |u(t,x)| < \infty.$$

Moreover, we use Lebesgue spaces and Sobolev spaces of mappings with values in other Banach spaces. Thus, we denote by $L^p(I;V)$ the space of all strongly measurable functions with

$$\|u\|_{L^p(I;V)} := \left(\int_I \|u\|_V^p \, dt \right)^{1/p} < \infty,$$

for $1 \leq p < \infty$ and

$$\|u\|_{L^\infty(I;V)} := \operatorname{ess\,sup}_{t \in I} \|u(t)\|_V < \infty.$$

We note that from Fubini's theorem follows $L^p(\Omega_T) = L^p(I; L^p(\Omega))$.

Next, we introduce the Hilbert space

$$W(0,T) := \left\{ v \; ; \; v \in L^2(I,V) \text{ and } \partial_t v \in L^2(I,V^*) \right\}.$$

The space $W(0,T)$ is endowed with the scalar product

$$(u,v)_{W(0,T)} = \int_I (u,v)_V \, dt + \int_I (\partial_t u, \partial_t v)_{V^*} \, dt.$$

The space $W(0,T)$ is continuously embedded into $C(I; L^2(\Omega))$, the space of all continuous functions from I into $L^2(\Omega)$, such that there exists a constant $C > 0$ satisfying

$$\|w\|_{C(I;H)} \leq C \|w\|_{W(0,T)} \quad \text{for all } w \in W(0,T), \tag{2.23}$$

see, e.g., Dautray & Lions [26]. Moreover, we have

$$W(0,T) \subset L^2(\Omega_T),$$

with a continuous embedding. In the following, we make the use of the Aubin-Lions lemma.

LEMMA 2.3.1 (Aubin-Lions lemma). *Let $Y \subset X \subset Z$ be Banach spaces. Suppose that the inclusion $Y \subset Z$ is a compact embedding. Moreover, let Y and Z be reflexive spaces. Then, for any $1 < p, q < \infty$ the space*

$$\{u \in L^p(I;Y) \; ; \; \partial_t u \in L^q(I;Z)\}$$

is compactly embedded into the space $L^p(I;X)$.

The proof of this result can be found in Temam [114]. By Rellich-Kondrashov theorem V is compactly embedded into H. Then, Aubin-Lions lemma yields that

$$W(0,T) \hookrightarrow\hookrightarrow L^2(\Omega_T).$$

Finally, we define the product space for the species concentrations

$$X := W(0,T) \times \cdots \times W(0,T), \tag{2.24}$$

consisting of d Hilbert spaces.

2.3.1. Regularity of solutions

In order to postulate the weak form of (2.22), we define for all $\phi \in V$ the spatial semilinear form $\bar{a} : V \times V \to I\!R$ as

$$\bar{a}(u)(\phi) := (D\,\nabla u, \nabla\phi) + (\nabla\cdot(v\,u), \phi) - (f(u) + E(u,t,x), \phi) - (w\,u + E_s(u,t,x), \phi)_{\Gamma_G}. \quad (2.25)$$

So as to incorporate the inhomogeneous boundary condition, let $\hat{u} \in W_2^{1,0}(\Omega_T)^d$ represent the inflow data, that is $\hat{u} = u^{\text{in}}$ on Γ_I for almost all $t \in I$. With this notation the variational form of problem (2.22) reads in short terms: Find $u \in \hat{u} + X$, such that

$$(\partial_t u, \phi) + \bar{a}(u)(\phi) = 0 \quad \text{and} \quad (u(0), \phi(0)) = (u^0, \phi(0)), \quad (2.26)$$

for almost all $t \in I$ and all $\phi \in V$. For simplicity, we introduce the definitions

$$(v, w)_I := \int_I (v(t), w(t))\,dt \quad \text{and} \quad a(u)(\phi) := \int_I \bar{a}(u(t))(\phi(t))\,dt,$$

and rewrite the weak formulation (2.26) in a more compact form

$$(\partial_t u, \phi)_I + a(u)(\phi) + (u(0), \phi(0)) = (u^0, \phi(0)) \quad \forall \phi \in X. \quad (2.27)$$

System (2.11) is of a rather general form. Before we begin with the analysis of the equations, we make the following assumptions concerning the data:

ASSUMPTION 2.3.1 (Data). *There holds*

(i) $\Omega \subset I\!R^n, n = 2, 3,$ *is a convex domain with Lipschitz boundary.*

(ii) *The wind field* $v : \Omega_T \to I\!R$ *is continuously differentiable with* $\nabla \cdot v = 0$.

(iii) *For the diffusion coefficients there holds*

$$0 < c_0 \le D(t,x) \le c_1, \quad c_0, c_1 \in I\!R.$$

(iv) *The emission term* $E(u,t,x) : I\!R^d \times \Omega_T \to I\!R$ *is measurable with respect to* $(t,x) \in \Omega_T$ *for all* $u \in I\!R^d$, *and at least two times continuously differentiable with respect to* u *for almost all* $(t,x) \in \Omega_T$. *For* $u = 0$ *the source term* E *and its derivatives up to order two are uniformly bounded by a constant* $K > 0$

$$\|E(0,\cdot,\cdot)\|_{L^\infty(\Omega_T)} + \|\partial_u E(0,\cdot,\cdot)\|_{L^\infty(\Omega_T)} + \|\partial_{uu} E(0,\cdot,\cdot)\|_{L^\infty(\Omega_T)} \le K.$$

(v) *The surface emission term* $E_s(u,t,x) : I\!R^d \times \Sigma_G \to I\!R$ *is measurable with respect to* $(t,x) \in \Sigma_G$ *for all* $u \in I\!R^d$, *and at least two times continuously differentiable with respect to* u *for almost all* $(t,x) \in \Sigma_G$. *For* $u = 0$ *the surface source term* E_s *and its derivatives up to order two are uniformly bounded by a constant* $K_s > 0$

$$\|E_s(0,\cdot,\cdot)\|_{L^\infty(\Sigma_G)} + \|\partial_u E_s(0,\cdot,\cdot)\|_{L^\infty(\Sigma_G)} + \|\partial_{uu} E(0,\cdot,\cdot)\|_{L^\infty(\Sigma_G)} \le K_s.$$

(vi) *The deposition velocity* w *is measurable for almost all* $(t,x) \in \Sigma_G$.

(vii) *In presence of radioactive decay, for the decay constant in* (2.21) *there holds*

$$\|\lambda(t)\|_{L^\infty(I)} \leq C,$$

for a constant $C \in \mathbb{R}$.

(viii) *The initial condition possesses the regularity* $u^0 \in L^\infty(\Omega_T)^d$ *and is componentwise positive* $u^0 \geq 0$.

We note that the assumptions on the domain and the wind field are satisfied by the most chemical transport models since the wind field v is usually obtained by the solution of the Navier-Stokes equations. The assumptions concerning the diffusion coefficients and emission terms are fulfilled by model (2.22), see also Chapter 7, Section 7.1.

System (2.11) is a weakly-coupled system of semilinear parabolic differential equations. The couplings occur due to the chemical reactions. Without any assumptions on the nonlinearity f in general blow-up can occur in finite time. Thus, we make the following assumptions concerning the structure and the differentiability properties of the nonlinearity:

ASSUMPTION 2.3.2 (Nonlinearity). *There holds*

(i) *The nonlinearity* $f_i = f_i(u) : \mathbb{R} \to \mathbb{R}, i = 1, \ldots, d$, *is at least two times continuously differentiable with respect to* u.

(ii) *The nonlinear source term* f *preserves the positivity of the solutions*

$$f_i(u) \geq 0, \quad \text{whenever } u_i = 0.$$

(iii) *There holds the following dissipative property: there exist* $a_i \in \mathbb{R}$ *and* $b_i \in \mathbb{R}$ *with* $a_i > 0$, $b_i \geq 0, i = 1, \ldots, d$, *such that for all* $u \in \mathbb{R}^d_+$ *there holds*

$$\sum_{i=1}^{d} a_i f_i(u) \leq \sum_{i=1}^{d} b_i u_i. \tag{2.28}$$

The differentiability properties and the quasi-positivity of the nonlinear term f are natural assumptions fulfilled by the presented mass kinetics model, see, e.g., Norman [89] and Manley et al. [78]. The dissipative property is assumed similarly to Pierre & Texier-Picard [93] (see also the survey article Pierre [92]) and is satisfied by many of chemical reaction mechanisms employed in simulation of atmospheric transport.

Since the emission terms are still rather general, we suppose that they are positive and of form (2.17) and, thus, independent of u, i.e., $E = E(t,x) \geq 0$ and $E_s = E_s(t,x) \geq 0$. The generalization of the following results in the presence, e.g., of radioactive decay and wet

deposition process is under the given assumptions straightforward. We state the following result concerning the existence and the regularity of weak solutions of problem (2.26).

PROPOSITION 2.3.1. *Let assumptions 2.3.1 and 2.3.2 be satisfied. Then, there exists a unique positive solution* $u \in \hat{u} + X \cap L^\infty(\Omega_T)^d$, *of problem* (2.26) *with* $\hat{u} = u^{in}$ *on* Σ_I. *Furthermore, there hold the following stability estimates*

$$\|u\|_{L^\infty(I;L^2(\Omega)^d)^d} \le C\Big(\|u^0\| + \|E\| + \|E_s\|_{L^2(\Gamma_G)} + \|w\|_{L^2(\Gamma_G)}\Big), \tag{2.29}$$

and

$$\|u\|_{W(0,T)} \le C\Big(\|u^0\| + \|E\|_I + \|E_s\|_{L^2(\Sigma_G)} + \|w\|_{L^2(\Sigma_G)}\Big), \tag{2.30}$$

with a constant C *that depends only on the data of problem* (2.26) *and not on the initial concentrations.*

PROOF. For the proof of existence and regularity of the positive solution, we refer to Pierre & Texier-Picard [93] and Fitzgibbon et al. [39] (see also Norman [89] and Manley et al. [78] for a more general problem with presence of Navier-Stokes and energy equations). The uniqueness of the solution can be shown by similar techniques as the stability estimate (2.30).

In order to show estimates (2.29) and (2.30), we set

$$\bar{u} := \sum_{i=1}^d a_i u_i, \quad \bar{E} := \sum_{i=1}^d a_i E_i, \quad \bar{E}_s := \sum_{i=1}^d a_i E_{s,i}, \quad \text{and} \quad \bar{f}(u) = \sum_{i=1}^d a_i f_i(u).$$

Then, there holds

$$(\partial_t \bar{u}, \phi) + (D\,\nabla\bar{u}, \nabla\phi) + (v \cdot \nabla\bar{u}, \phi) = (\bar{f}(u) + \bar{E}, \phi) + (w\,\bar{u} + \bar{E}_s, \phi)_{\Gamma_G}, \tag{2.31}$$

for all $\phi \in W(0,T)$ and almost all $t \in I$. We test equation (2.31) with $\phi = \bar{u}$, use the ellipticity condition in Assumption 2.3.1, (iii), and obtain

$$\frac{1}{2}\frac{d}{dt}\|\bar{u}\|^2 + c_0\Big(\|\bar{u}\|_V^2 - \|\bar{u}\|^2\Big) + (v\,\nabla\bar{u}, \bar{u}) \le (w\,\bar{u} + \bar{E}_s, \bar{u})_{\Gamma_G} + (\bar{f}(u) + \bar{E}, \bar{u}), \tag{2.32}$$

for almost all $t \in I$. For the convection term on the left-hand side, we obtain using the definition of the vector space V, the sign of $v \cdot n$ in the boundary conditions (2.13) and (2.14), and Assumption 2.3.1, (ii),

$$(v\,\nabla\bar{u}, \bar{u}) = \frac{1}{2}\int_\Omega v\,\nabla\bar{u}^2\,dx = \frac{1}{2}\int_\Omega (\nabla\cdot v)\bar{u}^2\,dx + \frac{1}{2}\int_\Gamma \bar{u}^2(v\cdot n)\,dS \ge 0. \tag{2.33}$$

Consequently, this positive term can be neglected. Using the dissipative property, we obtain for the nonlinear term on the right-hand side

$$(\bar{f}(u), \bar{u}) \le \|\bar{f}(u)\|\,\|\bar{u}\| \le \|\sum_{i=1}^d b_i f_i(u)\|\,\|\bar{u}\| \le C\|\bar{u}\|^2, \tag{2.34}$$

for some C depending only on a_i and b_i. For the volumetric emission term, we obtain by the help of the Cauchy-Schwartz and Young inequalities

$$(\bar{E}, \bar{u}) \leq C\|\bar{E}\|^2 + C\|\bar{u}\|^2, \tag{2.35}$$

where C depends on the constant K in Assumption 2.3.1, (iv). Due to $L^2(\Gamma_G) \hookrightarrow H^1(\Omega)$, we obtain using the Young inequality again

$$(\bar{E}_s, \bar{u})_{\Gamma_G} \leq \|\bar{E}_s\|_{L^2(\Gamma_G)}\|\bar{u}\|_{L^2(\Gamma_G)} \leq C\|\bar{E}_s\|^2_{L^2(\Gamma_G)} + \frac{c_0}{4}\|\bar{u}\|^2_V, \tag{2.36}$$

with the constant c_0 from Assumption 2.3.1, (iii). The boundary term including the deposition velocity is treated similarly,

$$(w\,\bar{u}, \bar{u})_{\Gamma_G} \leq C\|w\|^2_{L^2(\Gamma_G)} + \frac{c_0}{4}\|\bar{u}\|^2_V. \tag{2.37}$$

Using the identity

$$\int_0^T \frac{d}{dt}\|\bar{u}(t)\|^2\,dt = \|\bar{u}(T)\|^2 - \|\bar{u}(0)\|^2, \tag{2.38}$$

integrating inequality (2.32) with respect to time, neglecting the positive terms on the left-hand side, and collecting the above estimates, we infer that

$$\max_{t\in\bar{I}} \|\bar{u}(t)\| \leq C\Big(\|\bar{u}^0\| + \|\bar{E}\| + \|\bar{E}_s\|_{L^2(\Gamma_G)} + \|w\|_{L^2(\Gamma_G)}\Big). \tag{2.39}$$

Since $a_i > 0$, $i = 1, \ldots, d$, this shows estimate (2.29). Integrating inequality (2.32), we obtain the same type of bound in $L^2(I;V)^d$. This fact implies that $\|\partial_t u\|_{L^2(I;V^*)}$ is uniformly bounded. Therefore, u is bounded in X and the assertion follows. □

The existence and the boundedness of the solutions of problem (2.26) rely strongly on the quasi-positivity of the concentrations and the dissipative property. Whereas Assumption 2.3.2, (ii) is always true due to the structure of the used mass kinetics, the dissipativeness must be considered more carefully. In the following, we verify this crucial property for two special chemical reaction chains later used in our numerical computations.

EXAMPLE 1

As first example, we consider the Chapman mechanism describing the ozone loss in the stratosphere. The reaction chain is given by

$$O_2 + h\nu \xrightarrow{k_1} O + O \tag{2.40}$$

$$O + O_2 + M \xrightarrow{k_2} O_3 + M \tag{2.41}$$

$$O_3 + h\nu \xrightarrow{k_3} O + O_2 \tag{2.42}$$

$$O + O_3 \xrightarrow{k_4} O_2 + O_2 \tag{2.43}$$

Here, M is a nonreactive species stabilizing the ozone O_3. We denote the unknowns by $u_1 = [O_3], u_2 = [O]$, and $u_3 = [O_2]$, where the square brackets stand for the corresponding concentration values. Accordingly to the used mass kinetics the nonlinearities are given by

$$\begin{aligned} f_1(u) &= k_2u_2u_3 - k_3u_1 - k_4u_1u_2, && (2.44)\\ f_2(u) &= 2k_1u_3 + k_3u_1 - k_2u_2u_3 - k_4u_1u_2, && (2.45)\\ f_3(u) &= -k_1u_3 - k_2u_2u_3 + k_3u_1 + 2k_4u_1u_2. && (2.46) \end{aligned}$$

Due to the high concentration of oxygen in comparison to the concentrations of other species, it is assumed to be constant over time, cf. Jacob [62]. Consequently, there holds $u_3 = \text{const}$ and $f_3(u) = 0$. Using this steady state approximation and adding up the nonlinearities $f_i(u), i = 1, 2, 3$, we infer dissipative property given in Assumption 2.3.2, (iv). For the numerical test involving this reaction mechanism, we refer to Chapter 6, Section 6.6.

EXAMPLE 2

In the second example, we consider a reaction chain describing the ozone loss in Polar regions, which includes six atmospheric constituents interacting with each other in four chemical reactions. The corresponding reaction chain is given by

$$\begin{aligned} Cl + O_3 &\xrightarrow{k_1} ClO + O_2 && (2.47)\\ ClO + NO &\xrightarrow{k_2} Cl + NO_2 && (2.48)\\ NO + O_3 &\xrightarrow{k_3} NO_2 + O_2 && (2.49)\\ NO_2 + O_2 + h\nu &\xrightarrow{k_4} NO + O_3 && (2.50) \end{aligned}$$

In this case the unknowns are denoted by $u_1 = [Cl], u_2 = [O_3], u_3 = [ClO], u_4 = [NO], u_5 = [NO_2]$, and $u_6 = [O_2]$. The nonlinear reaction terms read as follows:

$$\begin{aligned} f_1(u) &= -k_1u_1u_2 + k_2u_3u_4, && (2.51)\\ f_2(u) &= -k_1u_1u_2 - k_3u_4u_2 + k_4u_5u_6, && (2.52)\\ f_3(u) &= -k_2u_3u_4 + k_1u_1u_2, && (2.53)\\ f_4(u) &= -k_2u_3u_4 - k_3u_4u_2 + k_4u_5u_6, && (2.54)\\ f_5(u) &= -k_4u_5u_6 + k_2u_3u_4 + k_3u_4u_2, && (2.55)\\ f_6(u) &= -k_4u_5u_6 + k_1u_1u_2 + k_3u_4u_2. && (2.56) \end{aligned}$$

In this case, we obtain

$$\sum_{i=1}^{6} f_i(u) = 0,$$

and, thus, dissipative assumption 2.3.2, (iv) is fulfilled with the constant $C = 0$. For the corresponding numerical calculations, we refer to Chapter 5, Section 5.5.

CHAPTER 3

Finite Element Discretization

In this chapter, we treat the discretization of the weak form of problem (2.26) by the Galerkin finite element method. We begin in Section 3.1 with the temporal discretization and introduce discontinuous Galerkin (dG) and continuous Galerkin (cG) methods. The spatial discretization is done by the continuous finite element method described in Section 3.1. Since the resulting equations are convection-dominated, they must be stabilized. To this end, we consider two stabilization schemes. The first residual-based streamline upwind Petrov-Galerkin scheme (SUPG), introduced in Subsection 3.3.1, allows to treat hyperbolic equations with the presented continuous finite elements. The second scheme is the local projection stabilization method (LPS) presented in Subsection 3.3.2.

3.1. Time discretization

This section is devoted to the temporal discretization of problem (2.26). First, we consider the discontinuous Galerkin method, which uses discontinuous trial and test functions. The second method uses continuous trial and discontinuous test functions and is called continuous Galerkin method.

To introduce the semi-discretization in time, we choose time points t_m for $0 \leq m \leq M$, such that

$$0 = t_0 < \cdots < t_m < \cdots < t_M = T.$$

Then, we partition the time interval $\bar{I} = [0, T]$,

$$\bar{I} = \{t_0\} \cup I_1 \cup \cdots \cup I_m \cup \cdots \cup I_M,$$

with subintervals $I_m := (t_{m-1}, t_m]$ of length $k_m := t_m - t_{m-1}$. The discretization parameter k is given as a piecewise constant function by $k|_{I_m} = k_m$, for $m = 1, \ldots, M$. On the subintervals I_m, we define the following semi-discrete spaces X_k^r and $\tilde{X}_k^r$, for $r \in \mathbb{N}_0$:

$$\begin{aligned} X_k^r &:= \left\{ v_k \in C(\bar{I}, H) \,;\, v_k|_{I_m} \in \mathcal{P}_r(I_m, V),\, m = 1, \ldots, M \right\}, \\ \tilde{X}_k^r &:= \left\{ v_k \in L^2(\bar{I}, V) \,;\, v_k|_{I_m} \in \mathcal{P}_r(I_m, V),\, m = 1, \ldots, M, \text{ and } v_k(t_0) \in H \right\}, \end{aligned}$$

where $\mathcal{P}_r$ denotes the space of polynomials up to degree r on I_m with values in V. Thus, X_k^r consists of functions which are continuous and piecewise polynomial with respect to time. This space is used as trial space in the continuous Galerkin method. The space $\tilde{X}_k^r$ consists of functions that may have discontinuities at the borders of the subintervals I_m. The space is used as trial and test space in the discontinuous Galerkin method and as test space in the continuous Galerkin method.

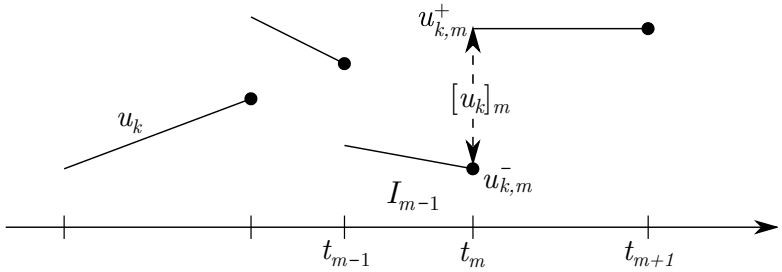

FIGURE 3.1: Notation of discontinuous functions u_k in the case $r = 1$

DISCONTINUOUS GALERKIN METHOD

To account for possible discontinuity of a function $u_k \in \tilde{X}^r_k$ at time points t_m, we introduce the notation

$$u^+_{k,m} := \lim_{\varepsilon \downarrow 0} u_k(t_m + \varepsilon), \quad u^-_{k,m} := \lim_{\varepsilon \downarrow 0} u_k(t_m - \varepsilon), \quad [u_k]_m := u^+_{k,m} - u^-_{k,m},$$

i.e., $u^+_{k,m}$ and $u^-_{k,m}$ are the limits "from above" and "from below" at time t_m, respectively, while $[u_k]_m$ is the corresponding "jump" of u_k at t_m, see Figure 3.1.

Then, the dG(r) semi-discretization of problem (2.26) seeks $u_k \in \tilde{X}^r_k$, such that

$$\sum_{m=1}^{M} (\partial_t u_k, \phi)_{I_m} + a(u_k)(\phi) + \sum_{m=0}^{M-1} ([u_k]_m, \phi^+_m) + (u^-_{k,0}, \phi^-_0) = (u^0, \phi^-_0) \quad \forall \phi \in \tilde{X}^r_k. \tag{3.1}$$

Here, $(u, \phi)_{I_m}$ is defined correspondingly to $(u, \phi)_I$

$$(u, \phi)_{I_m} := \int_{I_m} (u(t), \phi(t))\, dt.$$

CONTINUOUS GALERKIN METHODS

The cG(r) discretization of problem (2.26) can be stated directly: Find $u_k \in X^r_k$, such that

$$(\partial_t u_k, \phi)_I + a(u_k)(\phi) + (u_k(0), \phi^-_0) = (u^0, \phi^-_0) \quad \forall \phi \in \tilde{X}^{r-1}_k. \tag{3.2}$$

3.2. Discretization in space

In this section, we present the discretization in space of the semi-discretized problems defined above by the continuous Galerkin finite element method. To this end, we consider the discretization with usual bi-/trilinear H^1-conforming elements as explained in standard literature; see, e.g., Ciarlet [25].

We consider two or three dimensional shape-regular meshes $\mathcal{T}_h = \{K\}$ consisting of quadrilateral or hexahedral non-degenerate cells K, which constitute a non-overlapping

covering of the computational domain Ω. The discretization parameter h is defined as a cellwise constant function by setting $h|_K := h_K$ with the diameter h_K of the cell K. We construct continuous V-conforming finite element spaces V_h^s by

$$V_h^s := \{v \in C(\bar{\Omega} \cap V) \; ; \; v|_K \in \mathcal{Q}^s(K), \, K \in \mathcal{T}_h\}. \tag{3.3}$$

Here, $\mathcal{Q}^s(K)$ consists of shape functions obtained via iso-parametric transformations of bi/trilinear polynomials in $\hat{\mathcal{Q}}^s(\hat{K})$ defined on the reference cell $\hat{K} = (0,1)^n$, $n = 2, 3$. The space of functions on the reference cell is given by

$$\hat{\mathcal{Q}}^s(\hat{K}) := \text{span}\left\{ \prod_{i=1}^{n} x_i^{\alpha_i} \; ; \; \alpha_i \in \{0, 1, \ldots, s\} \right\}.$$

The space $\mathcal{Q}^s$ is defined using the transformation $T_K : \hat{K} \to K$ as

$$\mathcal{Q}^s(K) = \left\{ v : K \to I\!R \; ; \; v \circ T_K \in \hat{\mathcal{Q}}^s(\hat{K}) \right\}.$$

To ease local mesh adaptation, we allow "hanging nodes" (at most one per face or edge) where the corresponding "irregular" nodal values are eliminated from the system by linear interpolation of neighboring regular nodal values (see Figure 3.2).

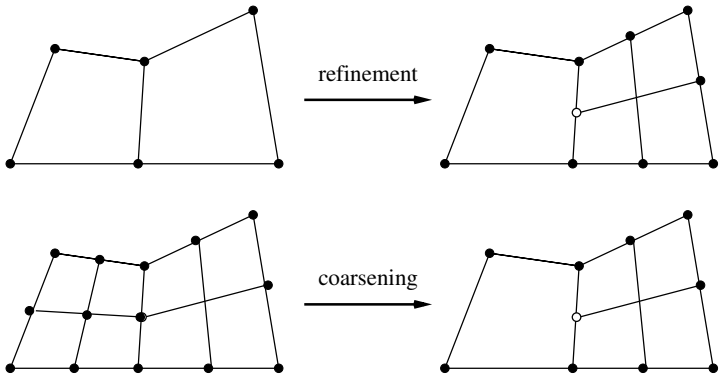

FIGURE 3.2: Mesh refinement and coarsening using "hanging nodes".

In order to use the meshes locally varying in time, we follow the procedure described in Meidner [81] and Becker [11]. Thus, we associate with each time point t_m a triangulation $\mathcal{T}_h^m$ and a corresponding finite element space $V_h^{s,m} \subseteq V$. By these means, we introduce the fully discrete space-time finite element spaces

$$\tilde{X}_{k,h}^{r,s} := \left\{ u_{kh} \in L^2(I, H) \; ; \; u_{kh}| \in \mathcal{P}_r(I_m, V_h^{s,m}), \, m = 1, \ldots, M, \text{ and } u_{kh}(0) \in V_h^{s,0} \right\}.$$

Due to the choice of the spaces $V_h^{s,m}$, there holds the inclusion $\tilde{X}_{k,h}^{r,s} \subseteq \tilde{X}_k^r$.

Using the definitions of these spaces the cG(s)dG(r) discretization of problem (2.26) seeks $u_{kh} \in X_{k,h}^{r,s}$ satisfying

$$\sum_{m=1}^{M} (\partial_t u_{kh}, \phi)_{I_m} + a(u_{kh})(\phi) + \sum_{m=0}^{M-1} ([u_{kh}]_m, \phi_m^+) + (u_{kh,0}^-, \phi_0^-) = (u^0, \phi_0^-) \quad \forall \phi \in \tilde{X}_{k,h}^{r,s}. \tag{3.4}$$

The formulation of the corresponding cG(s)cG(r) discretization on dynamically changing meshes in time is more involved. In this case, we must ensure the global continuity in time of functions in the trial space. To this end, we follow the approach described in Becker [11]. We choose $\{\tau_0, \tau_1, \ldots, \tau_r\}$ to be a basis of $\mathcal{P}_r(I_m, I\!R)$ satisfying

$$\tau_0(t_{m-1}) = 1, \;\; \tau_0(t_m) = 0, \;\; \text{and} \;\; \tau_i(t_{m-1}) = 0, \; i = 1, \ldots, r.$$

Next, we define the spaces

$$X_{k,h}^{r,s,m} := \text{span}\left\{ \tau_i u_i \; ; \; u_0 \in V_h^{s,m-1}, \, u_i \in V_h^{s,m}, \, i = 1, \ldots, r \right\}.$$

By the help of these spaces, we define the trial space for the cG(s)cG(r) discretization as

$$X_{k,h}^{r,s} := \left\{ u_{kh} \in C(\bar{I}, H) \; ; \; u_{kh}|_{I_m} \in X_{k,h}^{r,s,m}, \, m = 1, \ldots, M \right\}.$$

Thus, the definition of $X_{k,h}^{r,s,m}$ ensures the continuity in time of all functions in $X_{k,h}^{r,s}$.

With these preparations the cG(s)cG(r) discretization seeks $u_{kh} \in X_{k,h}^{r,s}$, such that

$$(\partial_t u_{kh}, \phi)_I + a(u_{kh})(\phi) + (u_{kh}(0), \phi_0^-) = (u^0, \phi_0^-) \quad \forall \phi \in \tilde{X}_{k,h}^{r-1,s}. \tag{3.5}$$

3.3. Stabilization

It is well known that the Galerkin discretizations are not appropriate for convection-dominated problems since the computed solution usually exhibits global spurious oscillations. For enhancing the stability and the accuracy, we need a stabilized formulation of the discrete equations. In this section, we present two types of the stabilization. The first is a residual-based stabilization technique and the second is the local projection stabilization scheme. In both methods an additional stabilization term is added to the fully discrete formulations.

3.3.1. Residual based stabilization

One of the most widely used stabilization approaches is the streamline upwind Petrov Galerkin method (SUPG) first proposed in Hughes & Brooks [59]. The additional terms in this case are given by

$$s_{\text{SUPG}}(u_{kh})(\psi) = \sum_{m=1}^{M} \left\{ \int_{I_m} \sum_{K \in \mathcal{T}_h} (\partial_t u_{kh} + \nabla \cdot (D \nabla u_{kh}) + v \nabla u_{kh} + f - E, \delta_{K,m} v_{kh} \nabla \psi)_K \right\}.$$

The term $(v\,\nabla u_{kh}, v\,\nabla\psi)$ is a streamline diffusion term. The other terms are due to the consistency of the method, i.e., the additional terms vanish for the continuous solution. The cellwise stabilization parameter $\delta_{K,m}$ is defined as

$$\delta_{K,m} = \delta_0 \frac{h_K^2}{\|D\|_K + h_K\|v\|_K + \frac{h_K}{k_m}}. \tag{3.6}$$

For details on the choice of this parameter $\delta_{K,M}$, we refer to Franca & Frey [40] or Braack et al. [21]. In our numerical computations, we set $\delta_0 = 0.3$.

Consequently, the stabilized discrete formulation for the cG(s)dG(r) discretization reads as follows: Find $u_{kh} \in \tilde{X}_{k,h}^{r,s}$, such that

$$\begin{aligned}\sum_{m=1}^{M} (\partial_t u_{kh}, \phi)_{I_m} + a(u_{kh})(\phi) + s_{\mathrm{SUPG}}(u_{kh}, \phi) + \sum_{m=0}^{M-1} ([u_{kh}]_m, \phi_m^+) \\ + (u_{kh,0}^-, \phi_0^-) = (u^0, \phi_0^-) \quad \forall \phi \in \tilde{X}_{k,h}^{r,s}.\end{aligned} \tag{3.7}$$

The corresponding formulation for the cG(s)cG(r) discretization seeks $u_{kh} \in X_{k,h}^{r,s}$, such that

$$(\partial_t u_{kh}, \phi)_I + a(u_{kh})(\phi) + s_{\mathrm{SUPG}}(u_{kh}, \phi) + (u_{kh}(0), \phi_0^-) = (u^0, \phi_0^-) \quad \forall \phi \in \tilde{X}_{k,h}^{r-1,s}. \tag{3.8}$$

The disadvantage of this stabilization method from implementational point of view is the appearance of second order derivatives in the stabilization terms which do not vanish for finite element methods of higher order. Furthermore, this scheme is not symmetric and, thus, two approaches "optimize-then-discretize" and "discretize-then-optimize" lead to different first order optimality conditions for optimization problems. It is difficult to choose a priori the approach leading to the more accurate solution. However, this stabilization scheme allows to treat hyperbolic problems discretized by continuous finite element methods, see Chapter 6 for a computational example.

3.3.2. Local projection stabilization

Another technique to stabilize the finite element discretizations of convection dominated problems is the local projection stabilization (LPS) originally proposed for the Stokes problem by Becker & Braack [13]. For the definition of the method, we introduce an interpolation operator $I_h : V_h^s \to \tilde{V}_h^s$ into a subspace $\tilde{V}_h^s \subseteq V_h^s$ which is given by

$$\tilde{V}_h^s = \begin{cases} V_{2h}^1 & \text{for } s = 1, \\ V_h^1 & \text{for } s = 2. \end{cases}$$

The nodal interpolation operator onto the mesh $\mathcal{T}_{2h}$ in the case $s = 1$ can be easily computed using the patch structure of the mesh. Additionally, we define a fluctuation operator

$$\pi : V_h^{s,m} \to V_h^{s,m}, \quad \pi := \mathrm{id} - I_h.$$

The defined operators can be extended in time by setting pointwise

$$(\pi u_{kh})(t) := \pi u_{kh}(t).$$

The additional stabilization terms are given by

$$s_{\mathrm{LPS}}(u_{kh}, \phi) := \sum_{m=1}^{M} \int_{I_m} s_h^m(u_{kh}(t), \phi(t))\, dt, \tag{3.9}$$

where

$$s_h^m(u_{kh}, \phi) := \sum_{K \in \mathcal{T}_h} (v \cdot \nabla(\pi u_{kh}), \delta_{K,m} v \cdot \nabla(\pi\phi))_K. \tag{3.10}$$

The cellwise defined parameter $\delta_{K,m}$ is given in the same way as in (3.6).

Consequently, the stabilized discrete formulation for the cG(s)dG(r) discretization reads as follows: Find $u_{kh} \in \tilde{X}_{k,h}^{r,s}$, such that

$$\begin{aligned} \sum_{m=1}^{M} (\partial_t u_{kh}, \phi)_{I_m} + a(u_{kh})(\phi) + s_{\mathrm{LPS}}(u_{kh}, \phi) + \sum_{m=0}^{M-1} ([u_{kh}]_m, \phi_m^+) \\ + (u_{kh,0}^-, \phi_0^-) = (u^0, \phi_0^-) \quad \forall \phi \in \tilde{X}_{k,h}^{r,s}. \end{aligned} \tag{3.11}$$

The corresponding stabilized discrete formulation for the cG(s)cG(r) discretization seeks $u_{kh} \in X_{k,h}^{r,s}$, such that

$$(\partial_t u_{kh}, \phi)_I + a(u_{kh})(\phi) + s_{\mathrm{LPS}}(u_{kh}, \phi) + (u_{kh}(0), \phi_0^-) = (u^0, \phi_0^-) \quad \forall \phi \in \tilde{X}_{k,h}^{r-1,s}. \tag{3.12}$$

The advantage of this method is that the nonphysical derivative with respect to time is avoided. Furthermore, the stabilization of optimization problems leads to symmetric first order optimality systems. Compared to the SUPG scheme this method is not consistent. However, the additionally introduced error is of the same order as the discretization error.

3.4. Solution aspects

Due to the discontinuity of the test functions the presented discretizations lead to the Padé schemes. Thus, the temporal discretization scheme dG(r) for $r = 0$ uses piecewise constant test and trial functions in time and consequently $\partial_t u_{kh}|_{I_m} = 0$.

We introduce the notation $U_m := u_{kh,m}^-$ for $m = 0, 1, \ldots, M$, and obtain the set of discrete equations for all $\phi \in V_h^{s,m}$

cG(s)dG(0) discretization:

$\mathbf{m = 0}$:

$$(U_0, \phi) = (u^0, \phi)$$

$\mathbf{m = 1, \ldots, M}$:

$$(U_m, \phi) + k_m \bar{a}(U_m)(\phi) = (U_{m-1}, \phi)$$

Here, we have evaluated the temporal integrals on the right-hand side by the box rule. Thus, we obtain the backward Euler method which is known to be a first order strongly A-stable Padé scheme. This time stepping scheme is dissipative and provides the damping of high-frequency error components. However, in Eriksson & Johnson [33] it was shown, that the approximation of the temporal integrals by the box rules has disadvantages compared to the exact evaluation of the integrals. Thus, especially for long time integrations, the use of higher order quadrature is advisable.

The use of piecewise linear trial functions in time, that is $r = 1$, leads to the Crank-Nicolson scheme if the temporal integrals are approximated by the trapezoidal rule. Here, we use the notation $U_m := u_{kh,m}$ and obtain for all $\phi \in V_h^{s,m}$

cG(s)cG(1) discretization:

$\mathbf{m = 0}$:

$$(U_0, \phi) = (u^0, \phi)$$

$\mathbf{m = 1, \ldots, M}$:

$$(U_m, \phi) + \frac{k_m}{2} \bar{a}(U_m)(\phi) = (U_{m-1}, \phi) - \frac{k_m}{2} \bar{a}(U_{m-1}, \phi)$$

The Crank-Nicolson scheme is known to be of the second order and has only little dissipation. However, it is not strongly A-stable so that it suffers from instabilities caused by rough perturbations in the data leading to the loss of regularity. This defect can be overcome by means of a sample damping procedure which preserves the order of discretization and does not increase the computational costs. For a detailed discussion of this issue, we refer to Rannacher [96].

Each time step of both discretization schemes requires the solution of quasi-stationary nonlinear system. They are solved by the means of the inexact Newton method. For the inner iteration we employ either the Krylov subspace methods such as the Generalized Minimal Method (GMRES) as described in Saad [102] or a multigrid iteration. For the latter choice, we use the strategy described in Becker & Braack [9] in order to obtain the optimal complexity. For more details, we refer to Chapter 6.

CHAPTER 4

Atmospheric Inverse Problem

In this chapter, we consider an inverse problem modeling the transport of chemical species in the Earth's atmosphere. Since the formulation of parameter identification problems depends on the ingredients of the problem, we first give a short overview about the existing techniques used for observation of atmospheric composition. Here, we concentrate mainly on the remote sensing methods. The obtained observations are often further used as input parameters by radiative transfer models, which are introduced in Section 4.2.

The main uncertain factors in modeling the atmospheric transport of chemical species are the sources in the free atmosphere and near the Earth's surface. This gives a rise to introduce parameters that scale the modeled source and sink terms, such that the solution of the problem matches the available observations as well as possible. This leads to the formulation of a calibration problem. In order to present a rather general analysis, we treat the initial concentrations as a further unknown parameter of the system.

It is important to know the stability properties of the resulting inverse problem in order to obtain reliable approximations of the solution. So in Section 4.3, we analyze the problem under consideration and show that even in the case of provided distributed observations the problem is ill-posed in the sense of Hadamard. To this end, we show that the inverse of the corresponding operator is discontinuous, and the solution of the problem does not continuously depend on the data. As a result, small errors in the provided observations can be arbitrarily largely amplified. Consequently, we need some kind of stabilization. For that reason, the next chapter is devoted to the regularization methods.

We close this chapter by showing the differentiability properties of the so-called parameter-to-solution mapping in Section 4.4 and give explicit representations of the derivatives. These are used in the analysis of regularization methods, on the one hand, and for the construction of the numerical methods, on the other.

4.1. Atmospheric retrieval techniques

In this section, we review the most important atmospheric retrieval techniques. Thereby, we concentrate mainly on remote sensing algorithms. These methods derive the atmospheric composition by analyzing the absorption properties of the radiative transfer and are distinguished depending on the platform, the radiation source, and sounding geometry. Thus, ground-based systems provide local measurements, whereas space-borne instruments can measure global distributions of atmospheric species. The obtained spectral distribution is

then used for further calculations, e.g., in radiative transfer models in order to deduce the concentrations of atmospheric constituents.

The measurements of the atmospheric composition are performed by analyzing the radiative absorption properties of chemical species. The radiation is characterized by its wavelength. In this regard the atmospheric species absorb the energy at different wavelengths. The methods for remote sensing differ in their dependence on the radiative source. Instruments based upon thermal emission operate in the long wavelength range. In this case, the atmospheric profile of chemical species is deduced from thermal images showing the temperature emission of molecules. Methods that utilize solar radiation operate in the short wavelength region. The concentrations are determined by the scattering and absorption properties of the species. Thus, ozone molecules absorb solar radiation strongly at short wavelengths in the range between 290 and 330 nm. This implies that if the measurement is performed by a space-borne spectrometer the photons cannot pass through the ozone layer. On the other hand, for longer wavelengths the protons can reach lower altitudes before the absorption process begins. This also allows to scan the atmosphere as a function of altitude, see also Zdunkowski, Trautmann & Bott [123].

Retrieval methods are further classified into active and passive. Active remote sensing techniques such as lidar (light detection and ranging) use laser pulses which are emitted and then collected by a detector. A network of ground-based lidar stations such as EARLINET (The European Aerosol Lidar Network) or SHADOZ (Southern Hemisphere Additional Ozonesondes Network) can provide dense spatially and temporally distributed chemical and meteorological atmospheric fields, see Rocadenbosch et al. [100] and Thomson et al. [115], respectively. Another source of local distributed measurements are coordinated field campaigns (see, e.g., Hall [51], Emmons et al. [29], Su et al. [112]). In this case, it is possible to perform the so-called in-situ measurements when the atmospheric composition is directly analyzed onboard of an aircraft or a balloon. These measurements are often used in order to validate the observations that are obtained from other sources or by numerical computations.

Passive remote sensing systems are positioned mainly onboard of satellites and use natural sources of radiation such as sun light and provide near real-time measurements. The instruments measure the radiation of the sunlight transmitted, reflected and scattered by the Earth's atmosphere or reflected by the surface. An example of such instrument is the GOME-2 (Global Ozone Monitoring Experiment 2) launched in 2006 onboard of the satellite ERS-2, which measures the atmospheric ozone, trace gases, and ultraviolet radiation. The form of the observations retrieved by such systems depends on the geometry of viewing. In this sense, we distinguish between nadir, limb, and occultation modes. In the nadir viewing the scanning is performed in down-looking direction. The resulting information is then given in form of integrated column densities. Limb sounding analyzes the radiative absorption for a range of tangential to the Earth paths with different vertical distributions. The retrieved information represents the vertical profile of atmospheric composition. The observational geometry in occultation mode is similar to limb but with sun or moon as light sources.

Thus, this monitoring is used during the sun and moon rise and set events. Some of the space-borne systems such as SCIAMACHY (Scanning Imaging Absorption Spectrometer for Atmospheric Chartography) and TES (Tropospheric Emission Spectrometer) can combine different monitoring geometries. This limb-nadir matching enables the reconstruction of three-dimensional concentration fields, see, e.g., Noël et al. [88] and Bowman et al. [20]. We note that atmospheric remote sensing is a challenging task since many trace gases such as CO and NO_2 show weak absorption properties.

4.2. Radiative transfer models

The spectral information obtained by remote sensing techniques is used in further computations in order to deduce the concentrations of atmospheric constituents. The most retrieval techniques rely upon the solution of radiative transfer models, see Doicu, Trautmann & Schreier [27]. This results in the formulation of inverse problems which must be solved for specific chemical species.

The radiative transfer models take into account such processes as photon absorption, scattering, and emission processes. The form of the equation can be derived analogously to the continuity equation for the mass in fluid mechanics. In the following, we consider a general form of the radiative transfer model employed in atmospheric applications for the reconstruction of concentrations of trace gases. For a detailed description of all involved processes in radiative transfer and modeling aspects, we refer to Zdunkowski, Trautmann & Bott [123].

We consider a medium $\Omega \subset \mathbb{R}^n$, $n = 2, 3$, which can represent a part of the atmosphere. We denote by $\mathcal{I}_\nu = \mathcal{I}(x, \nu)$ the radiation intensity, where x denotes the spatial variable and ν the frequency. The nonstationary form of radiative transfer equation for the radiation intensity is given by

$$\frac{1}{v_c}\partial_t \mathcal{I}_\nu + n \cdot \nabla \mathcal{I}_\nu + \sigma_{e,\nu}\mathcal{I}_\nu - \frac{\sigma_{s,\nu}}{4\pi}\int\limits_{S^2} P'(\tau, n)\mathcal{I}_\nu \, d\tau = f_\nu, \tag{4.1}$$

where n is the unit vector pointing in the direction of the solid angle $d\tau$ of the unit sphere S^2, v_c the propagation speed of photons, and P' the phase function. The function $\sigma_{s,\nu} = \sigma_{s,\nu}(x, \nu)$ is the scattering coefficient, and $\sigma_{e,\nu} = \sigma_{e,\nu}(x, \nu)$ denotes the extinction coefficient given as the sum of absorption and scattering coefficients

$$\sigma_{e,\nu} = \sigma_{a,\nu} + \sigma_{s,\nu}.$$

The scattering coefficient describes the absorption properties of the specific gas in the atmosphere. The source function f_ν describes the change of photons due to emission. In view of high values of propagation speed the term including the time derivative is usually neglected in atmospheric applications.

For a black body the source term is given in terms of the Planck function $B = B(\Theta, \nu)$ which depends on the local temperature and the frequency

$$f_\nu(x, \nu) = \sigma_a B(\Theta, \nu). \tag{4.2}$$

The absorption coefficient can be related to the species by

$$\sigma_{a,\nu} = \sum_i \kappa_i(x, \nu) c_i(x) + b(x, \nu),$$

where b is the volume absorption coefficient, κ_i and c_i the absorption cross sections and concentration profile for a gas, respectively.

The scattering can be neglected in the case of the clear sky environment. The radiative transfer equation in this case reads as follows:

$$n \cdot \nabla \mathcal{I}_\nu + \sigma_{a,\nu} \mathcal{I}_\nu = \sigma_a B_\nu. \tag{4.3}$$

However, in the presence of clouds the scattering becomes to play an important role. For the boundary conditions the incoming radiative transfer is prescribed. Thus, we impose

$$\mathcal{I}_\nu(x) = \mathcal{I}^{\text{in}}(x), \tag{4.4}$$

on the inflow part of the boundary $\Gamma_I = \{x \in \Gamma \ ; \ n \cdot n_\Gamma < 0\}$, where n_Γ denotes the outward pointing unit normal vector.

We introduce the space

$$Z := \Big\{ \mathcal{I}_\nu \in L^2(\Omega) \ ; \ n \cdot \nabla_x \mathcal{I} \in L^2(\Omega) \Big\}. \tag{4.5}$$

Then, the weak formulation of problem (4.3) reads: Find $\mathcal{I}_\nu \in Z$, such that

$$(n \cdot \nabla \mathcal{I}_\nu, \phi) + (\sigma_{a,\nu} \mathcal{I}_\nu, \phi) = (\sigma_a B_\nu, \phi) \quad \forall \phi \in L^2(\Omega). \tag{4.6}$$

The above problem can be solved using the Galerkin discretization as described in Chapter 3. Since the system is hyperbolic, it needs to be stabilized. To this end, the SUPG stabilization can be employed. For more details on the numerical treatment and modeling aspects of the forward problem, we refer to Kanschat et al. [70] and Meinköhn et al. [84].

To reconstruct the unknown concentration profile $c(x)$, corresponding inverse problem must be solved. However, for weakly absorbing trace gases the retrieval techniques based on the radiative transfer models yield only integrated quantities. In the case of nadir sounding mode, we obtain so-called vertical column densities, i.e., the concentrations are integrated over the height. In the limb operational mode, we obtain slant column densities, which means that concentrations are integrated over paths of light. For technical and theoretical details concerning the reconstruction of unknown concentration with the help of Laplace transformation, we refer to Bal & Ren [6].

In the following, we assume to be given either integrated or distributed form of measurements. In this case, we must take into account that the observations are contaminated by noise due to the instrumental accuracy and approximative solution of the radiative transfer equation. Furthermore, as shown the form of the radiative transfer model depends on the local cloud coverage. Neglecting scattering may result in errors in measurements which are stronger than the signal. To this end, it is customary first to analyze the supplied cloud maps. The analysis can be accomplished by the means of the image processing techniques such as image segmentation. The study of the supplied cloud coverage images results in a large amount of information needed to be processed, and, thus, makes the use of adaptive techniques unavoidable. We consider this issue in Chapter 6, Section 6.2, where the minimization of the so-called Mumford-Shah functional leading to the segmentation of clouds is considered. Numerical calculations of the inverse problem corresponding to the radiative transfer model (4.6) aiming at the identification of the unknown profile $c(x)$ are performed in Chapter 6, Section 6.4.

4.3. Analysis of the inverse problem

The main uncertain factors in modeling of transport of atmospheric constituents are the emissions in the free atmosphere and the surface sources. In this section, we consider the calibration of problem (2.26). Here, we restrict ourselves to the case where the parameters are only space dependent. In order to present a rather general analysis, we treat the initial concentration of system (2.26) as a further unknown parameter. The aim of this section is to show that the resulting inverse problems are ill-posed in the sense that the inverse of the corresponding solution operator is not continuous. Consequently, small data in the available observations may be amplified arbitrarily.

First, we postulate the calibration problem as an operator equation. To this end, we introduce the measurement operator

$$\begin{aligned} \mathcal{C} : X &\to Y, \\ u &\mapsto g, \end{aligned}$$

which maps the function $u \in X$ into the measurement space Y. Here, the space X is defined accordingly to (2.24), and the choice of the space of measurements Y depends on the given particular observations. Then, we consider the following inverse problem: Given observations $g^\delta \in Y$ find $(u, \mu, \beta, \chi) \in X \times Q$, such that

$$\begin{aligned} \partial_t u - \nabla \cdot (D\,\nabla u) + v \cdot \nabla u &= f(u) + \mu(x) E(u,t,x) && \text{in } \Omega_T, \\ u &= u^{\text{in}} && \text{on } \Sigma_I, \\ D\,\partial_n u &= 0 && \text{on } \Sigma_O, \\ D\,\partial_n u - w\,u &= \beta(x) E_s(u,t,x) && \text{on } \Sigma_G, \\ u(0) &= \chi(x) && \text{in } \Omega, \\ \mathcal{C}(u) &= g^\delta && \text{in } \Omega_T, \end{aligned} \tag{4.7}$$

for unknown concentrations of chemical species $u = (u_1, \dots, u_d)^T$, unknown calibration parameters $\mu = (\mu_1, \dots, \mu_{d'})^T$ and $\beta = (\beta_1, \dots, \beta_{d'})^T$, and initial conditions $\chi = (\chi_1, \dots, \chi_{d'})^T$ with $d' \leq d$. The upper index δ in the overspecification condition $\mathcal{C}(u) = g^\delta$ corresponds to the noise level, i.e., we have perturbed observations satisfying

$$\|g - g^\delta\|_Y \leq \delta. \tag{4.8}$$

In the following, we will show that even in the case of distributed measurements the above inverse problem is ill-posed. Thus, we assume that we are given measurements in Ω_T, for example, from a lidar network or as a solution of a radiative transfer model. In this case the observation operator is given as identity $\mathcal{C} = \mathrm{id}$. Since only function values and not derivative values can be measured, we set

$$Y := L^2(\Omega_T)^d. \tag{4.9}$$

Next, we define

$$Q := Q_1 \times Q_2 \times Q_3, \quad Q_1 := L^\infty(\Omega)^{d'}, \quad Q_2 := L^\infty(\Gamma_G)^{d'}, \quad Q_3 := Q_1. \tag{4.10}$$

The corresponding weak form of the inverse problem (4.7) reads as follows: Given observations $g^\delta \in Y$ find $u \in \hat{u} + X$ and $q := (\mu, \beta, \chi) \in Q$, such that

$$\begin{aligned} (\partial_t u, \phi)_I + (D\,\nabla u, \nabla\phi)_I + (v \cdot \nabla u, \phi) + (u(0), \phi(0)) &= (f(u), \phi)_I \\ +(\mu(x)E(t,x), \phi)_I + (w\,u + \beta(x)E_s(t,x), \phi)_{\Sigma_G} + (\chi(x), \phi(0)) \quad \forall \phi \in X, \quad &(4.11) \\ \mathcal{C}(u) = g^\delta. \end{aligned}$$

Here, $\hat{u} \in W_2^{1,0}(\Omega_T)^d$ represents again the inflow boundary condition, that is $\hat{u} = u^{\mathrm{in}}$ on the inflow boundary Σ_I.

For this weak formulation, we define the parameter-to-solution mapping

$$\begin{aligned} S : Q &\to X, \\ q &\mapsto u(q), \end{aligned} \tag{4.12}$$

which maps the parameter vector $q \in Q$ to the corresponding solution $u \in X$. Finally, we introduce the forward operator F as the composition

$$F : Q \to Y, \quad F = \mathcal{C} \circ S. \tag{4.13}$$

With these preparations problem (4.7) can be equivalently rewritten as the following nonlinear operator equation

$$F(q) = g^\delta. \tag{4.14}$$

The next lemma states the continuity properties of the parameter-to-solution mapping S.

LEMMA 4.3.1. *Let $p, q \in Q$. Then, there exists a constant $c > 0$, such that*

$$\|F(q) - F(p)\|_Y \leq c\|q - p\|_Q. \tag{4.15}$$

PROOF. We follow closely the proof given in Tröltzsch [118] and Neitzel & Vexler [85].

We denote by $u := F(q)$ and $\bar{u} := F(p)$. The difference $y := u - \bar{u}$ fulfills the equation

$$\begin{aligned}(\partial_t y, \varphi)_I + (D\,\nabla y, \nabla\phi)_I + (v \cdot \nabla y, \phi)_I + (y(0), \phi(0)) = (f(u) - f(\bar{u}), \phi)_I \\ + ((\mu - \bar{\mu})E, \phi)_I + ((\beta - \bar{\beta})E_s, \phi)_{\Gamma_G} + (\chi - \bar{\chi}, \phi(0)) \quad \forall \phi \in X.\end{aligned} \tag{4.16}$$

By the main theorem of calculus for vector-valued functions, we obtain

$$f_\xi(t,x) := f(u) - f(\bar{u}) = \int_0^1 \partial_u f(\bar{u} + \xi(u - \bar{u}))\, d\xi\, y, \tag{4.17}$$

which is componentwise bounded in $L^\infty(\Omega_T)$ due to Proposition 2.3.1. Thus, problem (4.16) is equivalent to the linear system of equations

$$\begin{aligned}(\partial_t y, \phi)_I + (D\nabla y, \nabla\phi)_I + (v\cdot\nabla y, \phi)_I + (f_\xi y, \phi)_I + (y(0), \phi(0)) = ((\mu - \bar{\mu})E, \phi)_I \\ + ((\beta - \bar{\beta})E_s, \phi)_{\Sigma_G} + (\chi - \bar{\chi}, \phi(0)) \quad \forall \phi \in X.\end{aligned} \tag{4.18}$$

The reaction term and the right-hand side of the system are bounded in $L^\infty(\Omega_T)$, and so the unique solvability follows from the result in Fitzgibbon et al. [39]. The assertion follows analogously as in Proposition 2.3.1. □

The next result shows two important properties of the operator F characterizing the stability of the atmospheric inverse problem.

PROPOSITION 4.3.1. *Operator $F(\cdot)$ defined in* (4.13) *is weakly sequentially closed and compact.*

PROOF. First, we show that the operator F is weakly sequentially closed. To this end, let $(q_n)_{n\in\mathbb{N}}$ be a sequence, such that

$$q_n \rightharpoonup q \quad \text{weakly in } Q. \tag{4.19}$$

Furthermore, we assume that the sequence $(u_n)_{n\in\mathbb{N}}$ given by $F(q_n) = u_n$ satisfies

$$u_n \rightharpoonup u \quad \text{weakly in } X. \tag{4.20}$$

Then, we must show that $Fq = u$.

We consider the sequence $y_n = f(u_n)$. From Proposition 2.3.1, we follow that u_n is bounded in $Y \cap L^\infty(\Omega_T)^d$. This implies the existence of a weakly convergent subsequence $(y_{n_k})_{k\in\mathbb{N}}$.

We denote this subsequence by $(y_n)_{n\in\mathbb{N}}$ again. Next, we reformulate problem (4.7) and consider the following linear parabolic system

$$\begin{aligned}(\partial_t u_n,\phi)_I + (D\,\nabla u_n,\nabla\phi)_I + (v\cdot\nabla u_n,\phi)_I + (u_n(0),\phi(0)) = (R_n,\varphi)_I \\ + (w\,u_n,\phi)_{\Sigma_G} + (\chi_n,\phi(0)) \quad \forall\phi\in X.\end{aligned} \tag{4.21}$$

Here, the right-hand side is given by

$$(R_n,\phi)_I := (y_n,\phi)_I + (\mu_n E,\phi)_I + (\beta_n E_s,\phi)_{\Sigma_G}.$$

Due to assumption (4.19) the term R_n converges weakly in $Y\times Q_1\times Q_2$

$$(R,\phi)_I = (y,\phi)_I + (\mu\,E,\phi)_I + (\beta\,E_s,\phi)_{\Sigma_G}.$$

Analogously, we obtain the convergence $u_n^0 \rightharpoonup \chi$ weakly in Q_3. Since the mapping $R_n\mapsto u_n$ is linear and continuous, we have the weak convergence of u_n to $\bar u\in X$ with the space X defined in (2.24). From the compact embedding $W(0,T)\hookrightarrow\hookrightarrow L^2(\Omega_T)$ (see the Aubin-Lions lemma 2.3.1), we may deduce the strong convergence

$$u_n\to\bar u \quad \text{in } Y. \tag{4.22}$$

From equality (4.17) and $\|u_n\|_{L^\infty(\Omega_T)}\le M$, we conclude

$$\|f(u_n)-f(\bar u)\|_I \le L(M)\|u_n-\bar u\|_I. \tag{4.23}$$

Using the above inequality, putting (u_n,q_n) into the variational formulation (4.11), and letting n to go to infinity proves the assertion.

Next, we prove the compactness of the operator F. Let $q\in Q$ and $(q_n)_{n\in\mathbb{N}}$ be a sequence in Q satisfying

$$q_n\rightharpoonup q \quad \text{weakly in } Q.$$

Then, we will to show that the image of Fq_n is pre-compact in Y.

Since q is bounded in Q, it is also bounded in $L^2(\Omega)^{d'}\times L^2(\Sigma_G)^{d'}\times L^2(\Omega)^{d'}$. The operator F is weakly sequentially closed, and so we can define the sequence $(Fq_n)_{n\in\mathbb{N}}$ given by $F(q_n)=u_n$. By the estimates in Proposition 2.3.1, we obtain

$$\|Fq_n\|_X \le C\|q_n\|_Q, \tag{4.24}$$

with a constant depending on E, E_s and the domain Ω. The assertion follows from the Aubin-Lions lemma 2.3.1. □

The result of the above proposition implies that the local inverses of F are discontinuous, see Engl et al. [32]. Consequently, problem (4.11) is ill-posed, and small errors in the observations can be arbitrarily amplified. An analogous situation occurs in the case of given

integral overdetermination condition, where the measurement operator and space are given by

$$\mathcal{C}(u(t,x)) = \int_{\Omega} u(t,x)\,dx \in Y, \quad Y := L^2([0,T])^d. \tag{4.25}$$

Since the operator $\mathcal{C}$ is linear and continuous, the corresponding forward operator F is compact. As a consequence, we need some kind of regularization. One possibility of the stabilization of the problem is the restriction of the definition domain of F to a compact set, see Rösch [101]. In this case the inverse F^{-1} is continuous as soon as it exists due to the Arzela-Ascoli theorem. However, this kind of the regularization can hardly be analyzed and yields no qualitative stability estimates. As a remedy, we consider in the next chapter construction and application of special regularization methods and show the stability of the regularized solutions.

4.4. Differentiability properties

In this section, we analyze the differentiability properties of the parameter-to-solution mapping S defined in (4.12). This is needed to state the stability estimates for the parameter variables, on the one hand, and convergence properties of the regularized solutions, on the other. Additionally, the exact form of the derivatives is used for the construction of numerical algorithms.

Before stating the differentiability properties of the parameter-to-solution mapping S, we recall the standard definitions of differentiability, which can be found, for example, in Jahn [64].

Definition 4.4.1 (Directional derivative). *Let X and Y be Banach spaces, $X_0 \subset X$ an open subset of X, and $f : X_0 \to Y$ a given mapping. If for two elements $x \in X_0$ and $\delta x \in X$ the limit*

$$f'(x)(\delta x) := \lim_{\epsilon \downarrow 0} \frac{f(x+\epsilon\delta x) - f(x)}{\epsilon}$$

exists, then $f'(x)(\delta x)$ is called the directional derivative of f at x in direction δx. If the limit exists for all $\delta x \in X$, then f is called directionally differentiable at x.

Definition 4.4.2 (Gâteaux derivative). *Let X and Y be Banach spaces, $X_0 \subset X$ an open subset of X. A directionally differentiable mapping $f : X_0 \to Y$ is called Gâteaux differentiable at $x \in X_0$ if the directional derivative $f'(x)$ is a continuous linear mapping from X to Y. $f'(x)$ is called Gâteaux derivative of f at x.*

Definition 4.4.3 (Fréchet derivative). *Let X and Y be Banach spaces, $X_0 \subset X$ an open subset of X, and $f : X_0 \to Y$ a given mapping. Furthermore, let be given an element $x \in X_0$. If there is a bounded linear mapping $f'(x) : X \to Y$ with the property*

$$\lim_{\|\delta x\|_X \to 0} \frac{\|f(x+\delta x) - f(x) - f'(x)(\delta x)\|_Y}{\|\delta x\|_X} = 0,$$

then $f'(x)$ is the Fréchet derivative of f at x, and f is called Fréchet differentiable at x.

REMARK 4.4.1. The given definition can be straightforward extended to higher order derivatives. We give here as example the second order Fréchet derivative. Let $f : X_0 \to Y$ be a Fréchet differentiable function at all $x \in X_0$. If the mapping $f' : X_0 \to L(X, Y)$ is Fréchet differentiable at $x \in X_0$, then f is called two times Fréchet differentiable at x. The second derivative is denoted by $(f')'(x) := f''(x)$.

In the next proposition, we state the differentiability properties of the parameter-to-solution mapping.

PROPOSITION 4.4.1. *The mapping S defined by* (4.12) *is two times continuously Fréchet differentiable.*

PROOF. The proof goes similarly as in Tröltzsch [118]. We consider the linear system

$$\begin{aligned}(\partial_t u, \phi)_I + (D\,\nabla u, \nabla\phi)_I + (v \cdot \nabla u, \phi)_I + (u(0), \phi(0)) = (\mu E, \phi)_I \\ + (w\,u + \beta E_s, \phi)_{\Gamma_G} + (\chi, \phi(0)),\end{aligned} \tag{4.26}$$

and define linear continuous operators as follows:

$$\begin{aligned}&\mathcal{G}_\Omega : Q_1 \to \hat{u} + X \cap L^\infty(\bar{\Omega}_T)^d, \quad u = \mathcal{G}_\Omega \mu \qquad \text{for } \beta = 0 \text{ and } \chi = 0,\\ &\mathcal{G}_\Gamma : Q_2 \to \hat{u} + X \cap L^\infty(\bar{\Omega}_T)^d, \quad u = \mathcal{G}_\Gamma \beta \qquad \text{for } \mu = 0 \text{ and } \chi = 0,\\ &\mathcal{G}_0 : Q_3 \to \hat{u} + X \cap L^\infty(\bar{\Omega}_T)^d, \quad u = \mathcal{G}_0 \chi \qquad \text{for } \mu = 0 \text{ and } \beta = 0,\end{aligned}$$

with $\hat{u} = u^{\text{in}}$ on Σ_I. By the help of these definitions, we can write the solution of the nonlinear system (4.11) in operator form

$$\mathcal{F}(u, q)(\phi) = (u, \phi)_I - (\mathcal{G}_\Omega(f(u) - \mu E), \phi)_I - (\mathcal{G}_\Gamma(w\,u + \beta E_s), \phi)_I - (\mathcal{G}_0 \chi, \phi(0)) = 0.$$

The operator $\mathcal{F}$ is of class C^2 since the corresponding Nemitskii operator $u \mapsto f(u)$ is due to Assumption 2.3.2 two times continuously Fréchet differentiable in $L^\infty(\Omega_T)$, see, e.g., Tröltzsch [118]. The linear system of equations

$$\mathcal{F}'_u(u, q)(w, \phi) = (p, \phi)_I, \tag{4.27}$$

admits for each $p \in L^\infty(\bar{\Omega}_T)$ a unique solution, see, e.g., Fitzgibbon et al. [39]. Thus, the application of the implicit function theorem proves the assertion. □

In the following corollar, we give the precise form of the first and second Fréchet derivatives of the parameter-to-state mapping S given in (4.12). In order to keep the resulting representations readable, we consider a single species.

COROLLAR 4.4.1. *The first derivative of the parameter-to-state mapping* $\delta u_i = S'(q_i)(\delta q_i)$ *for* $\delta q_i := (\delta\mu_i, \delta\beta_i, \delta\chi_i)$ *is given by*

$$\begin{aligned}(\partial_t \delta u_i, \phi)_I + (D\,\nabla\delta u_i, \nabla\phi)_I + (v\nabla\delta u_i, \phi)_I + (\delta u_i(0), \phi(0)) = (f'_{i,*}(u)\delta u_i, \phi)_I \\ + (w\,\delta u_i, \phi)_{\Sigma_G} + (\delta\mu_i E_i, \phi)_I + (\delta\beta_i E_{i,s}, \phi)_{\Sigma_G} + (\delta\chi_i, \phi(0)) \quad \forall \phi \in X.\end{aligned} \tag{4.28}$$

Here, $f'_{i,*}$ *denotes the rows of the Jacobian* $J_{ij} = (\partial_j f_i)_{i,j=1}^d$.

Let $\bar{u}_i := S'(q_i)(\bar{q}_i)$ *for* $\bar{q}_i := (\bar{\mu}_i, \bar{\beta}_i, \bar{\chi}_i)$ *and* $\delta u_i = S'(q_i)(\delta q_i)$ *for* $\delta q_i := (\delta\mu_i, \delta\beta_i, \delta\chi_i)$. *Then, the second derivative* $\delta^2 u_i := S''(q_i)(\bar{q}, \delta q)$ *is the solution of*

$$\begin{aligned}(\partial_t \delta^2 u_i, \varphi)_I + (D\,\nabla\delta^2 u_i, \nabla\phi)_I + (v\,\nabla\delta^2 u_i, \phi)_I + (\delta^2 u_i(0), \phi(0)) \\ = (f'_{i,*}(u)\delta^2 u_i, \phi)_I - (f''_{i,*}(u)(\delta u_i, \bar{u}_i), \phi)_I \quad \forall \phi \in X,\end{aligned} \tag{4.29}$$

where $f''_{i,*}$ *denotes the tensor* $H_{ikl} = (\partial_k \partial_l f'_{i,*})_{k,l=1}^d$.

PROOF. The first assertion can be proven by taking the total derivative of the weak formulation (4.11). The form of the second derivative is obtained similarly by differentiating equation (4.28). Details can be found in Becker [11]. □

CHAPTER 5

Regularization of Inverse Problems

In this chapter, we treat the regularization methods for ill-posed problems. Thus, we consider inverse problems formulated as operator equations where the direct inversion of the corresponding operator cannot be done in a stable way. To this end, we describe the approximation of the generalized inverse by a family of regularization operators. This variational approach is widely used in the field of chemical data assimilation methods (see, e.g., Carmichael et al. [24], Zhang & Sandu [124], and Hakami et al. [50]).

We begin in Section 5.1 with a general definition of regularization methods. We consider some concrete schemes such as ordinary and iterated Tikhonov regularization and Landweber iteration. The extension of the linear regularization methods to the nonlinear problems is not obvious. The corresponding regularization concept is described in Subsection 5.1.2.

The performance of any regularization method depends on the choice of the parameters. Here, we distinguish between a priori, a posteriori, and heuristic parameter choice rules. One of the most widely used a posteriori methods is the Morozov's discrepancy principle introduced in Section 5.2. Usually it is assumed that the operator corresponding to the inverse problem is given exactly. We consider a special case where the inverse problem under consideration is perturbed. So in order to access the stability estimates in this case, we consider a modified Morozov's discrepancy principle accounting for general perturbations. In Section 5.2.3, we discuss heuristic parameter choice rules. Although they do not lead in general to a convergent algorithm, they are approved in many applications to be robust and accurate regularization schemes for a fixed noise level.

In Section 5.3, we present numerical methods for the solution of the regularized problems. To this end, we consider the Lagrange-Newton and the direct Newton methods for optimization problems. Furthermore, we provide a discussion about the advantages of both solution algorithms. We close this chapter by presenting a numerical example describing the loss of ozone due to the chemical reactions with chlorine (Cl) and chlorine monoxide (ClO). Here, we compare ordinary and iterated Tikhonov regularization methods for different noise levels.

5.1. Regularization methods

In this section, we discuss regularization methods of ill-posed problems. We introduce a general form of a convergent regularization method leading to the construction of different algorithms. In this sense, we consider ordinary and iterated Tikhonov regularization schemes. Furthermore, we introduce the Landweber iteration in which the number of iterations serves

as regularization parameter. We begin with a general linear operator equation and after that consider the extensions to nonlinear problems.

5.1.1. Regularization of linear problems

As a prototype for a general linear inverse problem, we consider the following operator equation

$$Kq = g^\delta, \tag{5.1}$$

with a linear operator $K : \mathcal{D}(K) \subset Q \to Y$ between two Hilbert spaces Q and Y. Here, $g^\delta \in Y$ represents the noisy data with a noise level δ, such that there holds

$$\|g - g^\delta\|_Y \leq \delta. \tag{5.2}$$

In the following, we assume the attainability of the "exact solution", that is for the exact data $g \in Y$ there exists an element $q^\dagger \in \mathcal{D}(K)$ satisfying

$$K(q^\dagger) = g. \tag{5.3}$$

Very often the generalized inverse of K denoted by $K^\dagger$ has an unbounded range. In this case small errors in data can be arbitrarily largely amplified. The main idea of the regularization methods is to replace problem (5.1) by a sequence of well-posed problems. The generalized inverse $K^\dagger$ is then approximated by a family of regularized operators $R_\alpha : Y \to Q$.

A regularization method consists of two ingredients. First of the sequence of operators $(R_\alpha)_{\alpha \in \mathbb{R}}$ with the property

$$\limsup_{\delta \to 0} \{\|R_{\alpha(\delta, u^\delta)} g^\delta - K^\dagger g\|_Q \; ; \; g^\delta \in Y, \, \|g - g^\delta\|_Y \leq \delta\} = 0, \tag{5.4}$$

and secondly of the so-called parameter choice rule $\alpha = \alpha(\delta, g^\delta)$ satisfying

$$\limsup_{\delta \to 0} \{\alpha(\delta, g^\delta) \; ; \; g^\delta \in Y, \, \|g - g^\delta\|_Y \leq \delta\} = 0. \tag{5.5}$$

For the construction of convergent regularization methods, we assume that the regularization operator has the form

$$R_\alpha g^\delta := y_\alpha(K^*K)K^* g^\delta, \quad y_\alpha \in C\Big(0, \|K^*K\|\Big), \tag{5.6}$$

where K^* is the adjoint operator of K. Furthermore, we define a parameter-dependent family of functions

$$r_\alpha(\nu) := 1 - \nu y_\alpha(\nu). \tag{5.7}$$

Then, it is easy to see that there holds

$$q^\dagger - q = r_\alpha(K^*K)q^\dagger. \tag{5.8}$$

Concerning the convergence of a regularization method in the case of given exact data there holds the following result.

PROPOSITION 5.1.1. *Let for all $\alpha > 0$ for the functions y_α the following conditions be fulfilled:*

$$|\nu y_\alpha(\nu)| \le C, \tag{5.9}$$

with some constant C, and

$$\lim_{\alpha\to 0} y_\alpha(\nu) = \frac{1}{\nu}, \tag{5.10}$$

for all $\nu \in (0, \|K\|^2)$. Then, for all $g \in Y$ there holds

$$\lim_{\alpha\to 0} y_\alpha(K^*K)K^*g = q^\dagger, \tag{5.11}$$

where $q^\dagger$ is the least-squares solution of problem (5.1).

PROOF. The proof can be found, e.g., in Engl, Hanke & Neubauer [30]. □

Thus, the form of convergent regularization methods depends on the definition of the function y_α which must satisfy the assumptions of the above proposition. For the ordinary Tikhonov regularization, we set

$$y_\alpha(\nu) = \frac{1}{\nu + \alpha}, \tag{5.12}$$

and, consequently,

$$r_\alpha(\nu) = \frac{\alpha}{\nu + \alpha}. \tag{5.13}$$

The regularized solution $q = q_\alpha^\delta$ is then characterized by the following minimization problem

$$\min_{q\in\mathcal{D}(K)} j(q) := \|Kq - g^\delta\|_Y^2 + \alpha\|q\|_Q^2. \tag{5.14}$$

For the iterated Tikhonov regularization there holds

$$y_\alpha(\nu) = \frac{(\nu+\alpha)^n - \alpha^n}{\nu(\nu+\alpha)^n} \quad \text{and} \quad r_\alpha(\nu) = \left(\frac{\alpha}{\nu+\alpha}\right)^n. \tag{5.15}$$

This is equivalent to the minimization of the following sequence of functionals

$$\min_{q\in\mathcal{D}(K)} j(q) := \|Kq - g^\delta\|_Y^2 + \alpha\|q - q^{n-1}\|_Q^2 \quad \text{for } n = 1, 2, \ldots, \tag{5.16}$$

with some initial value $q^0 \in Q$. Here, the choice of the initial value is not crucial since the above functional is strictly convex, and so the optimization problem admits a unique solution. Consequently, a typical value $q^0 = 0$ can be chosen.

One of the simplest iterative regularization methods is the Landweber iteration which bases on the normal equation

$$K^*Kq = K^*g,$$

and is given by the fixed-point iteration

$$q^n = q^{n-1} - \omega K^*(Kq^n - g^\delta) \quad \text{for } n = 1, 2, \ldots, \tag{5.17}$$

with a damping parameter ω. The standard choice for the initial value is again $q_0 = 0$. Thus, we obtain

$$y_n(\nu) = \sum_{j=0}^{n-1} (1-\nu)^j \quad \text{and} \quad r_\alpha(\nu) = (1-\nu)^n. \tag{5.18}$$

In this case only the number of iterations n serves as regularization parameter.

5.1.2. Regularization of nonlinear problems

The extension of the linear regularization methods to nonlinear problems is not obvious. In this case no general adjoint operators can be defined, see, e.g., Marchuk [79]. We consider as a starting point the nonlinear operator equation of the form

$$F(q) = g^\delta, \tag{5.19}$$

where $F : \mathcal{D}(F) \subset Q \to Y$ is a continuous nonlinear operator between two Hilbert spaces Q and Y, and g^δ represents the perturbed observations, such that (5.2) holds. Here, as in the linear case, we assume the attainability of the solution, i.e., the existence of an element $q^\dagger \in \mathcal{D}(F)$, such that there holds

$$F(q^\dagger) = g. \tag{5.20}$$

We assume that the nonlinear operator F is given by the composition $F = \mathcal{C} \circ S$ with some measurement operator $\mathcal{C}$ and the parameter-to-solution mapping S corresponding to the problem

$$\mathcal{A}(q, u) = 0, \tag{5.21}$$

with a (nonlinear) operator $\mathcal{A}(\cdot, \cdot)$.

Motivated by the linear case the construction of ordinary Tikhonov regularization consists in replacing equation (5.19) by the optimization problem

$$\min_{q \in \mathcal{D}(F)} j(q) := \|F(q) - g^\delta\|_Y^2 + \alpha \|q - q^*\|_Q. \tag{5.22}$$

In contrast to the linear case the choice of the element q^* is crucial since in general nonlinear Tikhonov functionals possess only locally unique solutions. In this situation the concept of the solution is changed, and we look for the q^*-minimum norm solution, i.e.,

$$F(q^\dagger) = g, \tag{5.23}$$

and

$$\|q^\dagger - q^*\|_Q = \min\{\|q - q^*\|_Q \ ; \ F(q) = g\}. \tag{5.24}$$

Such q^* can incorporate the prior knowledge of the exact solution $q^\dagger$. For the existence of the solution of the optimization problem (5.22) there holds the following result.

PROPOSITION 5.1.2. *Let $F : Q \to Y$ be a continuous weakly sequentially closed operator. Then, for $\alpha > 0$ there exists a locally unique solution $q \in Q$ of the optimization problem* (5.22).

PROOF. Since $j(q) \geq 0$ there exists an infinum

$$j^* := \inf_{q \in Q} j(q). \tag{5.25}$$

Consequently, we can define a minimizing sequence $(q_i)_{i \in I\!N}$, that is

$$j(q_i) \to j^* \quad \text{as } i \to \infty.$$

Next, we consider the set

$$\mathcal{Q}_{ad} := \{q \in Q \, ; \, j(q) \leq c\},$$

which is nonempty since

$$j(q^*) = \|F(q^*) - g^\delta\|_Y^2 < \infty.$$

Furthermore, there holds

$$\alpha \|q - q^*\|_Q^2 \leq c \quad \forall q \in \mathcal{Q}_{ad}.$$

From here and $\alpha > 0$, we may deduce that there exists a constant $K > 0$, such that

$$\|q\|_Q \leq K.$$

Since Q is a Hilbert space, we can extract a weakly convergent sequence which is also denoted by $(q_i)_{i \in I\!N}$, such that

$$q_i \rightharpoonup q \text{ in } Q \quad \text{as } i \to \infty.$$

The sequence $(F(q_i))_{i \in I\!N}$ is bounded due to

$$\|F(q_i) - g^\delta\|_Y^2 \leq c.$$

Consequently, there exists a weakly convergent subsequence (also denoted by $(F(q_i))_{i \in I\!N}$), such that

$$F(q_i) \rightharpoonup y \text{ in } Y \text{ as } i \to \infty.$$

Since F is weakly sequentially closed, we deduce that $y = F(q)$ and, as a consequence,

$$j(q) = \lim_{i \to \infty} j(q_i) = j^*.$$

This implies the result. □

We want to apply this result to the atmospheric inverse problem (4.11) regularized by the ordinary Tikhonov method. The corresponding problem reads

$$\min_{q \in Q} \|F(q) - g^\delta\|_Y + \alpha \|q - q^*\|^2. \tag{5.26}$$

Here, the operator F is given by (4.13), and g^δ represent either distributed or integrated measurements that are perturbed. In the case of distributed measurements the space Y is chosen accordingly to (4.9). We set Y as in (4.25) for the integrated observations. There holds the following result.

COROLLAR 5.1.1. *Problem* (5.26) *admits a locally unique solution* $q = (\mu, \beta, \chi) \in Q$ *with corresponding optimal state* $u \in X$. *Here, the spaces* Q *and* X *are defined accordingly to* (4.10) *and* (2.24)*, respectively.*

PROOF. The assertion follows immediately from Lemma 4.3.1 and Proposition 4.3.1. □

We note that for the calibration parameters $\mu(x)$ and $\beta(x)$ the selection criteria can be chosen as $\mu^*(x) = 1$ and $\beta^*(x) = 1$, respectively. The prior knowledge for the unknown initial condition $\chi(x)$ is usually given in form of corresponding perturbed observations. It can be shown that the regularized solution $q = q_\alpha$ depends continuously on the data for a fixed value α, and the minimizer of (5.22) converges towards a q^*-minimum-norm solution of (5.19). The corresponding results can be found in Engl, Hanke & Neubauer [30].

The solution of the nonlinear problem (5.19) or (5.26) can be approximated analogously to the linear case by iterative regularization algorithms. So the operator equation (5.19) can be solved by Newton method which requires in each step the solution of the following linear problem

$$F'(q^n)(q^{n+1} - q^n) = g^\delta - F(q^n). \tag{5.27}$$

However, the problem of inversion of the derivative $F'(\cdot)$ is in general ill-posed so that the above equation must be further stabilized by regularization methods for linear problems. This leads to the Levenberg Marquardt and iteratively regularized Gauss-Newton methods. Alternatively, problem (5.19) can be solved by the nonlinear Landweber iteration given by

$$q_k = q_{k-1} + \omega F'(q_{k-1})^*(g^\delta - F(q_{k-1})), \tag{5.28}$$

with a damping parameter ω. A detailed analysis of these iterative forms of the regularization can be found in Kaltenbacher, Neubauer & Scherzer [68].

The iterated Tikhonov regularization method applied to the nonlinear equation (5.19) or (5.26) is given by the following sequence of optimization problems

$$\min_{q \in \mathcal{D}(F)} j_n(q) := \|F(q) - g^\delta\|_Y^2 + \alpha \|q - q_{n-1}\|^2, \quad n = 1, 2, \ldots \tag{5.29}$$

In this case the initial value $q_0 = q^*$ serves analogously to the ordinary Tikhonov functional as a prior guess for the unknown parameters. The existence and stability properties in this case can be stated analogously to the ordinary Tikhonov regularization method.

5.2. Parameter choice rules

The characterization of a convergent regularization method in Proposition 5.1.1 is given in the case of provided exact data g. For the perturbed observations there holds the following error estimate

$$\begin{aligned} \|q_\alpha^\delta - q^\dagger\| &\le \|R_\alpha g^\delta - R_\alpha g\| + \|R_\alpha g - q^\dagger\| \\ &\le \delta\|R_\alpha\| + \|R_\alpha F(q^\dagger) - q\|. \end{aligned} \tag{5.30}$$

The second term on the right-hand side converges to zero for $\alpha \to 0$. However, if the range of the corresponding operator is not closed, then, due to the Banach-Steinhaus theorem there holds $\|R_\alpha\| \to \infty$ as α tends to zero. Thus, in order to construct a convergent regularization method in the case of perturbed measurements, the right-hand side of (5.30) must be minimized. This leads to the construction of appropriate parameter choice rules for α. The parameter choice rules with $\alpha = \alpha(\delta)$, depending only on the noise level δ, are called a priori parameter choice rules. If α also depends on actual data g^δ, then, $\alpha = \alpha(\delta, g^\delta)$ is called a posteriori parameter choice rule. Noise-free rules, i.e., if α depends only on δ, cannot lead to a convergent regularization method as it was shown in Bakushinksii [5].

5.2.1. A priori parameter choice rules

The convergence of any regularization method can be arbitrarily slow if the range of the operator is not closed, cf. Schock [106]. In order to guarantee optimal convergence rates of the regularized solutions to the exact solution, certain assumptions need to be made. For linear problems most often it is assumed that the following general source condition must be fulfilled:

$$q^\dagger = B^\zeta w, \quad w \in Q, \ \|w\|_Y \le \rho, \tag{5.31}$$

with a bounded linear operator B. The most common choice is to use $B = (K^*K)^\zeta$ with parameter $\zeta \in (0, \frac{1}{2})$. We assume that there exist constants c and ζ_0 such that the following condition holds:

$$\nu^\zeta |r_\alpha(\nu)| \le c\alpha^\zeta, \quad 0 \le \zeta \le \zeta_0, \tag{5.32}$$

with the function $r_\alpha(\cdot)$ defined in (5.7). The constant ζ_0 is called a qualification of the regularization method. With assumptions (5.31) and (5.32), we obtain the following error estimates:

$$\|q - q^\dagger\|_Q \le c\alpha^\zeta \quad \text{and} \quad \|Kq - Kq^\dagger\|_Y \le c\alpha^{\zeta+\frac{1}{2}}\rho. \tag{5.33}$$

The choice of the regularization parameter $\alpha^{\zeta+\frac{1}{2}} = c\,\delta$ leads to the optimal convergence rate

$$\|q^\delta - q^\dagger\|_Q \le c\delta^{\frac{2\zeta}{2\zeta+1}}, \tag{5.34}$$

see, e.g., Engl, Hanke & Neubauer [30] or Tautenhahn & Jin [113]. The qualification of the ordinary and iterated Tikhonov regularization methods are $\zeta_0 = 1$ and $\zeta_0 = n$, respectively. This provides the best possible convergence rates $O(\delta^{\frac{2}{3}})$ and $O(\delta^{\frac{2n}{2n+1}})$, respectively, cf. Engl,

Hanke & Neubauer [30]. The obtained convergence rates cannot be further improved and correspond to the so-called saturation levels of the regularization methods.

In order to show the convergence rates for the regularization methods applied to the nonlinear problem (5.19), additional assumptions must be made depending on the particular method. We consider the ordinary Tikhonov regularization applied to problem (5.19). The next result yields the best possible convergence rate of $O(\delta^{\frac{2}{3}})$ for a specific parameter choice for α.

PROPOSITION 5.2.1. *Let $\mathcal{D}(F)$ be convex and F Fréchet-differentiable with*

$$\|F'(q^\dagger) - F'(q)\|_Y \leq \gamma \|q^\dagger - q\|_Q, \tag{5.35}$$

in a neighborhood of $q^\dagger \in Q$. Furthermore, let the following source condition be satisfied: There exists an element $\omega \in Y$, such that

$$q^\dagger - q^* = (F'(q^\dagger)^* F(q^\dagger))^\zeta \omega \quad \text{with } \gamma\|\omega\|_Y < 1 \text{ and } \zeta \in [1/2, 1]. \tag{5.36}$$

Then, for the choice $\alpha = O(\delta^{\frac{2}{2\zeta+1}})$, we obtain

$$\|q - q^\dagger\|_Q \leq C(\omega, \zeta)\delta^{\frac{2}{2\zeta+1}}. \tag{5.37}$$

PROOF. For the proof, we refer, e.g., to Kirsch [71] or Engl, Kunisch & Neubauer [31]. □

The convergence rates for the iterated Tikhonov regularization and for the Newton-types methods with corresponding source conditions can be found in Scherzer [104] and Kaltenbacher et al. [69], respectively. For the convergence analysis of the nonlinear Landweber iteration, we refer to Hanke et al. [52].

5.2.2. A posteriori parameter choice rules

The result of Proposition 5.2.1 yields the convergence rate $O(\delta^{\frac{2}{3}})$ with a constant C depending on the smoothness condition (5.36). However, the value of $\|\omega\|_Y$ and of ζ in (5.36) are in general not available. As a consequence, it is impossible to obtain the optimal constant C_{opt} for the a priori parameter choice rule. Due to this reason in practical applications the regularization parameter α is usually determined by a posteriori rules. This allows to obtain optimal convergence rates using only the noise level δ and the calculated approximation.

One of the most widely used a posteriori methods is the Morozov's discrepancy principle. It suggests the choice of the regularization parameter α in such a way that the error due to the regularization is equal to the error due to the observation data. Thus, α is given as the solution of the following nonlinear equation:

$$\|F(q) - g^\delta\|_Y = \delta. \tag{5.38}$$

This choice of the regularization parameter guarantees that, on the one hand, the discrepancy is equal to the noise level δ and, on the other hand, α is not too small. Thus, this stopping criterion requires the solution of the inverse problem for several different values of α. The discrepancy principle used with the ordinary Tikhonov regularization and Landweber method yields convergence rates for linear and nonlinear problems up to $O(\delta^{\frac{1}{2}})$, see, e.g., Groetsch [47] or Tautenhahn & Jin [113] and Hanke et al. [52], respectively. However, the regularization parameter satisfying the discrepancy principle (5.38) may not exist for a general nonlinear operator. For linear operators the simple condition

$$\|K(q) - g^\delta\|_Y \leq \delta \leq \|g^\delta\|_Y,$$

ensures the solvability of equation (5.38), see Kirsch [71]. In the nonlinear case severe additional assumptions must be made, see Kravaris & Seinfeld [73]. The assumptions can be weakened using the modified discrepancy principle

$$\tau_1 \delta \leq \|F(q) - g^\delta\|_Y \leq \tau_2\, \delta \quad \text{for some } 1 < \tau_1 \leq \tau_2. \tag{5.39}$$

For more details, we refer to Ramlau [95].

Usually the stability estimates for the a posteriori parameter choice rules are derived under the assumption that the exact solution of the operator equation is available. However, perturbations can occur due to errors in the model or by the need of the discretization. The case of the perturbed Tikhonov functional has been considered in Neubauer & Scherzer [86]. We extend the presented stability estimates by using the Morozov's discrepancy principle as stopping rule. To this end, we consider problem (5.19) with a perturbed operator F_η. We introduce the Tikhonov functional

$$j_\eta(q_\eta) := \|F_\eta(q_\eta) - g^\delta\|_Y^2 + \alpha\|q_\eta - q^*\|_Q^2, \tag{5.40}$$

where q_η denotes the perturbed regularized solution. The exact Tikhonov functional $j(\cdot)$ with corresponding regularized solution q are given by equation (5.22). As before, the q^*-minimum-norm solution is denoted by $q^\dagger$. We assume that the perturbation of problem (5.22) is given by η, such that there holds

$$j_\eta(q_\eta) - j(q) \leq \eta. \tag{5.41}$$

The error term is kept of a rather general form. The regularization parameter α is then determined as the solution of the scalar nonlinear equation

$$\|F(q_\eta) - g^\delta\|_Y = \delta + \sqrt{\eta}. \tag{5.42}$$

For this perturbed discrepancy principle, we obtain the following result concerning the convergence rate.

PROPOSITION 5.2.2. *Let $\mathcal{D}(F)$ be convex, and let F be Fréchet differentiable with*

$$\|F'(q^\dagger) - F'(q)\|_Y \leq \gamma \|q^\dagger - q\|_Q, \tag{5.43}$$

for all $q \in \mathcal{D}(F)$. Moreover, let the following source condition be satisfied: There exists an element $\omega \in Y$, such that

$$q^\dagger - q^* = F'(q^\dagger)^* \omega \quad \text{with } \gamma \|\omega\|_Y < 1. \tag{5.44}$$

For the noise level and the perturbation of the operator F let (5.2) *and* (5.41) *hold. If the regularization parameter α is chosen in such a way that the discrete discrepancy equation* (5.42) *is fulfilled, we obtain the following error estimate*

$$\|q_\eta - q^\dagger\|_Q \leq c(\delta + \eta^{1/2})^{1/2}.$$

PROOF. The proof goes along the lines for general a priori parameter choice rules for α provided in Engl, Hanke & Neubauer [30] (see also Engl, Kunisch & Neubauer [31] and Tautenhahn & Jin [113]).

Due to the minimizing property of q there holds

$$\begin{aligned} j_\eta(q_\eta) &\leq \|F(q) - g^\delta\|_Y^2 + \alpha \|q - q^*\|_Q^2 + \eta \\ &\leq \|F(q^\dagger) - g^\delta\|_Y^2 + \alpha \|q^\dagger - q^*\|_Q^2 + \eta \\ &\leq \delta^2 + \eta + \|q^\dagger - q^*\|_Q^2. \end{aligned} \tag{5.45}$$

As in Engl, Hanke & Neubauer [30], we obtain

$$\begin{aligned} j(q_\eta) &\leq \delta^2 + \eta + \alpha\Big(\|q^\dagger - q^*\|_Q^2 + \|q_\eta - q^\dagger\|_Q^2 - \|q_\eta - q^*\|_Q^2\Big) \\ &= \delta^2 + \eta + 2\alpha \langle q^\dagger - q^*, q^\dagger - q_\eta \rangle_Q. \end{aligned} \tag{5.46}$$

Condition 5.43 implies that

$$F(q_\eta) = F(q^\dagger) + F'(q^\dagger)(q_\eta - q^\dagger) + r_\alpha,$$

with

$$\|r_\alpha\|_Q \leq \frac{\gamma}{2} \|q_\eta - q^\dagger\|_Q^2.$$

We obtain from the source condition (5.44)

$$\|F(q_\eta) - g^\delta\|_Y^2 + \alpha \|q_\eta - q^\dagger\|_Q^2 \leq \delta^2 + \eta + 2\alpha \langle \omega, F'(q^\dagger)(q^\dagger - q_\eta) \rangle_Y.$$

Combining the above estimates leads to

$$\|F(q_\eta) - g^\delta\|_Y^2 + \alpha \|q_\eta - q^\dagger\|_Q \leq \delta^2 + \eta + 2\alpha\delta\|\omega\|_Y + 2\alpha\|\omega\|_Y \|F(q_\eta) - g^\delta\|_Y + \alpha\gamma\|\omega\| \|q_\eta - q^\dagger\|_Q^2,$$

and, thus, to

$$\|F(q_\eta) - g^\delta\|_Y^2 + \alpha(1 - \gamma\|\omega\|_Y)\|q_\eta - q^\dagger\|_Q^2 \leq \delta^2 + \eta + 2\alpha\delta\|\omega\|_Y + 2\alpha\|\omega\|_Y\|F(q_\eta) - g^\delta\|_Y.$$

Taking into account the discrete discrepancy equation (5.42) gives

$$\begin{aligned}\alpha(1 - \gamma\|\omega\|_Y)\|q_\eta - q^\dagger\|_Q^2 &\leq \delta^2 + \eta + 2\alpha\delta\|\omega\|_Y + 2\alpha\|\omega\|_Y(\delta + \sqrt{\eta}) - (\delta + \sqrt{\eta})^2 \\ &\leq 2\alpha\|\omega\|_Y(2\delta + \sqrt{\eta}).\end{aligned} \tag{5.47}$$

This together with the smallness assumption in the source condition (5.44) implies the assertion. □

We note that the source conditions are rather difficult to verify for nonlinear inverse problems, especially for parameter identification for partial differential equations. If using the Morozov's discrepancy principle for the atmospheric inverse problem (4.11), then under the assumption that (5.44) is satisfied, we may conclude from the above result that large errors in the parameters can be expected in the case of perturbations in wind field in regions with large gradients of the concentration. The other source of the error may come from the discretization if meteorological fields are given with a rather coarse resolution. In this case the discretization error can dominate over the noise level.

5.2.3. Heuristic parameter choice rules

All convergent regularization methods in the case of the perturbed measurements rely upon a known observation level. In applications with unknown noise level data-driven methods must be used. We just mention for completeness some of the most popular heuristic parameter choice rules.

An interesting approach is described by Kunisch & Zou [74] and refined in Xie & Zou [121], where the model functions are used in order to estimate the noise level $\|g - g^\delta\|_Y$. Another popular heuristic method is the L-curve criterion proposed by Hansen [54], which bases on the Tikhonov regularization. In this method the norm of the regularized solution is plotted versus the norm of the data term for a number of parameters α in a logarithmic scale. The corresponding graph has under certain conditions the L-shape. The value of the regularization parameter α is then determined by choosing the point of maximum curvature. This choice is a good compromise between the data fitting and the penalization the norm of the reconstruction. This method is widely used due to its simple structure and applicability to statistical ill-posed problems, i.e., when δ represents Gaussian white noise where the Morozov's discrepancy principle fails. Other widely used methods are the quasi-optimality criterion developed by Tikhonov & Arsenin [116] and Hanke-Raus rule, see Hanke & Raus [53]. The first one chooses a sequence of geometrically decaying regularization parameters and minimizes the distance between two consecutive regularized solutions, see

Tikhonov & Arsenin [116]. The second one chooses the regularization parameter α by minimizing

$$\frac{1}{\sqrt{\alpha}}\|F(q) - g^{\delta}\|_Y.$$

Although as shown in Bakushinskii [5] such heuristic methods in the worst case do not converge, they can lead to good reconstructions in many practical applications.

5.3. Algorithmic aspects

In this section, we describe the solution algorithms in order to treat the discussed inverse problems regularized by the ordinary or iterated Tikhonov-type methods. For simplicity, we rewrite problem (5.22) in form of a general optimal control problem

$$\min_{\{u,q\}\in V\times Q} J(u,q) = J_1(u) + J_2(q), \tag{5.48}$$

subject to the constraint

$$A(u,q)(\phi) = 0 \quad \forall \phi \in V, \tag{5.49}$$

with cost functional $J(\cdot,\cdot)$. The semilinear form $A(\cdot,\cdot)(\cdot) = A(t;\cdot,\cdot)$ denotes a possibly time-dependent nonlinear equation in variational form corresponding to (5.21). We prefer this notation in order to treat elliptic and parabolic problems simultaneously. The state space V and the control space Q are assumed to be Hilbert spaces.

There are mainly two classes of algorithms for the solution of optimal control problems of the type (5.48, 5.49) corresponding to the indirect and direct approaches. In the first case the optimization problem is converted into a boundary value problem which can be solved, for example, by Lagrange-Newton method. The second approach treats problem (5.48, 5.49) directly. This can be accomplished by the Newton method for optimization problems applied to the equivalent reduced formulation of the optimal control problem

$$\min_{q\in Q} j(q) = J(S(q),q), \tag{5.50}$$

with the reduced cost functional $j(\cdot) : Q \to I\!R$. Here, we denote by $S : Q \to V$ the solution operator of the state equation

$$A(S(q),q)(\phi) = 0 \quad \forall \phi \in V. \tag{5.51}$$

5.3.1. Newton-type methods

In order to introduce the Lagrange-Newton method, we employ the Lagrange principle and define the Lagrangian $\mathcal{L} : V \times Q \times V \to I\!R$ by

$$\mathcal{L}(u,q,\lambda) := J(u,q) - A(u,q)(\lambda), \tag{5.52}$$

where $\lambda \in V$ denotes the associated adjoint state. We assume that there is a locally unique minimum $\{u, q\} \in V \times Q$ of problem (5.48,5.49) which is characterized as corresponding to a stationary point $\{u, q, \lambda\} \in V \times Q \times V$ of the Lagrangian. Thus, the triplet $\{u, q, \lambda\} \in V \times Q \times V$ is determined by the first-order optimality condition (so-called KKT system)

$$\mathcal{L}'_u(u, q, \lambda)(\cdot) = 0 \quad \Leftrightarrow \quad J'_1(u)(\psi) - A'_u(u, q)(\psi, \lambda) = 0 \quad \forall \psi \in V, \tag{5.53}$$

$$\mathcal{L}'_q(u, q, \lambda)(\cdot) = 0 \quad \Leftrightarrow \quad J'_2(q)(\varphi) - A'_q(u, q)(\varphi, \lambda) = 0 \quad \forall \varphi \in Q, \tag{5.54}$$

$$\mathcal{L}'_z(u, q, \lambda)(\cdot) = 0 \quad \Leftrightarrow \quad -A(u, q)(\phi) = 0 \quad \forall \phi \in V, \tag{5.55}$$

where we call (5.53) the adjoint, (5.54) the control, and (5.55) the state equation. In order to define the Lagrange-Newton method, we need the Hessian operator of the Lagrangian $\mathcal{L}(\cdot, \cdot, \cdot)$. For $x = \{u, q, \lambda\}$, we define

$$H(x) = \begin{pmatrix} \mathcal{L}''_{uu}(x)(\cdot,\cdot) & \mathcal{L}''_{uq}(x)(\cdot,\cdot) & \mathcal{L}''_{u\lambda}(x)(\cdot,\cdot) \\ \mathcal{L}''_{qu}(x)(\cdot,\cdot) & \mathcal{L}''_{qq}(x)(\cdot,\cdot) & \mathcal{L}''_{q\lambda}(x)(\cdot,\cdot) \\ \mathcal{L}''_{\lambda u}(x)(\cdot,\cdot) & \mathcal{L}''_{\lambda q}(x)(\cdot,\cdot) & 0 \end{pmatrix}. \tag{5.56}$$

Then, the Newton increment $\delta x^n = \{\delta u^n, \delta q^n, \delta \lambda^n\}$ is given by the linear system

$$H(x^n) \begin{pmatrix} \delta u^n \\ \delta q^n \\ \delta \lambda^n \end{pmatrix} = - \begin{pmatrix} \mathcal{L}'_u(x^n) \\ \mathcal{L}'_q(x^n) \\ \mathcal{L}'_\lambda(x^n) \end{pmatrix}, \tag{5.57}$$

and the Newton update without damping reads

$$\{u^{n+1}, q^{n+1}, \lambda^{n+1}\} = \{u^n, q^n, \lambda^n\} + \{\delta u^n, \delta q^n, \delta \lambda^n\}. \tag{5.58}$$

The direct solution approach solves the optimization problem (5.50) directly. We consider the linearization of this problem. The starting point is again the first order optimality condition, which in this case reads

$$j'(q)(\varphi) = 0 \quad \forall \varphi \in Q. \tag{5.59}$$

The direct Newton method applied to this problem requires the solution of the linear system

$$j''(q)(\delta q, \varphi) = -j'(q)(\varphi) \quad \forall \varphi \in Q. \tag{5.60}$$

In order to calculate the second derivatives of the reduced functional $j(\cdot)$, we define the so-called additional adjoint equation: Find $\delta z \in X$, such that

$$A'_u(u, q)(\psi, \delta z) = -A_{uu}(u, q)(\delta u, \psi, \lambda) - A''_{qu}(u, q)(\delta q, \psi, \lambda) + J''_1(u)(\delta u, \psi) \quad \forall \psi \in V, \tag{5.61}$$

for a direction $\delta q \in Q$, where $\delta u = S'(q)(\delta q)$.

Using the above definitions the form of the derivatives of the reduced functional is given in the following proposition.

PROPOSITION 5.3.1. *By the help of the adjoint state $\lambda \in V$ defined by* (5.53) *the first derivative of the reduced cost functional in direction $\delta q \in Q$ is given by*

$$j'(q)(\delta q) = \alpha(q - q^*, \delta q)_Q - A'_q(u, q)(\delta q, \lambda). \tag{5.62}$$

Further, let $\delta u = S'(q)(\delta q)$ be the solution of the tangent equation

$$A'_u(u, q)(\delta u, \phi) + A'_q(u, q)(\delta q, \phi) = 0 \quad \forall \phi \in V, \tag{5.63}$$

and $\delta z \in V$ the solution of the additional adjoint equation (5.61)*. Then, the second derivative is given by*

$$\begin{aligned} j''(q)(\delta q, \varphi) = \alpha(\delta q,\varphi)_Q - A_{qq}(u, q)(\delta q, \varphi, \lambda) \\ - A''_{uq}(u, q)(\delta u, \varphi, \lambda) - A'_q(u, q)(\varphi, \delta z). \end{aligned} \tag{5.64}$$

PROOF. The proof is given by direct calculations. □

We now summarize the direct Newton algorithm for optimization problems:

Newton algorithm for optimization problems

(1) Choose an initial q_0 and set $k = 0$.
(2) Compute u^k, i.e., solve the state equation (5.55).
(3) Compute λ^k, i.e., solve the adjoint equation (5.53).
(4) Compute δu^k, i.e., solve the tangent equation (5.63).
(5) Compute the derivative $j'(q^k)(\varphi)$ according to (5.62).
(6) Compute the derivative $j''(q^k)(\delta q, \varphi)$ according to (5.64).
(7) Compute update δq, i.e., solve the linear system (5.60).
(8) Set $q^{k+1} = q^k + \omega \delta q$.
(9) Stop if stopping criterion is satisfied. Else set $k = k + 1$ and go to (2).

Both presented solution algorithms correspond to the inexact Newton methods since the linear systems in (5.57) and (5.60), respectively, are usually solved by some iterative solver only approximately. For the direct approach in the case of distributed unknown parameters Krylov-space methods using only matrix-vector products are used. By this way the expensive procedure of the assembling the Hessian is avoided. The most common choice for stopping criteria for these Newton-type methods uses the first-order optimality condition. Thus, for the indirect approach the residual of system (5.53, 5.54, 5.55) is to be reduced by a sufficiently

small factor, which depends on the particular application. For the direct Newton method for optimization problems usually

$$\|j'(q^k)\|_Q < \mathrm{TOL}, \tag{5.65}$$

is claimed.

There are various pros and cons of the indirect approach. It leads to a system with a saddle-point character. This makes the solution process for the linear solver more involved. Especially in nonstationary situations arising large algebraic systems require the use of special space-time solvers. Furthermore, the iterates are infeasible with respect to the state equation. Although the presented direct approach requires the solution of additional auxiliary problems, it leads to a more stable solution algorithm. However, the structure of the Lagrange-Newton method allows for the separation of the errors in inner and outer iterations with respect to a quantity of interest, as it is presented in Chapter 6. Moreover, this solution approach allows the use of multigrid method leading to an algorithm with the optimal complexity. For more details concerning this issue, we refer to Hinze et al. [57]. For a further discussion about the relations between the both approaches, we refer to Becker [11] and Meidner [81].

5.3.2. Morozov's discrepancy principle

Next, we consider the implementation of the unperturbed Morozov's discrepancy principle for Tikhonov-type regularization methods. For the iterated Tikhonov regularization this reads as follows:

$$k_*(\delta, g^\delta) := \inf\{k \in I\!N; \ \big| \ \|F(q^k) - g^\delta\| < \delta\}, \tag{5.66}$$

i.e., the iteration is stopped if the error reaches the noise level. This stopping criterion requires only one computation of the residual in each iteration. The parameter α in (5.29) can be chosen to be constant, so the simplest choice is to set $\alpha = 1$. Another possibility is to use a geometric sequence of the regularization parameters $\alpha_n = \alpha p^{n-1}$ for an initial starting value α and $0 < p < 1$. The latter case corresponds to the so-called nonstationary iterative Tikhonov method and can lead to a smaller k^*.

The calculation of the optimal parameter α for the ordinary Tikhonov regularization via Morozov's discrepancy principle requires an additional optimization process. Thus, in order to solve the discrepancy equation (5.42), we introduce the scalar function

$$i(\alpha) := \|F(q) - g^\delta\|^2 - \delta^2. \tag{5.67}$$

So $i(\alpha) = 0$ is equivalent to equation (5.42). This can be solved, for example, by the standard Newton method. To this end, we consider the evaluation of the derivatives of the function $i(\alpha)$. We denote by $x = (u, q, \lambda)$ and introduce an auxiliary Lagrange functional $\mathcal{M} = I\!R \times V \times Q \times V \to I\!R$

$$\mathcal{M}_\alpha(x, x_1) = \|F(q) - g^\delta\|_Y^2 + \mathcal{L}'_x(x)(x_1).$$

Here, we use the notation $x_1 = (u_1, q_1, \lambda_1)$. The form of the derivative $i'(\alpha)$ is given in the following proposition.

PROPOSITION 5.3.2. *Let $y = (u, q, \lambda, u_1, q_1, \lambda_1)$ be a stationary point of $\mathcal{M}$. Then, there holds*

$$i'(\alpha) = -2\alpha^2 (q - q^*, q_1)_Q. \tag{5.68}$$

PROOF. The proof can be found in Griesbaum, Kaltenbacher & Vexler [45]. □

For the calculation of the stationary point y the following problem must be solved

$$\mathcal{L}_{xx}(x)(\delta x, x_1) = -i'(u)(\delta u) \quad \forall \delta x = (\delta u, \delta q, \delta z) \in V \times Q \times V. \tag{5.69}$$

This can be seen by taking the total derivative of the auxiliary Lagrangian $\mathcal{M}$. Problem (5.69) is linear. Thus, using the computed approximation x the computation of the derivative $i'(\cdot)$ corresponds to one additional step of the Newton-type algorithm and, consequently, can be performed almost without additional effort. The algorithm for the computation of the optimal parameter choice for $\alpha = \alpha(\delta, g^\delta)$ is given as follows:

Calculation of regularization parameter α

(1) Choose initial $\alpha_0 > 0$ and set $k = 0$.

(2) Solve problem (5.48, 5.49) approximately by a Newton-type method.

(3) Solve the additional auxiliary problem (5.69).

(4) Apply one Newton step to the Morozov's discrepancy equation
$$\alpha^{k+1} = \alpha^k - \frac{i(\alpha^k)}{i'(\alpha^k)}.$$

(5) Solve problem (5.48, 5.49) approximately with calculated $\alpha(\delta, g^\delta)$.

(6) Stop if stopping criterion is satisfied. Else set k = k + 1 and go to (2).

The presented algorithm can be extended by accounting for the model perturbations. Each step of the Newton iteration requires the solution of the optimization problem (5.48, 5.49). This suggests the use of adaptive techniques for the optimization procedure. This can be accomplished by using optimized meshes as presented in Kaltenbacher, Kirchner & Vexler [67]. For the case of perturbations due to the discretization and the inexact solution of algebraic systems, we refer to Chapter 6.

5.4. Discrete equations for atmospheric inverse problem

As shown in the previous section Newton-type algorithms require the solution of the auxiliary problems. In this section, we derive the form of these additional problems for the atmospheric inverse problem (4.11) and describe their discretization. The discretization of the related problems such as radiative transfer model is handled in numerical examples. Furthermore, the presented solution algorithms can be directly transferred to the discrete level. The equations are stabilized by the LPS scheme for which the two approaches "discretize-then-optimize" and "optimize-then-discretize" coincide.

In order to shorten the notation, we redefine the spatial semilinear form $\bar{a}(\cdot)(\cdot)$ given in (2.25) by introducing the dependency on the unknown parameter $q := (\mu, \beta, \chi) \in Q$

$$\begin{aligned}\bar{a}(u,q)(\phi) := (D\,\nabla u, \nabla\phi) + (v\cdot\nabla u, \phi) - (f(u),\phi) - (\mu(x)E(u,t,x),\phi)\\ - (wu + \beta(x)E_s(u,t,x),\phi)_{\Gamma_G}.\end{aligned} \tag{5.70}$$

Here, we use the spaces Q and X defined accordingly to (2.24) and (4.10), respectively. Next, we introduce the semilinear form $a : X \times Q \times X \to I\!R$

$$a(u,q)(\phi) := \int_I \bar{a}(u(t),q)(\phi(t))\,dt. \tag{5.71}$$

With these preparations the atmospheric inverse problem (4.11) can be written in the following compact form: Find $u \in \hat{u} + X$ and $q := (\mu, \beta, \chi) \in Q$, such that

$$\begin{aligned}(\partial_t u, \phi)_I + a(u,q)(\phi) + (u(0),\phi(0)) = (\chi,\phi(0)) \quad \forall\phi \in X,\\ \mathcal{C}(u) = g^\delta.\end{aligned} \tag{5.72}$$

Next, we state the precise form of the equations related to the inverse problem (4.11) describing the transport of atmospheric constituents needed by the Newton-type methods as described in Subsection 5.3.1. To this end, we note that the semilinear form $A(t;\cdot,\cdot)(\cdot)$ defined in (5.49) reads in this case as follows:

$$A(t;u,q)(\phi) = (\partial_t u,\phi) + a(u,q)(\phi) + (u(0),\phi(0)) - (\chi,\phi(0)). \tag{5.73}$$

The functionals are given by

$$J_1(u) = \|\mathcal{C}(u) - g^\delta\|_Y^2 \quad \text{and} \quad J_2(q) = \alpha\|q - q^*\|^2, \tag{5.74}$$

with an appropriately chosen regularization parameter α.

We first derive the weak form of the adjoint equation corresponding to (5.53). This is given as follows: Find $\lambda \in X$, such that

$$-(\psi,\partial_t\lambda)_I + a'_u(u,q)(\psi,\lambda) + (\psi(T),\lambda(T)) = 2(\mathcal{C}(u) - g^\delta,\psi) \quad \forall\psi \in X, \tag{5.75}$$

for the vector-valued functions $\lambda = (\lambda_1, \ldots, \lambda_d)^T$ and $\psi = (\psi_1, \ldots, \psi_d)^T$. Using integration by parts and observing that $v \cdot n = 0$ on the ground-level part of the boundary Σ_G, we obtain for a species i

$$\begin{aligned} a'_u(u_i, q_i)(\psi_i, \lambda_i) = (D\,\nabla\lambda_i, \nabla\psi_i)_I - (\nabla\cdot(v\lambda_i), \psi_i)_I - (f'_{i,*}(u)^T\lambda_i, \psi_i)_I \\ +(\lambda_i\, u_i, \psi_i)_{\Sigma_O} - (w\,\lambda_i, \psi_i)_{\Sigma_G}, \end{aligned} \tag{5.76}$$

where $f'_{i,*}(u)$ denotes the the i-th row of the Jacobian $(\partial_i f_k(u))_{i,k=1}^d$.

The control equation corresponding to (5.54) is given by: Find $q := (\mu, \beta, \chi) \in Q$, such that

$$a'_q(u, q)(\varphi, \lambda) = J'_2(q)(\varphi) \quad \forall \varphi \in Q, \tag{5.77}$$

where $\lambda \in X$ is the solution of the adjoint problem (5.75). The derivative of the semilinear form $a(\cdot,\cdot)(\cdot)$ and the functional $J_2(\cdot)$ are given by

$$a'_q(u, q)(\varphi, \lambda) = (\lambda\, E(t, x), \varphi)_I + (\lambda\, E_s(t, x), \varphi)_{\Sigma_G} + (\lambda(0), \varphi(0)), \tag{5.78}$$

and

$$J'_2(q)(\varphi) = 2\alpha(\mu(x) - \mu^*, \varphi_\mu) + 2\alpha\,(\beta(x) - \beta^*, \varphi_\beta)_{\Gamma_G} + 2\alpha\,(\chi(x) - \chi^*, \varphi_\chi), \tag{5.79}$$

for all $\varphi = (\varphi_\mu, \varphi_\beta, \varphi_\chi) \in Q$.

The weak form of the tangent equation corresponding to (5.62) obtained by the total differentiation of the state equation (5.72) with respect to q in the direction $\delta q = (\delta q_\mu, \delta q_\beta, \delta q_\chi)$ reads as follows: Find $\delta u \in X$, such that

$$\begin{aligned} (\partial_t \delta u, \phi)_I + a'_u(u, q)(\delta u, \phi) + (\delta u_0^-, \phi_0^-) \\ = -a'_q(u, q)(\delta q, \phi) + (\delta q_\chi(0), \phi_0^-) \quad \forall \phi \in X. \end{aligned} \tag{5.80}$$

The precise form is given in Corollar 4.4.1 by equation (4.28).

The additional adjoint equation corresponding to (5.61) is given by: Find $\delta z \in X$ satisfying

$$\begin{aligned} -(\psi, \partial_t \delta z)_I + a'_u(u, q)(\psi, \delta z) + (\psi(T), \delta z(T)) = -a''_{uu}(u, q)(\delta u, \psi, \lambda) \\ - a''_{qu}(u, q)(\delta q, \psi, \lambda) + 2(\mathcal{C}'(u)(\delta u), \psi) \quad \forall \psi \in X. \end{aligned} \tag{5.81}$$

In order to formulate the second derivatives of the semilinear form $a(\cdot,\cdot)(\cdot)$, we introduce the tensor $H_{ikl}(f(u)) = \left(\partial_i\partial_k f_l(u)\right)_{i,k,l=1}^d$. Then, we obtain for a species i

$$a''_{uu}(u_i, q_i)(\delta u_i, \psi_i, \lambda_i) = (H_{ikl}(f(u))\lambda_i, \psi_i). \tag{5.82}$$

For the mixed second derivative, we obtain $a''_{qu}(u, q)(\delta q, \psi, \lambda) = 0$.

The unknown parameters $q \in Q$ can be discretized using the cG(s)-scheme as for the state variable as described in Chapter 3 or by cellwise constant functions. In both cases, we denote the discrete control space by $Q_d \subset Q$ and the discretized control variable by $q_\sigma \in Q_d$. Other related discrete variables are marked by the index σ. In order to stabilize the discrete convection-dominated auxiliary problems, we employ the LPS scheme. In the following, we present analogously as for the state equation two different discretization schemes.

DISCONTINUOUS GALERKIN METHOD

First, we state the discretization of the above equations by the cG(s)dG(r) discretization as described in Chapter 3. To this end, we use the stabilization bilinear form $s_{\mathrm{LPS}}(\cdot,\cdot)$ defined in (3.9).

Adjoint equation: Find $\lambda_\sigma \in X_{k,h}^{r,s}$ satisfying

$$\begin{aligned} -\sum_{m=1}^{M}(\psi,\partial_t\lambda_\sigma)_{I_m} + a_u'(u_\sigma,q_\sigma)(\psi,\lambda_\sigma) + s_{\mathrm{LPS}}(\psi,\lambda_\sigma) - \sum_{m=0}^{M-1}(\psi_m^-,[\lambda_\sigma]_m) \\ + (\phi_M^-,\lambda_{\sigma,M}^-) = 2(\mathcal{C}(u_\sigma)-g^\delta,\psi) \quad \forall\psi\in\tilde{X}_{k,h}^{r,s}. \end{aligned} \tag{5.83}$$

Tangent equation: Find $\delta u_\sigma \in X_{k,h}^{r,s}$, such that

$$\begin{aligned} -\sum_{m=1}^{M}(\partial_t\delta u_\sigma,\phi)_{I_m} + a_u'(u_\sigma,q_\sigma)(\delta u_\sigma,\phi) + s_{\mathrm{LPS}}(\delta u_\sigma,\phi) + \sum_{m=0}^{M-1}([\delta u_\sigma]_m,\phi_m^+) \\ + (\delta u_{\sigma,0}^-,\phi_0^-) = -a_q'(u_\sigma,q_\sigma)(\delta q,\phi) + (\delta q_\chi(0),\phi_0^-) \quad \forall\phi\in\tilde{X}_{k,h}^{r,s}, \end{aligned} \tag{5.84}$$

for direction $\delta q = (\delta q_\mu, \delta q_\beta, \delta q_\chi) \in Q_d$.

Additional adjoint equation: Find $\delta z_\sigma \in \tilde{X}_{k,h}^{r,s}$, such that

$$\begin{aligned} -\sum_{m=1}^{M}(\psi,\partial_t\delta z_\sigma)_{I_m} + a_u'(u_\sigma,q_\sigma)(\psi,\delta z_\sigma) + s_{\mathrm{LPS}}(\psi,\delta z_\sigma) - \sum_{m=0}^{M-1}(\psi_m^-,[\delta z_\sigma]_m) \\ + (\psi_M^-,\delta z_{\sigma,M}^-) = -a_{uu}''(u_\sigma,q_\sigma)(\delta u_\sigma,\psi,\lambda_\sigma) + 2(\mathcal{C}'(u_\sigma)(\delta u_\sigma),\psi) \quad \forall\psi\in\tilde{X}_{k,h}^{r,s}, \end{aligned} \tag{5.85}$$

CONTINUOUS GALERKIN METHOD

Next, we summarize the discretization of the above equations by the continuous Galerkin method.

Adjoint equation: Find $\lambda_\sigma \in \tilde{X}_{k,h}^{r-1,s}$, such that

$$\begin{aligned} -\sum_{m=1}^{M}(\psi,\partial_t\lambda_\sigma)_{I_m} + a_u'(u_\sigma,q_\sigma)(\psi,\lambda_\sigma) + s_{\mathrm{LPS}}(\psi,\lambda_\sigma) - \sum_{m=0}^{M-1}(\psi_m,[\lambda_\sigma]_m) \\ + (\psi_M,\lambda_{\sigma,M}^-) = 2(\mathcal{C}(u_\sigma)-g^\delta,\psi) \quad \forall\psi\in X_{k,h}^{r,s}. \end{aligned} \tag{5.86}$$

Tangent equation: Find $\delta u_\sigma \in X_{k,h}^{r,s}$, such that

$$\begin{aligned} (\partial_t\delta u_\sigma,\phi)_I + a_u'(u_\sigma,q_\sigma)(\delta u_\sigma,\phi) + s_{\mathrm{LPS}}(\delta u_\sigma,\phi) + (\delta u_{\sigma,0},\phi_0^-) \\ = -a_q'(u_\sigma,q_\sigma)(\delta q,\phi) + (\delta q_\chi(0),\phi_0^-) \quad \forall\phi\in\tilde{X}_{k,h}^{r-1,s}, \end{aligned} \tag{5.87}$$

for direction $\delta q = (\delta q_\mu, \delta q_\beta, \delta q_\chi) \in Q_d$.

Additional adjoint equation: Find $\delta z_\sigma \in \tilde{X}_{k,h}^{r-1,s}$, such that

$$\begin{aligned} -\sum_{m=1}^{M}(\psi,\partial_t\delta z_\sigma)_{I_m} + a_u'(u_\sigma,q_\sigma)(\psi,\delta z_\sigma) - \sum_{m=0}^{M-1}(\psi_m,[\delta z_\sigma]_m) + (\psi_M,\delta z_{\delta,M}) \\ = -a_{uu}''(u_\sigma,q_\sigma)(\delta u_\sigma,\psi,\lambda_\sigma) + 2(\mathcal{C}'(u_\sigma)(\delta u_\sigma),\psi) \quad \forall \psi \in X_{k,h}^{r,s}. \end{aligned} \tag{5.88}$$

For the derivation of the time-stepping methods involving a general semilinear form $a(\cdot,\cdot)(\cdot)$, we refer to Meidner [81].

5.5. Numerical example

In this section, we examine the approximation properties of ordinary and nonstationary iterated Tikhonov regularization methods and compare the corresponding computational effort. For this purpose, we consider the chemical reaction chain describing the ozone loss in Polar region presented in Chapter 2, Example 2. The reaction mechanism includes five atmospheric constituents interacting with each other in four chemical reactions. The aim of the computations is to reconstruct all concentrations, whereas the source term and initial condition of chlorine are unknown. The given integrated measurements are perturbed by different levels of Gaussian noise. In order to cope with the convection-dominated character, the equations are stabilized by the local projection method as explained in Chapter 3.

For convenience, we state the reaction chain again:

$$\begin{aligned} Cl + O_3 &\xrightarrow{k_1} ClO + O_2 \\ ClO + NO &\xrightarrow{k_2} Cl + NO_2 \\ NO + O_3 &\xrightarrow{k_3} NO_2 + O_2 \\ NO_2 + O_2 + h\nu &\xrightarrow{k_4} NO + O_3 \end{aligned}$$

The reaction rates are given by

$$\begin{aligned} k_1 &= 7.9 \cdot 10^{-12}\,\mathrm{cm}^{-3}\,\mathrm{molec}^{-1}\,\mathrm{s}^{-1}, \qquad k_2 = 2.7 \cdot 10^{-11}\,\mathrm{cm}^{-3}\,\mathrm{molec}^{-1}\,\mathrm{s}^{-1}, \\ k_3 &= 1.8 \cdot 10^{-15}\,\mathrm{cm}^{-3}\,\mathrm{molec}^{-1}\,\mathrm{s}^{-1}, \qquad k_4 = 10^{-2}\,\mathrm{s}^{-1}. \end{aligned}$$

The initial concentrations are set to be equal $u_{O_3}^0 = u_{ClO}^0 = u_{NO}^0 = u_{NO_2}^0 = 10^7\,\mathrm{molec\,cm}^3$. For the chlorine the initial concentration is supposed to be unknown, $u_{Cl}^0 = \chi(x)$. We consider a time period of one hour. The calculations are carried out in a domain of dimensions $\Omega = 6\,\mathrm{km} \times 4\,\mathrm{km}$. Furthermore, we assume an isothermal atmosphere with temperature $\Theta = 298\,\mathrm{K}$, such that the dependency of reaction rates on the temperature can be dropped. Furthermore, we use as diffusivity tensor $D = (D_{11}, D_{22})$ with $D_{11} = 3 \cdot 10^{-5}\,\mathrm{cm}^2\,\mathrm{s}^{-1}$ and $D_{22} = 10^{-4}\,\mathrm{cm}^2\,\mathrm{s}^{-1}$. The wind field is given by $v = (30\,\mathrm{m/s}, 10\,\mathrm{m/s})$. As boundary conditions, we prescribe the pollutant flux for Cl to be $10^7\,\mathrm{molec\,cm}^{-2}\,\mathrm{s}^{-1}$.

The chemical reaction terms are modeled accordingly to the mass kinetics as described in Chapter 2 and are given by (2.51) - (2.56). Furthermore, we assume the emission term for chlorine to be of the following form:

$$E_{Cl}(t,x) = \frac{M}{2\,\pi\sigma^2}\mu(x)\exp\left(-\frac{(x-x_c)^2+(y-y_c)^2}{2\sigma^2}\right).$$

Here, the emitted pollutant mass is $M = 10\,\mathrm{kg}$. The parameters in the emission term are set to be $\sigma = 0.3$, $x_c = 0.5$, and $y_c = 1$. The unknown profile of the emission $\mu(x)$ constitutes the second unknown parameter in the chemical system.

Thus, as the solution space we choose X as defined in (2.24) for the unknown concentrations and $Q := L^2(\Omega) \times L^2(\Omega)$ for the unknown parameters $q := (\mu, \chi) \in Q$. We use integrated observations as overspecification condition. The observation operator $\mathcal{C} : X \to Y$ and the measurement space Y are given by

$$\mathcal{C}(u_i) = \int_\Omega u_i(t,x)\,dx \in Y_i, \quad Y_i := L^2(I),\ i = 1,\dots,6.$$

In order to calculate the integrated measurements, we solve the corresponding forward problem on a finer temporal and spatial mesh for the following choice of parameters:

$$\chi^\dagger(x) = \begin{cases} 10^{-3}(x_1+x_2) & \text{if } 0 \le x_1 \le 2, \\ 0 & \text{else,} \end{cases}$$

and

$$\mu^\dagger(x) = x_1 + x_2.$$

The perturbed measurements are given by

$$g^\delta = g + \delta \sum_{n=1}^{6} \|\mathcal{C}(u_i)\|_{Y_i} \frac{r}{\|r\|_{Y_i}},$$

where r denotes the uniformly distributed random noise, $g = \mathcal{C}(u)$, and δ the percentage of the perturbation. We compare the ordinary and iterated Tikhonov regularization methods for different choices of the noise level δ. The Tikhonov functional is given by

$$J(u,q) = \sum_{n=1}^{6} \|\mathcal{C}(u_i) - g_i^\delta\|^2_{L_2(I)} + \alpha\|q - q^*\|.$$

For the nonstationary iterated Tikhonov regularization, we set for each noise level $\alpha_0 = \delta$ which is reduced in each iteration by the factor $p = \frac{4}{5}$. The initial value for the unknown parameters is chosen accordingly to $q^0 = 0$. For the ordinary regularization, we set also $q^* = 0$.

We solve the inverse problem on a spatial mesh with 3 506 nodes. For the discretization in time, we divide the interval $I = [0,T]$ into $M = 40$ subintervals of equal length. The

TABLE 5.1: Ordinary Tikhonov regularization

δ	It	$\frac{\|q_\sigma - q^\dagger\|_Q}{\|q^\dagger\|_Q}$	α
1.00e-02	5	3.31e-02	2.27e-03
2.00e-02	5	4.54e-01	7.14e-03
4.00e-02	7	6.27e-01	9.48e-03
8.00e-02	8	8.71e-01	1.17e-02

TABLE 5.2: Iterated Tikhonov regularization

δ	It	$\frac{\|q_\sigma - q^\dagger\|_Q}{\|q^\dagger\|_Q}$	α
1.00e-02	5	3.41e-02	3.28e-03
2.00e-02	4	4.49e-01	8.19e-03
4.00e-02	4	6.30e-01	1.64e-02
8.00e-02	4	8.69e-01	3.28e-02

problem is then discretized using the cG(1)cG(1)-scheme and solved by the direct Newton method for optimization problems. The corresponding results are presented in Tables 5.1 and 5.2.

From the second column, we can observe that the nonstationary iterated Tikhonov regularization needs less computational effort almost for each noise level in order to satisfy the Morozov's discrepancy principle. Especially for larger noise levels, we can observe a double work saving. Furthermore, for the ordinary regularization, we need a smaller regularization parameter α which can influence the stability properties of the employed iterative solver. However, in the present case, we can conclude that both solution strategies have comparable approximation properties.

CHAPTER 6

Adaptivity

The purpose of this chapter is to derive adaptive algorithms for the solution of problems governed by partial differential equations. The method is based on a posteriori error estimates which assess the different contributions of the error. Thus, the accuracy in the algebraic solution process can be balanced with that due to discretization using computable a posteriori error estimates in which the outer nonlinear and inner linear iteration errors are separated from the discretization error. This results in effective stopping criteria for the algebraic iteration, which are elaborated particularly for Newton-type methods.

The concept of adaptivity is well accepted in the context of finite element discretizations, see, e.g., Verfürth [119], Babuška & Stouboulis [4], Bangerth & Rannacher [7]. However, usually a posteriori error estimates are developed for the generally unknown exact discrete solutions. Although, the convergence properties of linear as well as nonlinear iterative methods such as the multigrid method or the Newton method are discussed in many publications (see, e.g., Bank & Dupont [8], Bramble [22], and Hackbusch [49]), there are only few results on a posteriori error estimation of the iteration error, which yield stopping criteria in balance with the discretization error.

First simultaneous a posteriori error estimates for discretization and iteration errors have been derived in Becker et al. [14] for the multigrid method applied to the Poisson equation and in Becker [10] for the Stokes equations. There, the errors are measured with respect to global L^2- and energy norms while the finite element discretization using uniform meshes. Later, related results for a special finite volume discretization have been derived in Jiranek et al. [65]. However, in many applications the error measured in global norms does not provide useful bounds for the error in terms of a given functional, so-called a quantity of interest. This has led to the concept of "goal-oriented" adaptivity based on duality techniques such as the Dual Weighted Residual (DWR) method described in Becker & Rannacher [17] and Bangerth & Rannacher [7]. The application of the DWR method to the simultaneous control of discretization and iteration errors has been developed in Meidner et al. [82] for various kinds of linear problems including as simplest model the Poisson equation but also linear saddle-point problems such as the Stokes system in fluid mechanics and the Karush-Kuhn-Tucker (KKT) system of linear-quadratic elliptic optimization problems. For the treatment of eigenvalue problems, we refer to Heuveline & Rannacher [56] and Rannacher et al. [99].

The developed error estimators are mainly based on results already published in Rannacher & Vihharev [98, 97]. However, we extend the concept presented there to the nonstationary inverse problems. The goal is to incorporate the iteration method into the adaptive solution process of a given problem. The developed approach is sufficiently general to include

weakly nonlinear diffusion-reaction problems with linear diffusion but nonlinear reaction terms, Euler-Lagrange equations stemming from image segmentation, and inverse problems involving radiative transfer models with state constraints. Related results in the context of energy-norm error control have been derived in El Alaoui et al. [1] for nonlinear monotone problems and more recently in Ern & Vohralik [35, 36] also for inexact Newton methods.

This chapter is organized as follows: In Section 6.1, we begin with an abstract stationary problem given in a variational form and derive a posteriori error estimates for a general fixed-point iteration. On this basis, we propose an adaptive method with balanced error contributions due to the discretization and the iterative solution. Thereby, we explain the practical realization of the presented algorithm. In Subsection 6.1.3, we consider a special case of Newton-type iterations. Here, we exploit the structure of the Newton algorithm and the DWR method and separate the algebraic error into contributions from the inner and outer iterations. The reliability and the efficiency of the proposed algorithm is shown by numerical examples in Section 6.2. The first example is concerned with a special form of a non-Lipschitz nonlinearity modeling chemical reactions in the case of interactions of gas-phase chemical species with aqueous surfaces. In the second example, we consider an application concerned with the denoising and the segmentation of the clouds from satellite observations. In Section 6.3, we consider general stationary inverse problems regularized by Tikhonov-type methods. We derive a posteriori error estimates for the resulting optimal control problems. Furthermore, we discuss the application of the proposed adaptivity concept to the Landweber iteration. The developed adaptive algorithm is applied in Section 6.4 to a radiative transfer model. The identification of the unknown concentrations constituting the reaction term of the equation requires to pose constraints to the state variable. We show the reliability and efficiency of the proposed adaptive method. We close the chapter by presenting error estimates for the nonstationary inverse problems. As a numerical example, we consider in Section 6.6 a chemical reaction chain describing the ozone loss.

6.1. Iteration error for steady problems

In this section, we present a posteriori error estimators for discretization and iteration errors for a general nonlinear partial differential equation in variational form. Based on the error estimators, we propose an adaptive algorithm in which the errors due to the discretization and the iterative solution of the discrete systems are balanced. The adaptive method is first derived for a general fixed-point iteration and after that extended to inexact Newton methods. Here, we exploit the structure of the DWR and Newton methods and separate algebraic error contributions due to the linearization and iterative computations in the inner iteration.

6.1.1. Iteration error for general fixed-point iteration

We consider an abstract model problem

$$\mathcal{A}(u) = 0 \quad \text{in } \Omega, \quad u = 0 \ \text{ on } \partial\Omega, \tag{6.1}$$

with a nonlinear elliptic operator $\mathcal{A}(\cdot)$, where Ω is a bounded domain in $\mathbb{R}^n$, $n \in \{2, 3\}$, with polygonal (polyhedral) boundary $\partial\Omega$. For simplicity, we impose homogeneous Dirichlet boundary conditions. However, the developed techniques can also be applied to problems with other types of boundary conditions. For the variational formulation of problem (6.1), we introduce the usual Sobolev Banach space $V := W_0^{1,p}(\Omega)$ for $1 < p < \infty$. With the semilinear form $A(\cdot)(\cdot)\colon V \times V \to \mathbb{R}$ associated to the operator $\mathcal{A}(\cdot)$, the weak formulation of problem (6.1) reads as follows: Find $u \in V$, such that

$$A(u)(\phi) = 0 \quad \forall \phi \in V. \tag{6.2}$$

We discretize this problem by a standard finite element method in finite dimensional spaces $V_h \times V_h \subset V \times V$ resulting in "discrete" problems

$$A(u_h)(\phi_h) = 0 \quad \forall \phi_h \in V_h, \tag{6.3}$$

which are equivalent to systems of nonlinear algebraic equations. Usually the a posteriori error estimators for the discretization error $u - u_h$ are derived under the assumption that the discrete problems (6.3) are solved exactly. This ensures the crucial property of Galerkin orthogonality,

$$A(u)(\phi_h) - A(u_h)(\phi_h) = 0, \quad \phi_h \in V_h. \tag{6.4}$$

In contrast, here, we assume that the discrete problems are solved only approximately and denote the obtained approximate solution in V_h by $\tilde{u}_h$ in contrast to the notation u_h for the "exact" discrete solution. Let the quantity of interest $J(u)$ of the computation be given in terms of a (nonlinear) functional $J(\cdot)\colon V \to \mathbb{R}$. Our goal is the derivation of an a posteriori error estimate with respect to the functional $J(\cdot)$. To this end, we define the Lagrange functional

$$\mathcal{L}(u, z) := J(u) - A(u)(z),$$

where $z \in V^*$ is a solution of the associated linear dual problem

$$A'(u)(\phi, z) = J'(u)(\phi) \quad \forall \phi \in V. \tag{6.5}$$

The corresponding discrete dual solution $z_h \in V_h$ is defined by the equation

$$A'(u_h)(\phi_h, z_h) = J'(u_h)(\phi_h) \quad \forall \phi_h \in V_h. \tag{6.6}$$

These problems are also supposed to be uniquely solvable. Then, there holds the following proposition.

PROPOSITION 6.1.1. *Let $\{\tilde{u}_h, \tilde{z}_h\} \in V_h \times V_h$ be approximations to the continuous solutions $\{u, z\} \in V \times V^*$ of the primal and dual problems* (6.2) *and* (6.5)*, respectively, obtained by any iterative process on the mesh $\mathcal{T}_h$. Then, there holds the following error representation:*

$$\begin{aligned} J(u) - J(\tilde{u}_h) = \tfrac{1}{2}\rho(\tilde{u}_h)(z - \tilde{z}_h) + \tfrac{1}{2}\rho^*(\tilde{u}_h, \tilde{z}_h)(u - \tilde{u}_h) \\ - \rho(\tilde{u}_h)(\tilde{z}_h) + \mathcal{R}_h^{(3)}, \end{aligned} \tag{6.7}$$

with the residual terms

$$\rho(\tilde{u}_h)(\cdot) := -A(\tilde{u}_h)(\cdot), \quad \rho^*(\tilde{u}_h, \tilde{z}_h)(\cdot) := J'(\tilde{u}_h)(\cdot) - A'(\tilde{u}_h)(\cdot, \tilde{z}_h).$$

The remainder term $\mathcal{R}_h^{(3)}$ *is cubic in the primal and dual errors* $\tilde{e} := u - \tilde{u}_h$ *and* $\tilde{e}^* := z - \tilde{z}_h$, *respectively,*

$$\begin{aligned}\mathcal{R}_h^{(3)} = & \tfrac{1}{2} \int_0^1 \Big\{ J'''(\tilde{u}_h + s\,\tilde{e})(\tilde{e}, \tilde{e}, \tilde{e}) - A'''(\tilde{u}_h + s\,\tilde{e})(\tilde{e}, \tilde{e}, \tilde{e}, \tilde{z}_h + s\tilde{e}^*) \\ & - 3\,A''(\tilde{u}_h + s\tilde{e})(\tilde{e}, \tilde{e}, \tilde{e}^*)) \Big\}\, s(s-1)\, ds.\end{aligned} \tag{6.8}$$

Proof. We set

$$x := \{u, z\}, \quad \tilde{x}_h := \{\tilde{u}_h, \tilde{z}_h\}, \quad L(x) := \mathcal{L}(u, z), \quad L(\tilde{x}_h) := \mathcal{L}(\tilde{u}_h, \tilde{z}_h).$$

With this notation there holds

$$L(x) - L(\tilde{x}_h) = \int_0^1 L'(\tilde{x} + s\,(x - \tilde{x}_h))(e)\, ds.$$

Using the general error representation for the trapezoidal rule

$$\int_0^1 f(s)\, ds = \tfrac{1}{2}(f(0) + f(1)) + \tfrac{1}{2} \int_0^1 f''(s)\, s\,(s-1)\, ds,$$

we conclude

$$L(x) - L(\tilde{x}_h) = \tfrac{1}{2} L'(\tilde{x}_h)(x - \tilde{x}_h) + \mathcal{R}_h^{(3)},$$

with the remainder term $\mathcal{R}_h^{(3)}$ given by (6.8). Recalling the particular structure of the functional $L(\cdot)$ and observing that u satisfies (6.2), we obtain

$$\begin{aligned} J(u) - J(\tilde{u}_h) &= L(x) + A(u)(z) - L(\tilde{x}_h) - A(\tilde{u}_h)(\tilde{z}_h) \\ &= L(x) - L(\tilde{x}_h) - A(\tilde{u}_h)(\tilde{z}_h) = \tfrac{1}{2} L'(\tilde{x}_h)(x - \tilde{x}_h) + \mathcal{R}_h^{(3)} - A(\tilde{u}_h)(\tilde{z}_h). \end{aligned}$$

The proof is completed by observing that

$$L'(\tilde{x}_h)(\cdot) = J'(\tilde{u}_h)(\cdot) - A'(\tilde{u}_h)(\cdot, \tilde{z}_h) - A(\tilde{u}_h)(\cdot).$$

□

The extra third residual term $\rho(\tilde{u}_h)(\tilde{z}_h)$ on the right-hand side of (6.7) would vanish if evaluated for the "exact" discrete solution u_h. In the present situation with an only approximate solution $\tilde{u}_h$, it will be used for estimating the iteration error.

6.1.2. Practical realization

The error representation (6.7) involves the unknown errors $z - \tilde{z}_h$ and $u - \tilde{u}_h$ as weights. Hence its evaluation requires the generation of reasonable approximations. We approximate the interpolations errors using the computed approximations $\tilde{z}_h$ and $\tilde{u}_h$ and patchwise interpolations into higher-order finite element spaces. To this end, we introduce the linear operator Π_h, which maps the computed solution to the approximations of the corresponding errors,

$$\Pi_h \tilde{z}_h := I_{2h}^{(2)} \tilde{z}_h - \tilde{z}_h \approx z - \tilde{z}_h, \qquad \Pi_h \tilde{u}_h := I_{2h}^{(2)} \tilde{u}_h - \tilde{u}_h \approx u - \tilde{u}_h.$$

The piecewise biquadratic (triquadratic) interpolation $I_{2h}^{(2)}$ can easily be computed if the underlying mesh provides a patch structure. That is, one can always combine four adjacent cells to a macro cell on which the biquadratic (bicubic) interpolation can be defined.

We obtain the following computable error estimator for the discretization error:

$$\begin{aligned} \eta_h &:= \tfrac{1}{2}\Big|\rho(\tilde{u}_h)(\Pi_h \tilde{z}_h) + \rho^*(\tilde{u}_h, \tilde{z}_h)(\Pi_h \tilde{u}_h)\Big| \\ &= \tfrac{1}{2}\Big|A(\tilde{u}_h)(\Pi_h \tilde{z}_h) - \tfrac{1}{2}\Big(J'(\tilde{u}_h)(\Pi_h \tilde{u}_h) + A'(\tilde{u}_h)(\Pi_h \tilde{u}_h, \tilde{z}_h)\Big)\Big|. \end{aligned} \tag{6.9}$$

This error representation is used for controlling the discretization error and for steering mesh refinement. For the latter purpose, the error estimator η_h must be localized to cellwise contributions. We describe the procedure for the primal residual term $\rho(\cdot)(\cdot)$. The contribution of the dual residual is computed in the same way. Thus, we consider the nodal basis $\{\phi_i, i = 1, 2, \ldots, N\}$ of V_h, where $N = \dim V_h$. Letting Z denote the coefficient vector of z_h, we have the representation

$$z_h = \sum_{i=1}^{N} \phi_i Z_i.$$

We can rewrite the error estimator as $\rho(u_h)(\Pi_h z_h) = \langle \Psi, Z \rangle$, where $\langle \cdot, \cdot \rangle$ denotes the Euclidian inner product on $\mathbb{R}^N$ and Ψ is given by $\Psi_i := \rho(u_h)(\Pi_h \phi_i)$. However, a direct localization of this term leads to an overestimation of the error due to the oscillatory behavior of the residuals. To avoid this, we introduce a filtering operator $\pi : \mathrm{id} - I_{2h}^h$, where I_{2h}^h is an interpolation operator in the space of bilinear (trilinear) finite elements defined on patches and denote by Z^π the coefficient vector of the filtered dual solution πz_h,

$$\pi z_h = \sum_{i=1}^{N} \phi_i Z_i^\pi.$$

Then, the properties of π and $I_{2h}^{(2)}$ and the linearity of the residual $\rho(\cdot)(\cdot)$ with respect to the weight imply $\rho(u_h)(\Pi_h z_h) = \langle \Psi, Z^\pi \rangle$. A further localization leads to nodewise error indicators

$$\rho(u_h)(\Pi_h z_h) = \sum_{i=1}^{N} \Psi_i Z_i^\pi.$$

The contributions of the dual residual are computed in the same way. Thus, we obtain

$$\eta_{h,i} = \frac{1}{2}|Z_i^\pi \Psi_i^u + U_i^\pi \Psi_i^z|,$$

where U_i^π and Ψ_i^y are defined analogously,

$$\Psi_i^z := \rho^*(u_h, z_h)(\Pi_h \phi_i),$$

and

$$\pi_h u_h = \sum_{i=1}^{N} \phi_i U_i^\pi.$$

For the mesh refinement the nodewise contributions $\eta_{h,i}$ are shifted to the corresponding cellwise contributions. Then, these error indicators are used to select the cells which have to be refined within the adaptive algorithm.

The additional term in representation (6.7) for the total error is used as estimator for the iteration error:

$$\eta_m := \Big|A(\tilde{u}_h)(\tilde{z}_h)\Big|, \tag{6.10}$$

while the cubic remainder $\mathcal{R}_h^{(3)}$ is neglected. This results in the error estimator

$$|J(u) - J(\tilde{u}_h)| \approx \eta = \eta_h + \eta_m. \tag{6.11}$$

The estimator η_m for the iteration error vanishes in the limit $\tilde{u}_h \to u_h$ and will therefore on each fixed mesh eventually fall below the estimator η_h for the discretization error. Surprisingly, this is true for any choice of the approximate dual solution $\tilde{z}_h \approx z_h$ indicating that the term η_m simply measures the deviation of $\tilde{u}_h$ from "Galerkin orthogonality", while the error $\tilde{z}_h - z_h$ only affects the size of the (neglected) remainder term.

Based on estimator (6.11) the algorithm for adaptively balancing discretization and nonlinear iteration errors reads as follows:

Adaptive fixed-point iteration

(1) Choose an initial discretization $\mathcal{T}_{h_0}$ and set $l = 0$.
(2) Choose an initial value $u_{h_l}^0$ and set $n = 0$.
(3) Apply one step of the nonlinear iteration $u_{h_l}^n \to u_{h_l}^{n+1}$.
(4) Solve the corresponding discrete dual problem for z_h^{n+1},
$$A'(u_h^{n+1})(\phi_h, z_h^{n+1}) = J'(u_h)(\phi_h) \quad \forall \phi_h \in V_h,$$
and evaluate the estimators $\eta_{h_l}^{n+1}$ and $\eta_{m_l}^{n+1}$.
(5) If $\eta_{h_l}^{n+1} + \eta_{m_l}^{n+1} \leq \mathrm{TOL}$ quit.
(6) If $\eta_{m_l}^{n+1} \geq \kappa\, \eta_{h_l}^{n+1}$ increment n and go to (3).
(7) Refine $\mathcal{T}_{h_l} \to \mathcal{T}_{h_{l+1}}$ using information from $\eta_{h_l}^{n+1}$.
(8) Increment l and go to (2).

As initial value in step (2) of the above algorithm, we use the values from the computations on the previous mesh, thus avoiding unnecessary iterations on fine meshes. In the numerical tests below this leads to rather small iteration errors already at the very beginning. We use an equilibration factor $\kappa = 0.1$. This ensures that the local mesh refinement results from the value of the discretization error estimator. Selecting an even smaller value does not improve the accuracy of the computed solution but increases the number of iterations. A larger value can affect the local mesh refinement. In order to reduce the computational work, we save the value η_{h_l} obtained on the current mesh. On the next finer mesh $\mathcal{T}_{h_{l+1}}$, we evaluate the discretization error estimator if for the iteration error estimator there holds $\eta_{m_{l+1}}^{n+1} \leq \kappa\, \eta_{h_l}^{n+1}$.

6.1.3. Inexact Newton method

As special choice of a fixed-point iteration, we consider an inexact Newton method. Then, solution process uses the following algorithm:

Adaptive inexact Newton method

(1) Choose an initial discretization $\mathcal{T}_{h_0}$ and set $l = 0$.

(2) Choose an initial value $u_{h_l}^0$ and set $n = 0$.

(3) Compute an approximate solution $\tilde{v}_{h_l}^n$ of the correction equation

$$A'(u_{h_l}^n)(v_{h_l}^n, \psi) = -A(u_{h_l}^n)(\psi) \quad \forall \psi \in V_{h_l},$$

by any iterative method $v_{h_l}^{n-1} \to v_{h_l}^n$.

(4) Update: $u_{h_l}^{n+1} = u_{h_l}^n + \vartheta_n\, \tilde{v}_{h_l}^n$ with some $\vartheta_n \in (0, 1]$.

(5) Compute an approximate solution $\tilde{z}_{h_l}^{n+1}$ of the linear dual problem

$$A'(u_{h_l}^{n+1})(\phi, z_{h_l}^{n+1}) = J'(u_{h_l}^{n+1})(\phi) \quad \forall \phi \in V_{h_l},$$

by any iterative method $z_{h_l}^n \to z_{h_l}^{n+1}$ and evaluate the corresponding error estimators $\eta_{h_l}^{n+1}$ and $\eta_{m_l}^{n+1}$.

(6) If $\eta_{h_l}^{n+1} + \eta_{m_l}^{n+1} \leq \mathrm{TOL}$ quit.

(7) If $\eta_{m_l}^{n+1} \geq \kappa\, \eta_{h_l}^{n+1}$ increment n and go to (3).

(8) Refine $\mathcal{T}_{h_l} \to \mathcal{T}_{h_{l+1}}$ using information from $\eta_{h_l}^{n+1}$.

(9) Increment l and go to (2).

As initial value for the Newton method in step (2), we use again the result from the previous coarser mesh, which again leads to rather small iteration errors already at the very

beginning. The evaluation of the discretization error estimator is done using the strategy described above.

For the further discussion, we define the following residuals corresponding to the interior linear iterations in steps (3) and (5) of the above algorithm:

$$\begin{aligned}\langle r_{h_l}^n, \cdot\rangle &:= A'(u_{h_l}^n)(\tilde{v}_{h_l}^n, \cdot) + A(u_{h_l}^n)(\cdot),\\ \langle d_{h_l}^n, \cdot\rangle &:= A'(u_{h_l}^{n+1})(\cdot, \tilde{z}_{h_l}^{n+1}) - J'(u_{h_l}^{n+1})(\cdot).\end{aligned}$$

For the exact Newton method the linear residual occurring due to the inexact solution of the correction equations vanishes, i.e., for the inner iterations of the primal and dual problems there holds $\langle r_h^n, \cdot\rangle \equiv 0$ and $\langle d_h^n, \cdot\rangle \equiv 0$. We aim at the equilibration of the errors due to the linearization, the iterative computations in the inner iteration, and the inexact solution of the dual problem. For this purpose, we consider the difference between two Newton iterates. For the sake of brevity, we consider a quadratic functional $J(\cdot) : V \to I\!R$. Using Taylor expansion and the definition of the dual problem, we obtain

$$\begin{aligned}J(u_h^{n+1}) - J(u_h^n) &= J(u_h^n + \vartheta_n \tilde{v}_h^n) - J(u_h^n)\\ &= \vartheta_n J'(u_h^n)(\tilde{v}_h^n) + \tfrac{1}{2}\vartheta_n^2 J''(u_h^n)(\tilde{v}_h^n, \tilde{v}_h^n)\\ &= \vartheta_n A'(u_h^n)(\tilde{v}_h^n, \tilde{z}_h^n) - \vartheta_n \langle d_h^n, \tilde{v}_h^n\rangle\\ &\quad + \tfrac{1}{2}\vartheta_n^2 J''(u_h^n)(\tilde{v}_h^n, \tilde{v}_h^n),\end{aligned} \tag{6.12}$$

and recalling the structure of the Newton method,

$$\begin{aligned}J(u_h^{n+1}) - J(u_h^n) = &- \vartheta_n A(u_h^n)(\tilde{z}_h^n) + \vartheta_n \langle r_h^n, \tilde{z}_h^n\rangle - \vartheta_n \langle d_h^n, \tilde{v}_h^n\rangle\\ &+ \tfrac{1}{2}\vartheta_n^2 J''(u_h^n)(\tilde{v}_h^n, \tilde{v}_h^n).\end{aligned} \tag{6.13}$$

The first term on the right hand side corresponds to the linearization error whereas the second and the third terms are due to the inexact solution of the correction equation for the primal problem and the solution of the dual problem. The last term occurs due to the quadratic structure of the error functional and it dominates over the residual terms of the linear problems. It vanishes, e.g., if $J(\cdot)$ is linear. Taking into account (6.13), we propose the following stopping criterion for the linear subiteration:

$$\max\{|\langle r_h^n, \tilde{z}_h^n\rangle|, |\langle d_h^n, \tilde{v}_h^n\rangle|\Big\} \leq \kappa \eta_{m_l}^n = \kappa\, |A(u_h^n)(\tilde{z}_h^n)|. \tag{6.14}$$

If we consider a linear error functional, we have the following representation for the full linear iteration error.

LEMMA 6.1.1. *Let v_h^n and $\tilde{v}_h^n$ be exact respectively inexact solutions of the correction equation in the Newton method starting from the preceding iterate u_h^n and with the Jacobi matrix assembled for u_h^n. Further, let $\tilde{z}_h^n$ be the inexact solution of the corresponding linear dual problem. Then, for the error in the next "inexact" iterate $u_h^{n+1} = u_h^n + \vartheta_n \tilde{v}_h^n$ and its*

"exact" analogue $\hat{u}_h^{n+1} := u_h^n + \vartheta_n v_h^n$ *with respect to a linear functional* $J(\cdot) : V \to \mathbb{R}$*, there holds*

$$J(\hat{u}_h^{n+1}) - J(u_h^{n+1}) = -\vartheta_n \langle r_h^n, \tilde{z}_h^n \rangle - \vartheta_n \langle d_h^n, v_h^n - \tilde{v}_h^n \rangle. \tag{6.15}$$

PROOF. By the definition of the Newton method there holds

$$J(\hat{u}_h^{n+1}) - J(u_h^{n+1}) = J(u_h^n + \vartheta_n v_h^n) - J(u_h^n + \vartheta_n \tilde{v}_h^n) = \vartheta_n J(v_h^n) - \vartheta_n J(\tilde{v}_h^n).$$

Now, we use the definition of the dual problem to obtain

$$\begin{aligned} J(\hat{u}_h^{n+1}) - J(u_h^{n+1}) &= \vartheta_n A'(u_h^n)(v_h^n, \tilde{z}_h^n) - \vartheta_n A'(u_h^n)(\tilde{v}_h^n, \tilde{z}_h^n) - \vartheta_n \langle d_h^n, v_h^n - \tilde{v}_h^n \rangle \\ &= -\vartheta_n A(u_h^n)(\tilde{z}_h^n) + \vartheta_n A(u_h^n)(\tilde{z}_h^n) - \vartheta_n \langle r_h^n, \tilde{z}_h^n \rangle \\ &\quad - \vartheta_n \langle d_h^n, v_h^n - \tilde{v}_h^n \rangle, \end{aligned}$$

which proves the assertion. □

REMARK 6.1.1. Under the same assumptions as in Lemma 6.1.1 for a quadratic functional there holds

$$\begin{aligned} J(\hat{u}_h^{n+1}) - J(u_h^{n+1}) &= -\vartheta_n \langle r_h^n, \tilde{z}_h^n \rangle - \vartheta_n \langle d_h^n, v_h^n - \tilde{v}_h^n \rangle \\ &\quad + \tfrac{1}{2}\vartheta_n^2 \Big(J''(u_h^n)(v_h^n, v_h^n) - J''(u_h^n)(\tilde{v}_h^n, \tilde{v}_h^n) \Big). \end{aligned} \tag{6.16}$$

The error representation (6.15) may be considered as additional justification of the stopping criterion (6.14). It is valid for any linear solver. If a multigrid method is used, then following the argument in Meidner et al. [82] the error representation (6.15) can be developed further into a form, which also allows to adaptively tune the inner smoothing iterations on each mesh level.

Next, we discuss how the developed adaptive algorithm can be applied to ill-posed problems regularized by the Landweber iteration. To this end, we consider the nonlinear operator equation (5.19) formulated as the constraint problem

$$\min_{q \in Q} j(q) = \|\mathcal{C}u - g^\delta\|_Y^2, \tag{6.17}$$

subject to

$$A(q, u)(\psi) = 0 \quad \forall \psi \in V, \tag{6.18}$$

where Q, V, and Y denote appropriate Hilbert spaces. The corresponding (nonlinear) operator F is given by the composition $F = \mathcal{C} \circ S$ with the linear observation operator $\mathcal{C} : V \to Y$ and the parameter-to-solution map $S : q \mapsto u(q)$. It is easy to see that one step of the Landweber iteration (5.28) requires the solution of the state equation (6.18) and the adjoint equation, which reads as

$$-A_u'(u, q)(\phi, z) = 2(\mathcal{C}u - g^\delta, \phi) \quad \forall \phi \in V. \tag{6.19}$$

This can be carried out by the adaptive inexact Newton method as described above. Obviously, for the update q^n there holds

$$F'(q)(\psi, F(q) - g^\delta) = A'_q(S(q), q)(\psi, z), \tag{6.20}$$

from where the update can be evaluated. Thus, in this case the discretization and iteration errors are measured with respect to functional (6.17). Alternatively, we can consider the functional $i(\cdot)$ defined in (5.67) corresponding to the Morozov's discrepancy principle

6.2. Numerical examples

In this section, we demonstrate the efficiency and reliability of the proposed adaptive algorithm. We compare the adaptive Newton method described above with a Newton method employing a residual based stopping criterion. To this end, we replace the adaptive stopping criterion in the Newton solver by requiring that the initial residual is to be reduced by a factor of 10^{-11}. Moreover, we employ the adaptive stopping rule for the linear solver in the inner Newton iteration. This will be analogously compared to the linear solver with a residual based rule. As in nonlinear case, we require that the initial residual must be reduced by a factor of 10^{-11}. The discretization error estimator will still be used for the construction of locally refined meshes and the error control. We denote this algorithm by *S I*, the adaptive Newton method with algebraic stopping criterion in the inner iteration as *S II*, and with an adaptive stopping rule as *S III*.

In the tables below, the following notation is used for the discretization error:

$$\begin{aligned} E_h := J(u) - J(u_h) \quad & \text{“exact” discretization error,} \\ \eta_h \quad & \text{estimator of discretization error,} \\ I^h_{\text{eff}} = \left|\frac{\eta_h}{E_h}\right| \quad & \text{effectivity index of discretization error estimator,} \end{aligned}$$

for the iteration error

$$\begin{aligned} E_m := J(u_h) - J(\tilde{u}_h) \quad & \text{“exact” iteration error,} \\ \eta_m \quad & \text{estimator of iteration error,} \\ I^m_{\text{eff}} = \left|\frac{\eta_m}{E_m}\right| \quad & \text{effectivity index of iteration error estimator,} \end{aligned}$$

and for the total error

$$\begin{aligned} E := J(u) - J(\tilde{u}_h) \quad & \text{total error,} \\ I^{\text{tot}}_{\text{eff}} = \left|\frac{\eta_h}{E_h}\right| \quad & \text{effectivity index of total error estimator.} \end{aligned}$$

We emphasize that the discretization and iterations error estimators η_h and η_m, respectively, depend on the computed approximations $\tilde{u}_h$ and $\tilde{z}_h$ and, thus, represent computable quantities.

6.2.1. Example 1

This example concerns the case of a non-differentiable nonlinearity (even non-Lipschitzian), in which the usual definition of the Newton method (or its semi-smooth variants; see Ito & Kunisch [61]) fails. In this case, we need to use some kind of regularization. Such nonlinearities occur due to chemical reactions in the case of interactions of gas-phase chemical species with aqueous surfaces. We will see that even in this "irregular" situation the derived a posteriori error estimators work well and can be used as the basis for an adaptive stopping criterion of the nonlinear iteration.

We consider the following steady-state nonlinear boundary value problem

$$-\nu\Delta u + f(u) = 0 \ \text{ in } \Omega, \quad u = g \ \text{ on } \partial\Omega, \tag{6.21}$$

where $\Omega := (-1,1)^2\backslash([0,0]\times[0,-1])$ is the slit domain shown in Fig. 6.1. Here, u denotes the concentration of a chemical species diffusing in a medium.

We consider a simple case of an isothermal mixed-order reaction such that the non-Lipschitzian nonlinearity is given by $f(u) = |u|^p$ with $p = 0.15$. We set the diffusivity of the medium to be equal $\nu = 10^{-1}$. On the slit part of the boundary, Γ_s, the boundary values are given by $g(x) = 0$ and on the remaining part, we prescribe the following values:

$$g(x) = \begin{cases} \exp(|x|)\sin(-\frac{1}{2}\pi\, x_1), & \text{if } x \in \Gamma_1, \\ \exp(|x|)\sin(\frac{1}{2}\pi\, x_2), & \text{if } x \in \Gamma_2, \\ \exp(|x|)\sin(\frac{1}{2}\pi\, x_1), & \text{if } x \in \Gamma_3, \\ \exp(|x|)\sin(-\frac{1}{2}\pi\, x_2), & \text{if } x \in \Gamma_4. \end{cases}$$

This problem is well posed with the choice $V = W_0^{1,2}(\Omega)$. The goal functional is given by point value $J(u) := u(a)$ at the point $a = (-0.75, -0.75)$. Since in this case the functional $J(\cdot)$ is not defined on the space V, it has to be regularized like

$$J_\varepsilon(u) := |B_\varepsilon(a)|^{-1} \int\limits_{B_\varepsilon(a)} u(x)\,dx = u(a) + O(\varepsilon^2),$$

where $B_\varepsilon(a) := \{z \in \Omega\ ;\ |z-a| \le \varepsilon\}$ is a ball with center a and radius $\varepsilon \approx TOL$.

In this situation there exists a so-called "dead core" in the interior of the domain where the solution is zero. In this region the nonlinearity is only Hölder continuous such that the usual definition of the Newton method fails. To overcome this problem, we use a difference quotient for approximating the directional derivative of the nonlinearity $f(\cdot)$ at points where it does not exist,

$$f'_\varepsilon(u,\phi) := \varepsilon^{-1}\Big(f(u+\varepsilon\phi) - f(u)\Big),$$

with a small $\varepsilon \approx h_{\min}$. This is then used as the coefficient for the nonlinearity in the dual problem as well as in the Newton iteration. Alternatively, we could also regularize

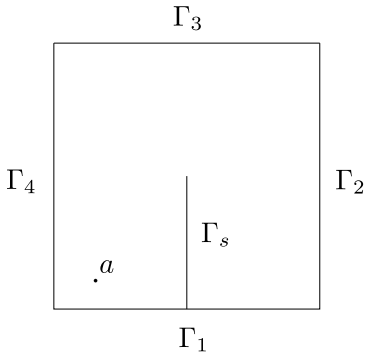

FIGURE 6.1: Configuration of Example 1, slit domain and point value evaluation

the problem itself following the approach proposed in Nochetto [87] by introducing the regularized functional

$$f_\varepsilon(u) := \begin{cases} u^p, & \text{if } \varepsilon^{1/(1-p)} \le u, \\ \varepsilon^{-1}u, & \text{if } 0 \le |u| \le \varepsilon^{1/(1-p)}, \end{cases}$$

which replaces the irregular functional in the variational formulation. The discrete weak form then seeks an $u_h \in g_h + V_h$ satisfying

$$A_\varepsilon(u_h)(\phi_h) := \nu(\nabla u_h, \nabla \phi_h) + (f_\varepsilon(u_h), \phi_h) = 0 \quad \forall \phi_h \in V_h, \tag{6.22}$$

where $g_h := I_h g$ is chosen as the nodal interpolation of g. Both approaches, the "approximation approach" as well as the "regularization approach", yield almost identical computational results, i.e., almost identical meshes with only slight differences in the number of nodes and structure of the refinement. Hence, in the following, we will consider only the above "approximation approach" since it only regularizes the solution process but keeps the problem to be solved unchanged. The locally refined meshes are depicted in Figure 6.2.

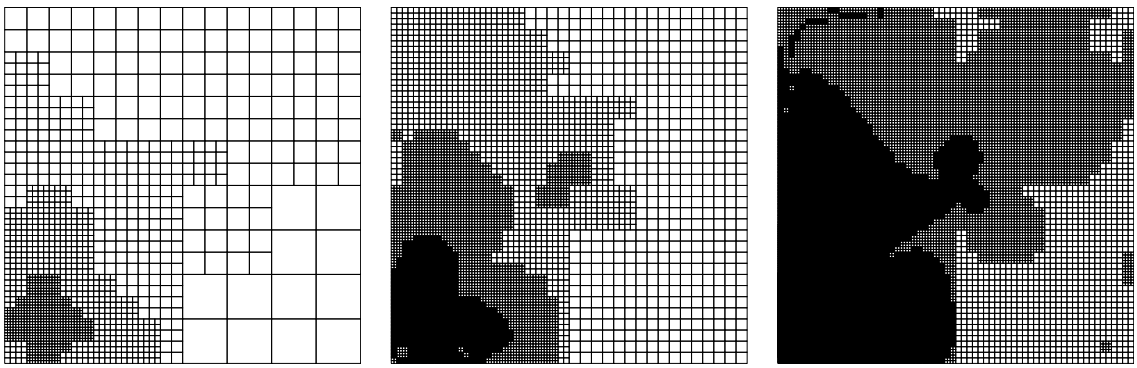

FIGURE 6.2: Example 1, locally refined meshes obtained by the adaptive solution process.

In order to access the "exact" discrete solutions ($S\,I$), we solve the problems by the Newton method using a multigrid algorithm in V-cycle form with 4 pre- and post-smoothing block-ILU steps as inner linear iteration. For both iterations the stopping criterion is that the initial residuals are reduced by a factor 10^{-15}. The approximate discrete solutions $\tilde{u}_h$ and $\tilde{z}_h$ are computed by an adaptive Newton method also using the same multigrid solver in the inner iteration (Alg. $S\,II$). Tables 6.1 and 6.2 show the development of the discretization and iteration errors and the a posteriori error estimators in the adaptive solution process on a coarse grid with 1 605 nodes and a fine grid with 222 917 nodes, respectively. These results demonstrate the sharpness of both error estimators. In this case, we would have stopped the Newton iteration in the adaptive algorithm already after the first step since then the discretization error dominates and carrying the iteration further would not improve the total error.

TABLE 6.1: Example 1, effectivity of the different error estimators on a coarse mesh with 1 605 knots ($S\,II$).

It	E_h	η_h	I^h_{eff}	E_m	η_m	I^m_{eff}
1	4.27e-03	5.13e-03	1.18	4.03e-04	4.03e-04	1.00
2	4.27e-03	5.13e-03	1.17	1.18e-05	1.18e-05	1.00
3	4.27e-03	5.13e-03	1.17	3.31e-07	3.31e-07	1.00
4	4.27e-03	5.13e-03	1.17	8.79e-09	8.79e-09	1.00
5	4.27e-03	5.13e-03	1.17	2.24e-10	2.24e-10	1.00
6	4.27e-03	5.13e-03	1.17	5.57e-12	5.57e-12	1.00

TABLE 6.2: Example 1, effectivity of the different error estimators on a fine mesh with 222 193 knots ($S\,II$).

It	E_h	η_h	I^h_{eff}	E_m	η_m	I^m_{eff}
1	1.30e-04	1.35e-04	1.04	8.54e-06	8.55e-06	1.00
2	1.30e-04	1.35e-04	1.04	2.71e-07	2.98e-07	1.10
3	1.30e-04	1.35e-04	1.04	3.53e-08	3.54e-08	1.00
4	1.30e-04	1.35e-04	1.04	7.37e-10	7.36e-10	1.00
5	1.30e-04	1.35e-04	1.04	2.63e-12	2.61e-12	0.99
6	1.30e-04	1.35e-04	1.04	4.68e-13	4.67e-13	1.00

Next, we present the convergence history of the mesh adaptation process. The corresponding values for the three algorithms $S\,I$, $S\,II$, and $S\,III$ described above are given in Tables 6.3, 6.4, and 6.5. The values of the error $E = |J(u) - J(\tilde{u}_h)|$ and of the total effectivity indices show that the use of the adaptive stopping criterion for the Newton method leads to a reliable algorithm. On all adapted meshes, we only need one Newton step in order to get

the linearization error ten times smaller than the discretization error. The values of the error E and the iteration error estimator η_m are almost identical in all cases. This demonstrates the efficiency and the reliability of the fully adaptive algorithm *S III*.

TABLE 6.3: Example 1, iteration with Alg. *S I* (iteration towards round-off error level).

N	#It	E	$\eta_h + \eta_m$	η_h	η_m	$I_{\text{eff}}^{\text{tot}}$
631	6	5.01e-03	5.00e-03	5.00e-03	1.08e-11	0.99
1 605	6	4.27e-03	5.13e-03	5.13e-03	5.57e-12	1.20
4 401	8	2.49e-03	2.53e-03	2.53e-03	6.38e-14	1.02
12 211	10	1.29e-03	1.19e-03	1.19e-03	8.46e-15	0.92
32 679	5	6.45e-04	5.79e-04	5.79e-04	2.17e-11	0.90
87 069	7	3.06e-04	2.84e-04	2.84e-04	1.42e-14	0.93
222 193	6	1.30e-04	1.35e-04	1.35e-04	4.68e-13	1.04

TABLE 6.4: Example 1, iteration with Alg. *S II* (adaptive stopping rule for the Newton iteration)

N	#It	E	$\eta_h + \eta_m$	η_h	η_m	$I_{\text{eff}}^{\text{tot}}$
631	2	5.01e-03	5.00e-03	5.00e-03	2.50e-05	0.99
1 605	1	4.27e-03	4.72e-03	5.13e-03	4.04e-04	1.11
4 401	2	2.49e-03	2.54e-03	2.53e-03	8.31e-06	1.02
12 211	1	1.29e-03	1.10e-03	1.19e-03	9.13e-05	0.85
32 679	1	6.45e-04	5.43e-04	5.78e-04	3.58e-05	0.84
87 069	1	3.06e-04	2.66e-04	2.84e-04	1.79e-05	0.87
222 193	1	1.30e-04	1.27e-04	1.35e-04	8.00e-06	0.98

Finally, we compare the algorithm *S II* with an algebraic stopping criterion in the inner iteration with the method *S III* which uses an adaptive stopping rule for the multigrid solver and the error for the dual problem. To this end, we consider the number of linear iterations needed on each mesh by both methods. The corresponding results are shown in Fig. 6.3. On all meshes in algorithm *S III*, we only need approximately 10 linear iterations in order to fulfill the adaptive stopping criterion. The method *S II* needs over 20 iterations in order to reduce the linear residual by the factor 10^{-11}.

TABLE 6.5: Example 1, iteration with Alg. *S III* (fully adaptive Newton iteration)

N	#It	E	$\eta_h + \eta_m$	η_h	η_m	$I_{\text{eff}}^{\text{tot}}$
631	2	5.01e-03	5.00e-03	5.00e-03	8.43e-06	0.99
1 605	1	4.27e-03	4.72e-03	5.13e-03	4.03e-04	1.10
4 401	2	2.49e-03	2.33e-03	2.52e-03	1.93e-04	0.94
12 211	1	1.29e-03	1.11e-03	1.19e-03	7.22e-05	1.03
32 679	1	6.45e-04	5.45e-04	5.78e-04	3.32e-05	0.86
87 069	1	3.06e-04	2.69e-04	2.84e-04	1.57e-05	0.89
222 193	1	1.30e-04	1.29e-04	1.35e-04	6.61e-06	0.99

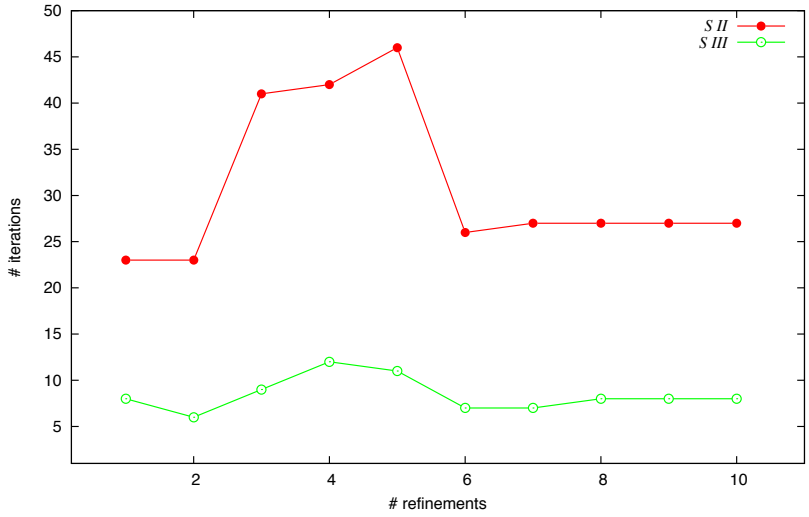

FIGURE 6.3: Example 1, number of interior linear iterations in dependence of refinement number.

6.2.2. Example 2

As described in Chapter 4, Section 4.2 neglecting the scattering in radiative transfer models may lead to large errors in computed measurements. Furthermore, the segmentation of clouds is needed for parametrization of wet deposition processes. Due to these reasons, it is customary to analyze the supplied cloud maps. This analysis can be carried out by application of image segmentation techniques. In this example, we show the efficiency of the adaptive algorithm applied to the task of simultaneous noise reduction and cloud segmentation from satellite observations.

We consider the minimization of the so-called Mumford-Shah functional

$$\mathcal{M}(u_1, S) := \frac{\gamma_1}{2} \int_{\Omega} (u_1 - g)^2 \, dx + \frac{\gamma_2}{2} \int_{\Gamma \setminus S} |\nabla u_1|^2 \, dx + \alpha \mathcal{H}^{d-1}(S). \tag{6.23}$$

Here, $\Omega \subset \mathbb{R}^d$ is the image domain with boundary Γ, $g \in L^\infty(\Omega)$ the perturbed image

intensity, $\mathcal{H}^{d-1}$ the one-dimensional Hausdorff measure, S the edge collection, γ_1, γ_2, and α are positive weights. We seek a smooth representation u_1 of g and an edge set S. In Ambrosio and Tortorelli [3] the functional $\mathcal{M}(\cdot,\cdot)$ is described by a sequence of elliptic functionals, which are defined by

$$\mathcal{E}_k(u) = \frac{\gamma_1}{2}\int\limits_{\Omega}(u_1-g)^2\,dx+\frac{\gamma_2}{2}\int\limits_{\Omega}(u_2^2+k_\epsilon)|\nabla u_1|^2\,dx+\alpha\int\limits_{\Omega}\left(\epsilon\,|\nabla u_2|^2+\frac{(1-u_2)^2}{4\epsilon}\right)dx, \quad (6.24)$$

for $u := (u_1, u_2)$ with small numbers $\epsilon \ll 1$ and $k_\epsilon \ll 1$. In this formulation the edge set S is described by a phase field $u_2(x)$ which is supposed to be small on S and close to one apart from edges.

The Euler-Lagrange equations corresponding to the energy functional (6.24) are given by

$$\begin{aligned} -\gamma_2\nabla\cdot\Big((u_2^2+k_\varepsilon)\nabla u_1\Big)+\gamma_1\,(u_1-g) &= 0 \quad \text{in } \Omega,\\ \partial_n u_1 &= 0 \quad \text{on } \Gamma,\\ -\epsilon\,\Delta u_2+\frac{\gamma_2}{2\alpha}\,|\nabla u_1|^2\,u_2+\frac{1}{4\epsilon}(u_2-1) &= 0 \quad \text{in } \Omega,\\ \partial_n u_2 &= 0 \quad \text{on } \Gamma. \end{aligned} \quad (6.25)$$

We set as solution space $V := H^1(\Omega)$. For the weak formulation of system (6.25), we introduce for all $\Phi = (\phi, \psi) \in V \times V$ the semilinear form

$$\begin{aligned} A(u)(\Phi) :=& (\gamma_2(u_2^2+k_\varepsilon)\nabla u_1, \nabla\phi) + (\gamma_1\,(u_1-g),\phi)\\ &+ (\varepsilon\nabla u_2, \nabla\psi) + \frac{\gamma_2}{2\alpha}(|\nabla u_1|^2\,u_2, \psi) + \frac{1}{4\epsilon}(u_2-1,\psi). \end{aligned}$$

Then, the corresponding weak formulation of system (6.25) seeks $u = (u_1, u_2) \in V \times V$ satisfying

$$A(u)(\Phi) = 0 \quad \forall \Phi = (\phi,\psi) \in V \times V. \quad (6.26)$$

As the input image, we consider a cloud map created by NASA's Earth observatory which is disturbed by ten percent, as can be seen in Figure 6.4. We consider the error functional given by the integral of the second component of the solution representing the contours of the clouds

$$J(u) := \int\limits_{\Omega} u_2(x)\,dx.$$

In this case the application of the DWR method corresponds to the formulation of an outer optimization problem, where the inner problem is given by the minimization of functional (6.24). The outer dual problem reads as follows: Find $z = (z_1, z_2)$, such that

$$\begin{aligned} (\gamma_2(u_2^2+k_\epsilon)\nabla z_1, \nabla\phi) + (\gamma_1\,z_1,\phi) + \frac{\gamma_2}{2}(u_2\nabla u_1\,z_2, \nabla\phi) = 0,\\ \epsilon(\nabla z_2,\nabla\psi) + 2\gamma_2(u_2\nabla u_1\nabla z_1,\psi) + \frac{\gamma_2}{2}(|\nabla u_1|^2 z_2,\psi) + \frac{1}{4\epsilon}(z_2,\psi) = (1,\psi), \end{aligned} \quad (6.27)$$

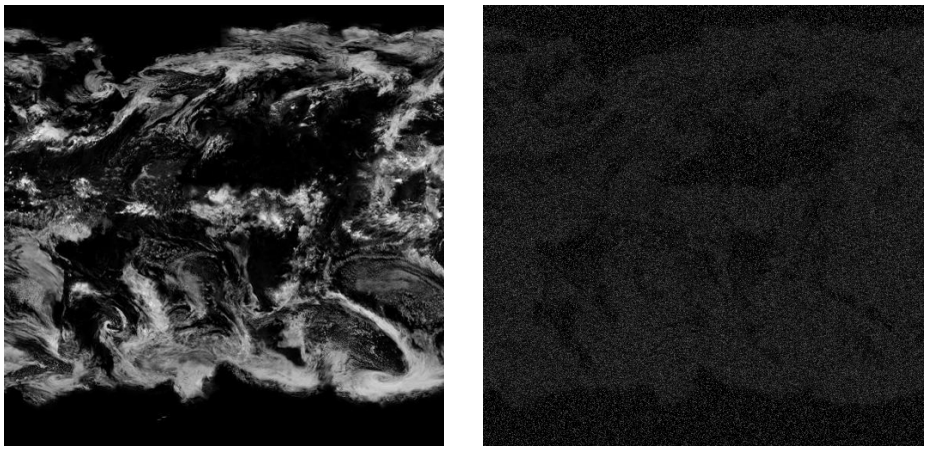

FIGURE 6.4: Example 2, cloud map observed by a satellite (source: NASA's Earth Observatory, data from public domain): original image (left), Gaussian noise added to the cloud map (right)

for all $\Phi = (\phi, \psi) \in V \times V$. We discretize the primal and dual systems by continuous Galerkin finite elements as described in Chapter 3, Section 3.2.

For substantiating the capabilities of the presented goal-oriented adaptive algorithm, we additionally introduce a heuristic error estimator based on the energy functional (6.24). To this end, using the "exact" discrete solution $u_h \in V_h$ and Galerkin orthogonality, we observe for the error $e_h := u - u_h$:

$$\|e\|_A := A(e_h, e_h) = A(e, u - \tilde{u}_h), \tag{6.28}$$

where $\tilde{u}_h$ denotes the approximated discrete solution. We use this identity for the construction of the error estimator

$$\eta_A := A(I_{2h}^{(2)} \tilde{u}_h - \tilde{u_h})(I_{2h}^{(2)} \tilde{u}_h - \tilde{u_h}). \tag{6.29}$$

The error estimator is localized employing the procedure described in Subsection 6.1.2.

The discrete problems are solved using the Newton method with a multigrid solver with V-cycle with two ILU-step for pre- and post-smoothing for the inner iteration. Due to the jumps of the solution along the contours the solution method may become unstable. In order to circumvent this problem, we formulate the Newton algorithm as a homotopy method. To this end, the computational mesh is successively coarsened. The resulting mesh hierarchy is then used in order to compute the starting values for the next refined mesh.

Although the image has many details, we show that the use of goal-oriented refined meshes leads to a significant computational reduction. To this end, we consider the solution processes on locally and uniformly refined meshes. In order to access the "exact" solution, we employ the Newton method on the uniformly refined hierarchy of meshes. The finest mesh is then given by the original resolution of 512×512 pixels of the cloud map where each pixel corresponds to two degrees of freedom. Figure 6.6 shows the logarithmic plot of

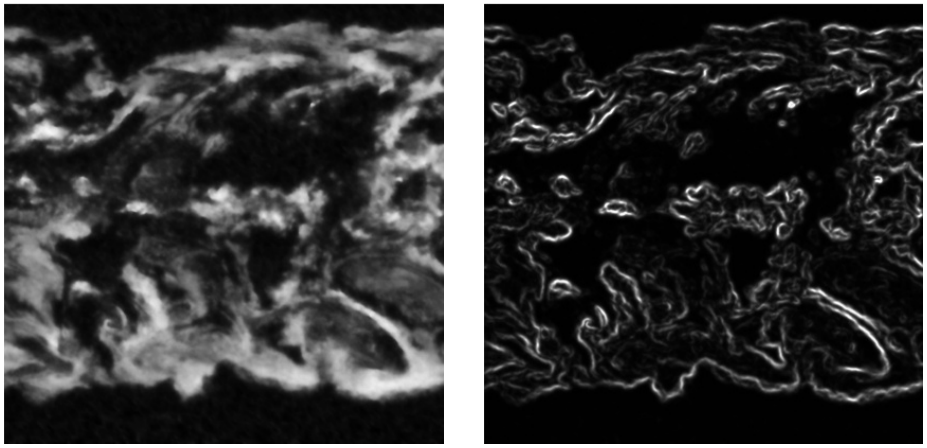

FIGURE 6.5: Example 2, computational results: reconstructed smoothed cloud map (left), and the corresponding contour solution (right)

error values in dependence of the degrees of freedom. Thus, with the chosen parameters, we achieve an accuracy of $|E| = 5 \cdot 10^{-4}$. In the case of uniformly refined meshes, we need to compute the solution on a mesh with 262 144 nodes. The computational process with the refinement based on the heuristic error estimator requires a mesh with 162 177 nodes. The goal-oriented refinement produces meshes which are strongly locally refined along the contours of the clouds (see Figure 6.7). In this case a mesh with 88 591 nodes is sufficient in order to calculate the solution with the same accuracy. The corresponding solution is shown in Figures 6.5.

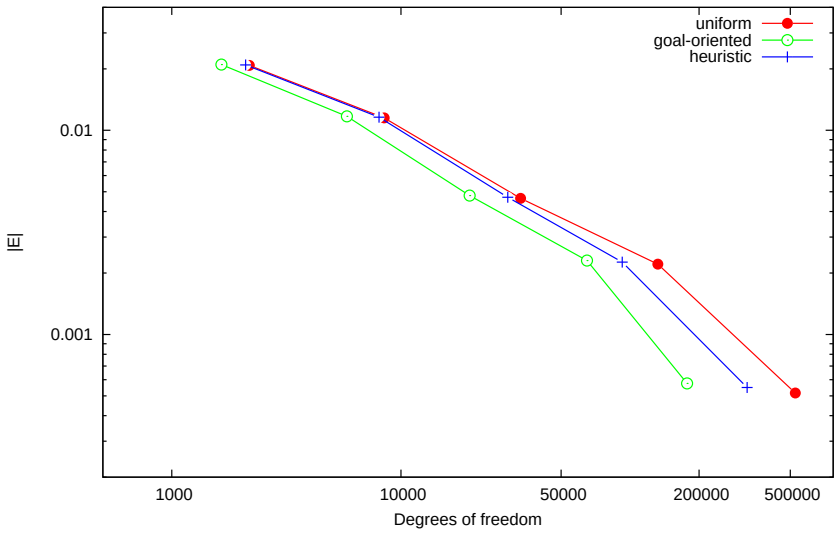

FIGURE 6.6: Example 2, error values E for uniformly and locally refined meshes

In order to show the reliability of the adaptive algorithms, we consider the effectivity indices of the derived error estimators on the locally refined meshes with 2 905 and 32 417 nodes. The corresponding values are shown in Tables 6.6 and 6.7, respectively.

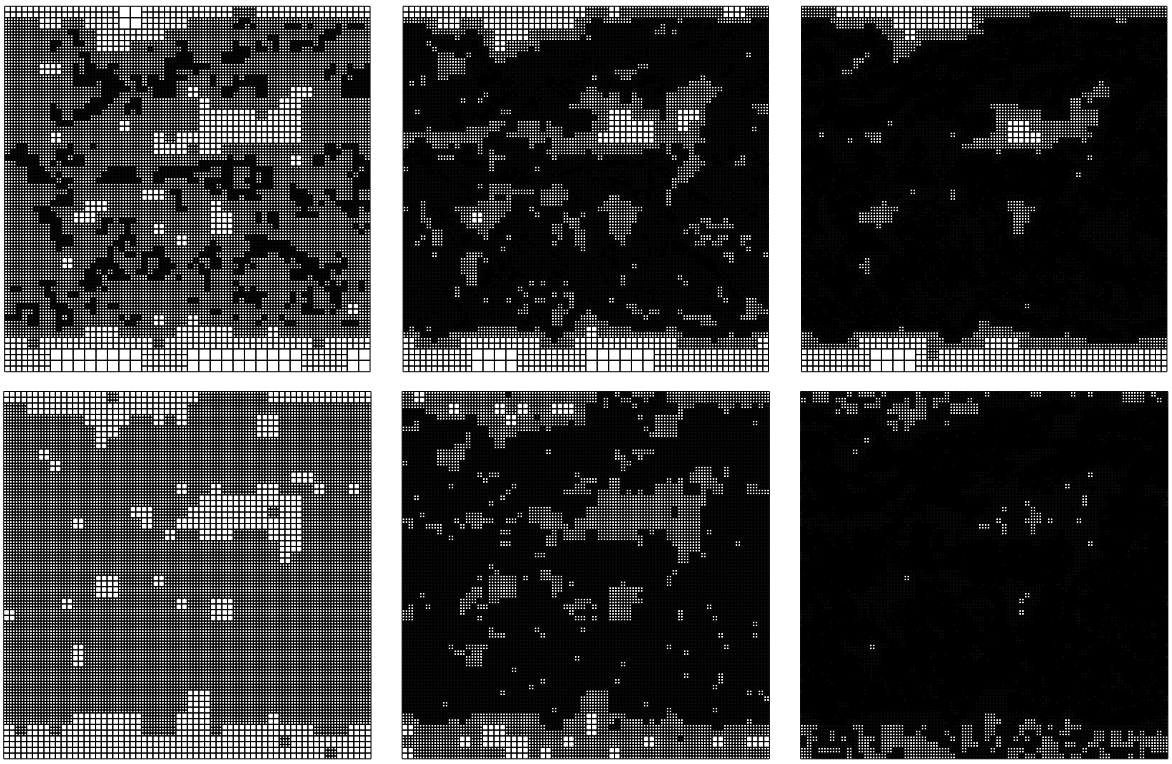

FIGURE 6.7: Example 2, goal-oriented refined meshes (top row) and meshes refined by the help of the heuristic error estimator η_A (bottom row)

TABLE 6.6: Example 2, effectivity of the error estimators for discretization and "exact" Newton iteration on a coarse mesh with 2 905 nodes.

It	E_h	η_h	I^h_{eff}	E_m	η_m	I^m_{eff}
1	1.17e-02	3.73e-03	0.32	1.49e-02	1.50e-02	1.01
2	1.17e-02	1.04e-02	0.89	2.67e-05	2.84e-05	1.06
3	1.17e-02	1.03e-02	0.88	2.28e-08	2.28e-08	1.00
4	1.17e-02	1.03e-02	0.88	1.24e-13	1.24e-13	1.00
5	1.17e-02	1.03e-02	0.88	0.00e+00	1.30e-18	inf

Next, we compare the computational time needed by different algorithms. At the first sight, the use of the DWR error estimation leads to a system of double size. However, the

TABLE 6.7: Example 2, effectivity of the error estimators for discretization and "exact" Newton iteration on a fine mesh with 32 417 nodes.

It	E_h	η_h	I_{eff}^h	E_m	η_m	I_{eff}^m
1	2.30e-03	3.27e-03	1.42	3.40e-03	3.36e-03	0.98
2	2.30e-03	2.04e-03	0.89	2.86e-05	2.86e-05	1.00
3	2.30e-03	2.02e-03	0.88	7.11e-07	7.33e-07	0.97
4	2.30e-03	2.03e-03	0.89	2.45e-08	2.58e-08	0.95
5	2.30e-03	2.02e-03	0.89	2.99e-11	2.90e-11	1.03
6	2.30e-03	2.02e-03	0.89	6.00e-16	6.12e-16	0.98
7	2.30e-03	2.02e-03	0.89	5.67e-21	1.89e-19	0.03

dual equation (6.27) is linear and corresponds to only one additional Newton step if we use the computed primal variables. Figure 6.8 depicts the CPU time for the algorithms based on optimized and uniformly refined meshes.

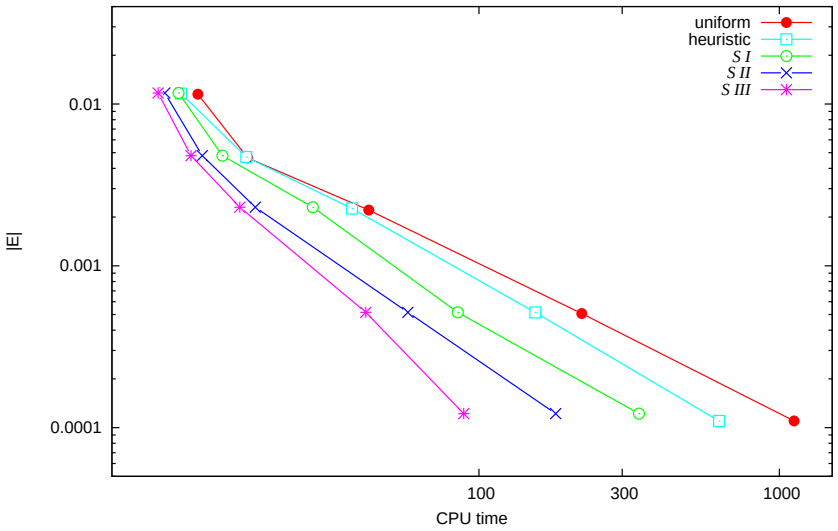

FIGURE 6.8: Example 2, comparison of the CPU time

The results show that the use of goal-oriented refined meshes (alg. $S\ I$) leads to an approximately two times faster method compared to the solution process on meshes refined by the help of the heuristic error estimator η_A. Compared to the solution method based on uniformly refined meshes, algorithm $S\ I$ is approximately three times faster. Furthermore, the algorithm $S\ II$ clearly outperforms the method $S\ I$ with an algebraic stopping criterion and is approximately two times faster. The use of the adaptive stopping criterion for the inner Newton iteration leads additionally to a double reduction of the computational effort.

Finally, we demonstrate the whole history of the solution process on goal-oriented refined meshes. The corresponding values are shown in Tables 6.8, 6.9, and 6.10. The error values E and the values of the error estimators show the reliability of the adaptive algorithms.

TABLE 6.8: Example 2, fully converged "exact" Newton iteration ($S\,I$).

N	#It	E	$\eta_h + \eta_m$	η_h	η_m	I_{eff}^{tot}
81	4	3.10e-02	2.65e-02	2.65e-02	6.97e-18	0.85
233	4	2.86e-02	5.74e-03	5.74e-03	3.68e-18	0.20
823	5	2.10e-02	8.32e-03	8.32e-03	3.35e-18	0.40
2905	5	1.17e-02	1.03e-02	1.03e-02	1.30e-18	0.88
9967	6	4.79e-03	4.37e-03	4.37e-03	5.44e-19	0.91
32417	7	2.30e-03	2.02e-03	2.02e-03	1.89e-19	0.88

TABLE 6.9: Example 2, "exact" Newton iteration with adaptive stopping criterion ($S\,II$).

N	#It	E	$\eta_h + \eta_m$	η_h	η_m	I_{eff}^{tot}
81	2	3.10e-02	2.65e-02	2.65e-02	5.47e-09	0.85
233	2	2.86e-02	5.74e-03	5.74e-03	2.05e-07	0.20
823	2	2.10e-02	8.34e-03	8.35e-03	7.46e-06	0.40
2905	2	1.17e-02	1.04e-02	1.04e-02	2.84e-05	0.89
9967	2	4.81e-03	4.61e-03	4.61e-03	1.61e-06	0.96
32417	2	2.34e-03	2.08e-03	2.04e-04	2.86e-05	0.89

TABLE 6.10: Example 2, "inexact" Newton iteration with adaptive stopping criterion ($S\,III$).

N	#It	E	$\eta_h + \eta_m$	η_h	η_m	I_{eff}^{tot}
81	2	3.10e-02	2.65e-02	2.65e-02	3.27e-09	0.85
233	2	2.86e-02	5.74e-03	5.74e-03	2.00e-07	0.20
823	2	2.10e-02	8.34e-03	8.35e-03	7.45e-06	0.40
2905	2	1.17e-02	1.04e-02	1.04e-02	2.84e-05	0.89
9967	2	4.81e-03	4.61e-03	4.61e-03	1.61e-06	0.96
32417	2	2.34e-03	2.08e-03	2.04e-04	2.86e-05	0.89

In order to compare the algorithms *S II* and *S III*, we consider the amount of the linear iterations needed for satisfying the corresponding stopping rule for the multigrid solver. The results are shown in Figure 6.9. In algorithm *S III*, we only need approximately 5-7 iterations in order to get the linear residual $\langle r_k, \tilde{z}_k \rangle$ ten times smaller than the linearization error estimator. For the method *S II* with the algebraic stopping criterion, we need approximately 16 linear iterations on each refinement level.

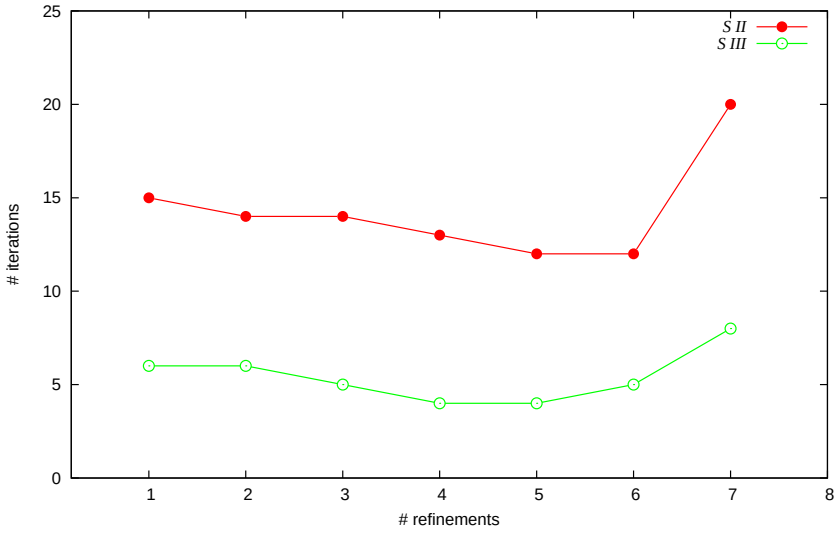

FIGURE 6.9: Example 2, number of linear iterations in dependence of refinement number

6.3. Application to the Tikhonov regularization

In this section, we derive the discretization and iteration error estimators for stationary inverse problems regularized by Tikhonov-type methods and solved by Newton algorithms as described in Chapter 5, Section 5.3. For the Newton-Lagrange method, we refine the iteration error estimator and separate it into contributions from the inner and outer iterations. On the basis of the error representations, we develop an adaptive method where the different error contributions are balanced. Most of the arguments are similar to those in the preceding sections.

We consider general (elliptic) optimal control problem (5.48, 5.49)

$$\min_{\{u,q\}\in V\times Q} J(u,q) = J_1(u) + J_2(q), \tag{6.30}$$

subject to

$$A(u,q)(\phi) = 0 \quad \text{for all } \psi \in V, \tag{6.31}$$

with cost functional $J(\cdot,\cdot)$ and a semilinear form $A(\cdot,\cdot)(\cdot)$. For simplicity, we assume the state space V and the control space Q to be Hilbert spaces. We assume that there is a locally unique minimum $\{u,q\} \in V \times Q$, which corresponds to a saddle-point of the Lagrange functional (5.52)

$$\mathcal{L}(u,q,z) = J(u,q) - A(u,q)(z).$$

In contrast to notation in (5.52), we denote the corresponding adjoint state by $z \in V$ indicating the dual variable in the DWR method. The triplet $\{u,q,z\} \in V \times Q \times V$ is determined by the first order optimality condition (5.53, 5.54, 5.55), which we state for convenience again:

$$\mathcal{L}'_u(u,q,z)(\cdot) = 0 \quad \Leftrightarrow \quad J'_1(u)(\psi) - A'_u(u,q)(\psi,z) = 0 \quad \forall \psi \in V, \tag{6.32}$$
$$\mathcal{L}'_q(u,q,z)(\cdot) = 0 \quad \Leftrightarrow \quad J'_2(q)(\varphi) - A'_q(u,q)(\varphi,z) = 0 \quad \forall \varphi \in Q, \tag{6.33}$$
$$\mathcal{L}'_z(u,q,z)(\cdot) = 0 \quad \Leftrightarrow \quad -A(u,q)(\phi) = 0 \quad \forall \phi \in V. \tag{6.34}$$

We consider the correction equations given by the Newton update (5.58), which are defined by the help of the Hessian operator $H(\cdot)(\cdot)$ in (5.56). Thus, the Newton correction equations are explicitly given by

$$\mathcal{L}''_{uu}(x^n)(\psi,\delta u^n) + \mathcal{L}''_{uq}(x^n)(\psi,\delta q^n) + \mathcal{L}''_{uz}(\psi,\delta z^n) = -\mathcal{L}'_u(x^n)(\psi), \tag{6.35}$$
$$\mathcal{L}''_{qu}(x^n)(\varphi,\delta u^n) + \mathcal{L}''_{qq}(x^n)(\varphi,\delta q^n) + \mathcal{L}''_{qz}(\varphi,\delta z^n) = -\mathcal{L}'_q(x^n)(\varphi), \tag{6.36}$$
$$\mathcal{L}''_{zu}(x^n)(\phi,\delta u^n) + \mathcal{L}''_{zq}(x^n)(\phi,\delta q^n) = -\mathcal{L}'_z(x^n)(\phi), \tag{6.37}$$

for all $\{\psi,\varphi,\phi\} \in V \times Q \times V$. The equation for the adjoint correction δz^n reads

$$\begin{aligned} J''_{1,uu}(u^n)(\psi,\delta u^n) - A''_{uu}(u^n,q^n)(\psi,\delta u^n,z^n) - A''_{uq}(u^n,q^n)(\psi,\delta q^n,z^n) \\ - A'_u(u^n,q^n)(\psi,\delta z^n) \;= A'_u(u^n,q^n)(\psi,z^n) - J'_{1,u}(u^n)(\psi), \end{aligned} \tag{6.38}$$

for all $\psi \in V$, where we have used the fact that $J''_{1,uq}(u)(\psi,\delta q^n) = 0$ and that the adjoint problem is linear, i.e., $A''_{uz}(u^n,q^n)(\psi,\delta z^n,\cdot) = A'_u(u^n,q^n)(\psi,\delta z^n)$. Then, the equation for the control correction δq^n takes the form

$$\begin{aligned} -A''_{qu}(u^n,q^n)(\varphi,\delta u^n,z^n) + J''_{2,qq}(q^n)(\varphi,\delta q^n) - A'_q(u^n,q^n)(\varphi,\delta z^n) \\ - A''_{qq}(u^n,q^n)(\varphi,\delta q^n,z^n) = A'_q(u^n,q^n)(\varphi,z^n) - J'_{2,q}(q^n)(\varphi), \end{aligned} \tag{6.39}$$

for all $\varphi \in Q$, where we have used $J''_{2,qu}(q^n)(\varphi,\delta u^n) = 0$ and the linearity of the control equation with respect to z, i.e., $A''_{qz}(u^n,q^n)(\varphi,\delta z^k,\cdot) = A'_q(u^n,q^n)(\varphi,\delta z^n)$. Finally, the equation for the primal correction δu^n is

$$-A'_u(u^n,q^n)(\delta u^n,\phi) - A'_q(u^n,q^n)(\delta q^n,\phi) = A(u^n,q^n)(\phi) \quad \forall \phi \in V. \tag{6.40}$$

The derivation of the error representation with respect to the cost functional is similar to Proposition 6.1.1.

PROPOSITION 6.3.1. *Let* $\{\tilde{u}_h, \tilde{q}_h, \tilde{z}_h\} \in V_h \times Q_h \times V_h$ *be an approximation to the solution* $\{u, q, z\} \in V \times Q \times V^*$ *of the KKT system (6.32) - (6.34) obtained by any iterative process on the mesh* $\mathcal{T}_h$ *. Then, there holds the following error representation:*

$$\begin{aligned} J(u,q) - J(\tilde{u}_h, \tilde{q}_h) = \tfrac{1}{2}\rho^*(\tilde{u}_h, \tilde{q}_h, \tilde{z}_h)(u - \tilde{u}_h) + \tfrac{1}{2}\rho^q(\tilde{q}_h, \tilde{z}_h)(q - \tilde{q}_h) \\ + \tfrac{1}{2}\rho(\tilde{u}_h, \tilde{q}_h)(z - \tilde{z}_h) - \rho(\tilde{u}_h, \tilde{q}_h)(\tilde{z}_h) + \mathcal{R}_h^{(3)}, \end{aligned} \tag{6.41}$$

where the residual terms are given by

$$\begin{aligned} \rho^*(\tilde{u}_h, \tilde{q}_h, \tilde{z}_h)(\cdot) &:= J_1'(\tilde{u}_h)(\cdot) - A_u'(\tilde{u}_h, \tilde{q}_h)(\cdot, \tilde{z}_h), \\ \rho^q(\tilde{q}_h, \tilde{z}_h)(\cdot) &:= J_2'(\tilde{q}_h)(\cdot) - A_q'(\tilde{u}_h, \tilde{q}_h)(\cdot, \tilde{z}_h), \\ \rho(\tilde{u}_h, \tilde{q}_h)(\cdot) &:= -A(\tilde{u}_h, \tilde{q}_h)(\cdot), \end{aligned}$$

and the remainder term $\mathcal{R}_h^{(3)}$ *is cubic in the errors* $e^u := u - \tilde{u}_h$, $e^q := q - \tilde{q}_h$, *and* $e^z := z - \tilde{z}_h$.

PROOF. Setting $e := x - \tilde{x}_h$ there holds

$$L(x) - L(\tilde{x}_h) = \int_0^1 L'(\tilde{x} + s\, e)(e)\, ds.$$

Using the general error representation for the trapezoidal rule

$$\int_0^1 f(s)\, ds = \tfrac{1}{2}(f(0) + f(1)) + \tfrac{1}{2}\int_0^1 f''(s)\, s\, (s-1)\, ds,$$

and observing that for $\delta y = \{\delta u, \delta q, \delta z\} \in V \times Q \times V$

$$L'(x)(y) = L_u'(x)(\delta u) + L_q'(x)(\delta q) + L_z'(x)(\delta z),$$

we conclude

$$L(x) - L(\tilde{x}_h) = \tfrac{1}{2}L'(\tilde{x}_h)(x - \tilde{x}_h) + \mathcal{R}_h^{(3)}.$$

Hence, recalling the particular structure of the functional $L(\cdot)$ and observing that u satisfies the state equation,

$$\begin{aligned} J(u,q) - J(\tilde{u}_h, \tilde{q}_h) &= L(x) + A(u,q)(z) - L(\tilde{x}_h) - A(\tilde{u}_h, \tilde{q}_h)(\tilde{z}_h) \\ &= L(x) - L(\tilde{x}_h) - A(\tilde{u}_h, \tilde{q}_h)(\tilde{z}_h) \\ &= \tfrac{1}{2}L'(\tilde{x}_h)(x - \tilde{x}_h) + \mathcal{R}_h^{(3)} - A(\tilde{u}_h, \tilde{q}_h)(\tilde{z}_h). \end{aligned}$$

Then, observing that for $y = \{\psi, \varphi, \phi\}$,

$$\begin{aligned} L'(\tilde{x}_h)(y) = J_1'(\tilde{u}_h)(\psi) - A_u'(\tilde{u}_h, \tilde{q}_h)(\psi, \tilde{z}_h) + J_2'(\tilde{q}_h)(\varphi) - A_q'(\tilde{u}_h, \tilde{q}_h)(\varphi, \tilde{z}_h) \\ - A(\tilde{u}_h, \tilde{q}_h)(\phi), \end{aligned}$$

the assertion follows. □

The separated error representation of the above proposition can be directly used as stopping criterion for the direct Newton method for optimization problems. The structure of the Lagrange-Newton method allows to refine the iteration error and to separate it into contributions from the outer and inner iterations.

Next, we analyze the error caused by solving the correction equations in Lagrange-Newton method only approximately. Let $x_h^n = \{u_h^n, q_h^n, z_h^n\} \in V_h \times Q_h \times V_h$ be the n-th Newton iterates on the discrete level $\mathcal{T}_h$. These are obtained by solving the discrete analogues of the Newton equations (5.57) only approximately by any linear iteration process, e.g., a multigrid method. To the corresponding approximate corrections $\widetilde{\delta x}_h^n = \{\widetilde{\delta u}_h^n, \widetilde{\delta q}_h^n, \widetilde{\delta z}_h^n\}$, we associate the linear iteration residuals

$$\begin{aligned}
\langle d_h^n, \cdot\rangle &:= -A'_u(u_h^n, q_h^n)(\cdot, z_h^n) + J'_{1,u}(u_h^n)(\cdot) + J''_{1,uu}(u_h^n)(\cdot, \widetilde{\delta u}_h^n) \\
&\quad - A''_{uu}(u_h^n, q_h^n)(\cdot, \widetilde{\delta u}_h^n, z_h^n) - A''_{uq}(u_h^n, q_h^n)(\cdot, \widetilde{\delta q}_h^n, z_h^n) - A'_u(u_h^n, q_h^n)(\cdot, \widetilde{\delta z}_h^n), \\
\langle g_h^n, \cdot\rangle &:= -A'_q(u_h^n, q_h^n)(\cdot, z_h^n) + J'_{2,q}(q_h^n)(\cdot) - A''_{qu}(u_h^n, q_h^n)(\cdot, \widetilde{\delta u}_h^n, z_h^n) \\
&\quad + J''_{2,qq}(q_h^n)(\cdot, \widetilde{\delta q}_h^n) - A'_q(u_h^n, q_h^n)(\cdot, \widetilde{\delta z}_h^n) - A''_{qq}(u_h^n, q_h^n)(\cdot, \widetilde{\delta q}_h^n, z_h^n), \\
\langle r_h^n, \cdot\rangle &:= -A(u_h^n, q_h^n)(\cdot) - A'_u(u_h^n, q_h^n)(\widetilde{\delta u}_h^n, \cdot) - A'_q(u_h^n, q_h^n)(\widetilde{\delta q}_h^n, \cdot).
\end{aligned}$$

In order to derive an adaptive stopping criterion for the inner linear iteration in the Newton steps, we consider the difference between two approximate Newton iterates: $x_h^{n+1} := x_h^n + \widetilde{\delta x}_h^n$ and x_h^n. For the corresponding error in the cost functional, we obtain by Taylor expansion:

$$\begin{aligned}
J(u_h^{n+1}, q_h^{n+1}) - J(u_h^n, q_h^n) &= J(u_h^n + \widetilde{\delta u}_h^n, q_h^n + \widetilde{\delta q}_h^n) - J(u_h^n, q_h^n) \\
&= J'_{1,u}(u_h^n)(\widetilde{\delta u}_h^n) + J'_{2,q}(q_h^n)(\widetilde{\delta q}_h^n) \\
&\quad + \tfrac{1}{2} J''_{1,uu}(u_h^n)(\widetilde{\delta u}_h^n, \widetilde{\delta u}_h^n) + \tfrac{1}{2} J''_{2,qq}(q_h^n)(\widetilde{\delta q}_h^n, \widetilde{\delta q}_h^n) \\
&\quad + O\Big(|\widetilde{\delta u}_h^n|^3 + |\widetilde{\delta q}_h^n|^3\Big).
\end{aligned}$$

By the above definitions of the correction residuals there holds

$$\begin{aligned}
J'_{1,u}(u_h^n)(\widetilde{\delta u}_h^n) + J'_{2,q}(q_h^n)(\widetilde{\delta q}_h^n) &= \langle d_h^n, \widetilde{\delta u}_h^n\rangle + A'_u(u_h^n, q_h^n)(\widetilde{\delta u}_h^n, z_h^n) \\
&\quad + \langle g_h^n, \widetilde{\delta q}_h^n\rangle + A'_q(u_h^n, q_h^n)(\widetilde{\delta q}_h^n, z_h^n) \;+\; \mathcal{R}_m,
\end{aligned}$$

with a second-order remainder $\mathcal{R}_m = O(|\widetilde{\delta u}_h^n|^2 + |\widetilde{\delta q}_h^n|^2 + |\widetilde{\delta z}_h^n|)$. Further, by definition, there holds

$$A'_u(u_h^n, q_h^n)(\widetilde{\delta u}_h^n, z_h^n) + A'_q(u_h^n, q_h^n)(\widetilde{\delta q}_h^n, z_h^n) = -\langle r_h^n, z_h^n\rangle - A(u_h^n, q_h^n)(z_h^n).$$

Combining the foregoing equations, we obtain the final result

$$\begin{aligned}
J(u_h^{n+1}, q_h^{n+1}) - J(u_h^n, q_h^n) &= \langle d_h^n, \widetilde{\delta u}_h^n\rangle + \langle g_h^n, \widetilde{\delta q}_h^n\rangle - \langle r_h^n, z_h^n\rangle \\
&\quad - A(u_h^n, q_h^n)(z_h^n) \;+\; O\Big(|\widetilde{\delta u}_h^n|^2 + |\widetilde{\delta q}_h^n|^2\Big).
\end{aligned} \tag{6.42}$$

If the state equation is linear in both the state as well as the control variables, the remainder term vanishes.

From the error representation (6.42) we draw the following conclusions: The difference in the cost functional for two consecutive approximate Newton iterates is essentially bounded by the linearization residual $\rho(u_h^n, q_h^n)(z_h^n)$ and the iteration residuals due to inexact solution of the linear correction equations. These are the leading error terms while the other terms, which are of higher-order in the corrections $\widetilde{\delta u}_h^n$ and $\widetilde{\delta q}_h^n$, can be neglected. Following this philosophy, we propose the following stopping criterion for the linear iteration within the Newton steps: Set

$$\eta_m^{n,\mathrm{out}} := |A(u_h^n, q_h^n)(z_h^n)|, \quad \eta_m^{n,\mathrm{in}} := \max\Big\{|\langle r_h^n, z_h^n\rangle|, |\langle d_h^n, \widetilde{\delta u}_h^n\rangle|, |\langle g^n, \widetilde{\delta q}_h^n\rangle|\Big\},$$

and iterate in the linear correction equations until

$$\eta_m^{n,\mathrm{in}} \leq \kappa\, \eta_m^{n,\mathrm{out}}, \tag{6.43}$$

with a small safety factor $\kappa = 10^{-1}$. Combining this with the stopping rule for the outer nonlinear Newton iteration obtained from Proposition 6.3.1,

$$\eta_m^{n,\mathrm{out}} \leq \kappa \eta_h^n, \tag{6.44}$$

where

$$\eta_h^n := \tfrac{1}{2}\Big|\rho^*(u_h^n, q_h^n, z_h^n)(\Pi_h u_h^n) + \rho^q(q_h^n, z_h^n)(\Pi_h q_h^n) + \rho(u_h^n, q_h^n)(\Pi_h z_h^n)\Big|,$$

we obtain a fully adaptive solution process in which the errors due to discretization as well as outer nonlinear and inner linear iterations are balanced. This strategy has been used in the numerical test discussed below.

We note that the proposed adaptive algorithm can be applied directly to the iterated stationary and nonstationary Tikhonov regularization methods.

6.4. Numerical example

In this section, we show the efficiency of the adaptive algorithm and the reliability of the developed discretization and iteration error estimators. We consider a radiative transfer model, where we aim at the identification of the unknown concentration profile in the case of a single trace gas. We treat the case without scattering. In order to guarantee a unique solvability of the regularized problem, we impose the inequality constraints on the state variable. For handling of these constraints, we use the barrier method. The corresponding optimal control problem is solved by the Newton-Lagrange method.

We consider a simplified model of the radiative transfer equation. We assume a clear sky environment and set the scattering coefficient equals to zero, $\sigma_{s,\nu} = 0$. Furthermore,

we assume that only one trace gas contributes to absorption or emission. Under these assumptions the system under consideration is given by

$$\begin{aligned} \nabla \mathcal{I}(x,\nu) + (q(x)+1)\mathcal{I}(x,\nu) &= f \qquad \text{in } \Omega, \\ \mathcal{I} &= \mathcal{I}^{\text{in}} \qquad \text{on } \Gamma_-, \end{aligned} \tag{6.45}$$

where $f \in L^2(\Omega)$ is supposed to be known. As the solution space for the state $\mathcal{I} \in V$, we set $V = Z$ and for the unknown parameter $Q = L^2(\Omega)$, where Z is given by (4.5). Here, for the sake of brevity, we consider a two-dimensional domain $\Omega := (0,1)^2$ with the boundary Γ, and the inflow part of the boundary given by

$$\Gamma_I = \{x \in \Gamma \,;\, n \cdot n_\Gamma < 0\}.$$

Here, n_Γ denotes the outward point unit vector and $n = (1,1)^T$.

The aim of the computations is to reconstruct the intensity $\mathcal{I}$ and to identify the absorption coefficient $q(x)$ from given distributed measurements $g \in Y$. Thus, the observation operator $\mathcal{C} : V \to Y$ is given as $\mathcal{C} = \text{id}$ and the measurement space as $Y = L^2(\Omega)$. We regularize the inverse problem by introducing the Tikhonov functional and consider the resulting optimal control problem

$$\min J(\mathcal{I}, q) = \frac{1}{2}\|\mathcal{I} - g\|^2 + \frac{\alpha}{2}\|q - q^*\|, \tag{6.46}$$

such that the state equation (6.45) is fulfilled. Since the problem admits a unique solution provided $\mathcal{I}$ does not vanish, we impose an one-sided state constraint and claim

$$\mathcal{I}(x) > \mathcal{I}_a \quad \text{in } \Omega. \tag{6.47}$$

The target is given by $g(x) = 1.01 - \sin(\pi x_1)\sin(\pi x_2)$. For the right-hand side, we prescribe

$$f(x) = \frac{10}{\sqrt{2\pi\sigma^2}} \exp\left(-\frac{1}{2\sigma^2}((x_1 - s_0)^2 + (x_2 - s_1)^2)\right),$$

with $\sigma = 0.49$, $s_0 = \frac{1}{2}$, and $s_1 = \frac{1}{2}$. Furthermore, we set $\mathcal{I}_a = 0$.

In order to solve this state-constrained optimal control problem, we employ an interior point method. Here, the inequality constraint is handled by a penalty/barrier approach, i.e., by adding certain penalty/barrier terms to the cost functional. We use the logarithmic or rational barrier functions

$$l_\gamma(u) := -\gamma \log(u - u_a), \qquad l_\gamma(u) := \frac{\gamma^\kappa}{(\kappa - 1)(u - u_a)^{\kappa - 1}}, \quad \text{for } \kappa > 1.$$

The barrier functional of order κ is constructed by integrating $l_\gamma(u)$ over Ω,

$$b_\gamma(u) := \int_\Omega l_\gamma(u(x))\, dx.$$

With this notation the augmented cost functional is given by

$$J_\gamma(\mathcal{I}, q) = J(\mathcal{I}, q) + b_\gamma(\mathcal{I}). \tag{6.48}$$

For any optimal solution $\{\mathcal{I}, q\} \in V \times Q$ there exists an adjoint solution $z \in V$, such that the triplet $\{u, q, z\} \in V \times Q \times V$ solves the following saddle point system:

$$\begin{aligned} (\nabla\psi, \nabla z) + ((q(x)+1)z, \psi) - (I - g, \psi) &= b'_\gamma(\psi, z) \quad \forall \psi \in V, \\ \alpha(\varphi, q) - (\varphi, \mathcal{I}z) &= 0 \qquad\quad \forall \varphi \in Q, \\ (\nabla\mathcal{I}, \nabla\phi) + ((q+1)\mathcal{I}, \phi) &= (f, \phi) \qquad \forall \phi \in V. \end{aligned} \tag{6.49}$$

Using conforming bilinear $\mathcal{Q}_1$ elements for discretizing of all three variables $\{u, q, z\}$ in associated finite element subspaces $V_h \subset V$ and $Q_h \subset Q$ leads to the discrete saddle point problems

$$\begin{aligned} (\nabla\psi_h, \nabla z_h) + ((q_h+1)z_h, \psi_h) - (\mathcal{I}_h, \psi_h) &= b'_\gamma(\psi_h, z_h) - (g, \psi_h) \quad \forall \psi_h \in V_h, \\ \alpha(\varphi_h, q_h) - (\varphi_h, \mathcal{I}_h z_h) &= 0 \qquad\quad \forall \varphi_h \in Q_h, \\ (\nabla\mathcal{I}_h, \nabla\phi_h) + ((q_h+1)\mathcal{I}_h, \phi_h) &= (f, \phi_h) \qquad \forall \phi_h \in V_h. \end{aligned}$$

Since the state equation and, consequently, the adjoint equation are hyperbolic, standard finite element techniques produce spurious oscillations. In order to cope with this instability, we stabilize both equations by applying the streamline diffusion modification as explained in Chapter 3, Section 3.3.

On the continuous level the barrier method is designed in such a way that the iterates remain feasible. However, this does not necessary hold on the discrete level. One of the possibilities to cope with this difficulty is to perform a pointwise modification of the computed Newton corrections as described in Schiela [105]. Here, we use a simple line search method ensuring that the computed Newton iterates lie in the feasible region. In this numerical test, we use the barrier functional of fourth-order, $\kappa = 4$, and set the parameter $\gamma = 10^{-7}$. Since we assume to be given exact measurements, we set $\alpha = 10^{-7}$. We solve the correction equations again by the multigrid method in V-cycle form with one step of block-ILU pre- and post-smoothing on each mesh level. For the "algebraic" stopping criterion, we require that the initial nonlinear and linear residuals are reduced by the factor 10^{-11}. In order to access the "exact" algebraic errors, we solve the discrete equations on each mesh additionally by the full Newton method.

In this case, boundary layers occur, and the "optimized" meshes obtained by this adaptive solution process are strongly refined near the boundary as shown in Figure 6.10. The corresponding solution reaching the value 0.01 in the middle of the domain and the calculated parameter are shown in Figure 6.11.

First, we examine the sharpness of the developed error estimators. Tables 6.11 and 6.12 show the convergence history on a coarse mesh with only 181 nodes and on a fine mesh with

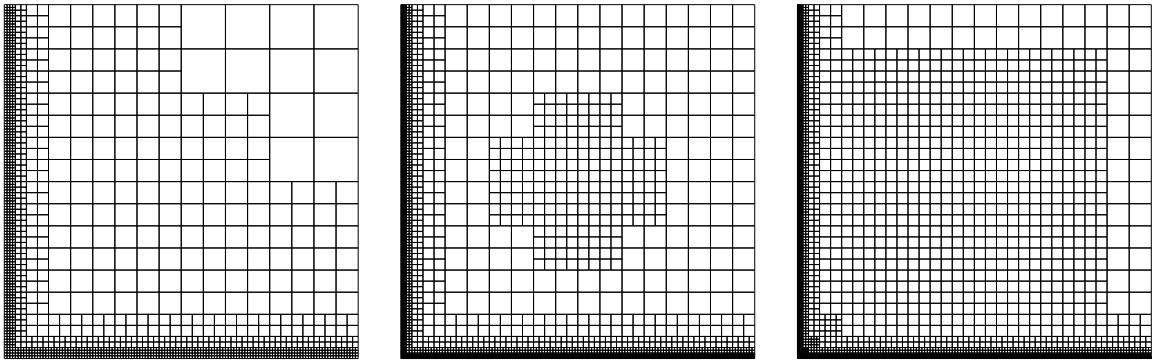

FIGURE 6.10: Example 3, locally refined meshes from the solution process

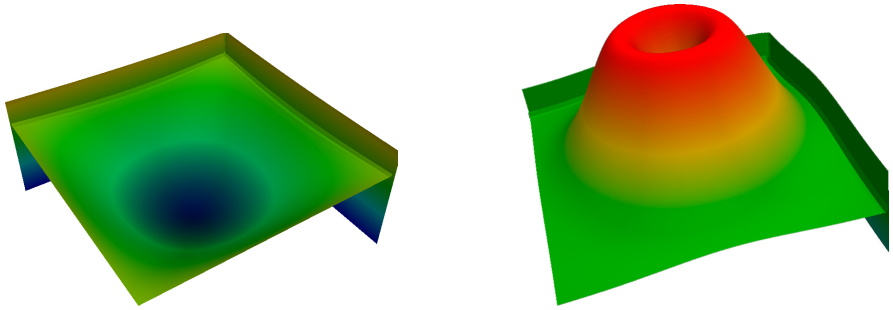

FIGURE 6.11: Example 3, reconstructed intensity with boundary layer (left) and optimal parameter (right).

TABLE 6.11: Example 3, effectivity of the error estimators for discretization and "exact" Newton iteration on a coarse mesh with 181 nodes.

It	E_h	η_h	I^h_{eff}	E_m	η_m	I^m_{eff}
1	1.76e-02	9.59e-03	0.55	1.53e-03	9.97e-07	0.00
2	1.76e-02	8.99e-03	0.51	6.58e-07	6.00e-07	0.91
3	1.76e-02	8.99e-03	0.51	6.98e-11	6.96e-11	1.00
4	1.76e-02	8.99e-03	0.51	3.47e-18	7.59e-18	2.19
5	1.76e-02	8.99e-03	0.51	1.04e-17	4.09e-19	0.04

29 157 nodes, respectively. These results demonstrate that the developed error estimators are efficient and reliable.

Then, in Tables 6.13, 6.14, and 6.15, we report the full history of the solution process for all three algorithms *S I*, *S II*, and *S III*. Finally, Fig. 6.12 shows the number of iterations needed by the multigrid solver in the inner linear iteration in each Newton step in order to fulfill the stopping criterions in the algorithms *S II* and *S III*. Again a substantial work saving is achieved by the adaptive stopping criterions.

TABLE 6.12: Example 3, effectivity of the error estimators for discretization and "exact" Newton iteration on a fine mesh with 29 157 nodes.

It	E_h	η_h	I^h_{eff}	E_m	η_m	I^m_{eff}
1	3.94e-05	9.61e-05	2.43	3.31e-05	5.68e-05	1.72
2	3.94e-05	4.31e-05	1.08	2.51e-07	2.44e-07	0.97
3	3.94e-05	4.27e-05	1.08	8.00e-09	7.98e-09	1.00
4	3.94e-05	4.27e-05	1.08	6.45e-13	6.44e-13	1.00
5	3.94e-05	4.27e-05	1.08	4.05e-17	4.06e-17	1.00

TABLE 6.13: Example 3, fully converged "exact" Newton iteration ($S\ I$).

N	#It	E	$\eta_h + \eta_m$	η_h	η_m	I^{tot}_{eff}
181	5	1.77e-02	9.00e-03	9.00e-03	4.09e-19	0.51
393	5	8.77e-03	4.53e-03	4.53e-03	1.61e-19	0.52
877	5	4.29e-03	2.26e-03	2.26e-03	1.19e-18	0.53
1 785	5	2.05e-03	1.13e-03	1.13e-03	8.71e-19	0.55
3 589	5	9.26e-04	5.60e-04	5.60e-04	1.10e-18	0.60
7 333	5	3.72e-04	2.72e-04	2.72e-04	1.26e-17	0.73
14 721	5	1.09e-04	1.20e-04	1.20e-04	1.54e-18	1.11
29 157	5	3.94e-05	4.27e-05	4.27e-05	4.06e-17	1.08

TABLE 6.14: Example 3, "exact" Newton iteration with adaptive stopping criterion ($S\ II$).

N	#It	E	$\eta_h + \eta_m$	η_h	η_m	I^{tot}_{eff}
181	2	1.77e-02	9.00e-03	9.00e-03	6.05e-07	0.51
393	2	8.77e-03	4.53e-03	4.53e-03	1.35e-07	0.52
877	2	4.29e-03	2.26e-03	2.26e-03	1.87e-07	0.53
1 785	2	2.05e-03	1.13e-03	1.13e-03	2.36e-07	0.55
3 589	1	9.34e-04	5.84e-04	5.67e-04	1.71e-05	0.63
7 333	1	3.78e-04	2.75e-04	2.71e-04	3.18e-05	0.72
14 721	2	1.08e-04	1.26e-04	1.27e-04	7.19e-07	1.18
29 157	2	3.95e-05	4.31e-05	4.29e-05	2.43e-07	1.09

TABLE 6.15: Example 3, "inexact" Newton iteration with adaptive stopping criterion (*S III*).

N	#It	E	$\eta_h + \eta_m$	η_h	η_m	I_{eff}^{tot}
181	2	1.77e-02	9.00e-03	9.00e-03	6.06e-07	0.51
393	2	8.77e-03	4.53e-03	4.53e-03	1.35e-07	0.52
877	2	4.29e-03	2.26e-03	2.26e-03	1.87e-07	0.53
1 785	2	2.05e-03	1.13e-03	1.13e-03	2.36e-07	0.55
3 589	1	9.34e-04	5.84e-04	5.67e-04	1.71e-05	0.63
7 333	1	3.78e-04	2.75e-04	2.72e-04	3.18e-05	0.72
14 721	2	1.08e-04	1.27e-04	1.28e-04	7.25e-07	1.19
29 157	2	3.97e-05	4.32e-05	4.30e-05	2.50e-07	1.09

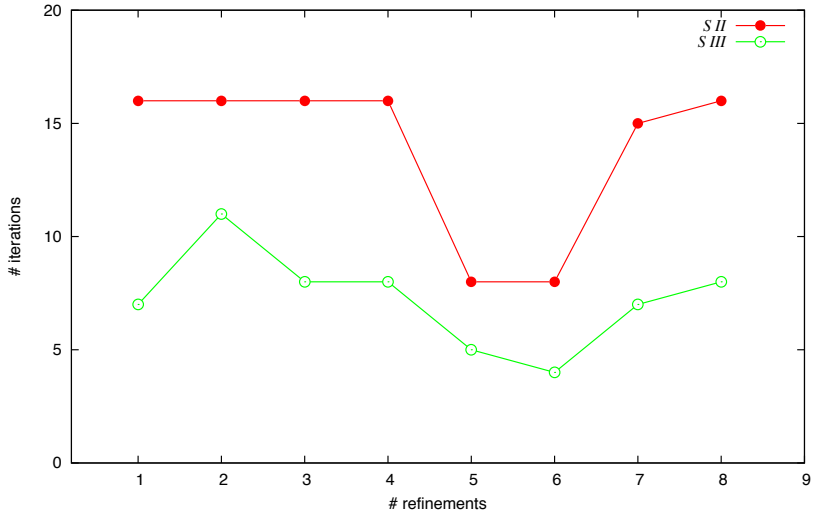

FIGURE 6.12: Example 3, number of linear iterations in dependence of refinement number

6.5. Error estimation for unsteady problems

In this section, we extend the concept of the adaptivity presented for the stationary problems to the nonstationary atmospheric inverse problems regularized by Tikhonov-type methods. For the discretization in time, we first consider the cG(s)dG(r) scheme whereas the extension to the continuous temporal discretization follows by the same arguments. The atmospheric inverse problem (5.72) regularized by the ordinary Tikhonov method is given by the following optimal control problem:

$$\min_{(u,q)\in X\times Q} J(u,q) := J_1(u) + J_2(q), \tag{6.50}$$

subject to

$$(\partial_t u, \phi)_I + a(u,q)(\phi) + (u(0), \phi(0)) = (\chi, \phi(0)) \quad \forall \phi \in X, \tag{6.51}$$

with the semilinear form $a(\cdot,\cdot)(\cdot)$ defined in (5.71) and $q = (\mu, \beta, \chi)$. Here, we keep the Tikhonov functional rather general allowing for different forms of available observations. We associate with problem (6.50, 6.51) the Lagrangian $\mathcal{L} : X \times Q \times X \to I\!R$ defined by

$$\mathcal{L}(u, q, z) := J(u, q) - (\partial_t u, z)_I - a(u, q)(z) + (\chi - u(0), z(0)), \tag{6.52}$$

where $z \in X$ denotes the associated adjoint state corresponding to the dual variable in the DWR method.

We aim at the separation of the total error into contributions due to the discretization and the iterative solution of the algebraic systems. To this end, we consider the different levels of the discretization of problem (6.50, 6.51). So the pure time discretized problem is given by

$$\min_{(u_k,q_k)\in\tilde{X}_k^r\times Q} J(u_k, q_k), \quad \text{subject to the state equation (3.1).} \tag{6.53}$$

The corresponding Lagrangian $\tilde{\mathcal{L}} : \tilde{X}_k^r \times Q \times \tilde{X}_k^r \to I\!R$ is defined as

$$\begin{aligned}\tilde{\mathcal{L}}(u_k, q_k, z_k) := J(u_k, q_k) &- \sum_{m=1}^{M} (\partial_t u_k, z_k)_{I_m} - a(u_k, q_k)(z_k) \\ &- \sum_{m=0}^{M-1} ([u_k]_m, z_{k,m}^+) + (\chi_k - u_{k,0}^-, z_{k,0}^-).\end{aligned} \tag{6.54}$$

The space-time discretized problem with parameter q kept not discretized reads as follows:

$$\min_{(u_{kh},q_{kh})\in\tilde{X}_{k,h}^{r,s}\times Q} J(u_{kh}, q_{kh}), \quad \text{subject to the state equation (3.4).} \tag{6.55}$$

Finally, the fully discrete problem is given by

$$\min_{(u_\sigma,q_\sigma)\in\tilde{X}_{k,h}^{r,s}\times Q_d} J(u_\sigma, q_\sigma), \quad \text{subject to the state equation (3.4).} \tag{6.56}$$

The Lagrange functionals associated with problems (6.55) and (6.56) are given analogously to (6.54) by adding the index h or replacing the index k by σ respectively. Then, we split the total error as follows:

$$\begin{aligned}J(u, q) - J(\tilde{u}_\sigma, \tilde{q}_\sigma) = J(u, q) &- J(u_k, q_k) \\ &+ J(u_k, q_k) - J(u_{kh}, q_{kh}) \\ &+ J(u_{kh}, q_{kh}) - J(\tilde{u}_\sigma, \tilde{q}_\sigma),\end{aligned}$$

where $(\tilde{u}_\sigma, \tilde{q}_\sigma)$ denotes the approximative solution of problem (6.56). We cite the following abstract result from Meidner [81] (see also Becker & Rannacher [17]).

LEMMA 6.5.1. *Let Y be a function space and L a three times Gâteaux differentiable functional on Y. Let y_1 be a stationary point of L on a subspace $Y_1 \subseteq Y$*

$$L'(y_1)(\delta y_1) = 0 \quad \forall \delta y_1 \in Y_1. \tag{6.57}$$

The Galerkin approximation of the above equation $y_2 \in Y_2 \subseteq Y$ satisfies

$$L'(y_2)(\delta y_2) = 0 \quad \forall \delta y_2 \in Y_2. \tag{6.58}$$

If the continuous solution y_1 satisfies additionally

$$L'(y_1)(y_2) = 0, \tag{6.59}$$

then, we have for arbitrary $\hat{y}_2 \in Y_2$ the error representation

$$L(y_1) - L(y_2) = \frac{1}{2} L'(y_2)(y_1 - \hat{y}_2) + \mathcal{R}, \tag{6.60}$$

where the remainder term $\mathcal{R}$ is given by the means of the error $e := y_1 - y_2$

$$\mathcal{R} = \frac{1}{2} \int_0^1 L'''(y_2 + se)(e, e, e)\, s\,(s-1)\, ds. \tag{6.61}$$

In order to apply the result of the above lemma, we consider the stationary points of $\mathcal{L}$ and $\tilde{\mathcal{L}}$ on different levels of discretization:

$$\begin{aligned}
\mathcal{L}'(u,q,z)(\phi,\varphi,\psi) &= 0 \qquad \forall (\phi,\varphi,\psi) \in X \times Q \times X, && (6.62)\\
\tilde{\mathcal{L}}'(u_k,q_k,z_k)(\phi_k,\varphi_k,\psi_k) &= 0 \qquad \forall (\phi_k,\varphi_k,\psi_k) \in \tilde{X}_k^r \times Q \times \tilde{X}_k^r, && (6.63)\\
\tilde{\mathcal{L}}'(u_{kh},q_{kh},z_{kh})(\phi_{kh},\varphi_{kh},\psi_{kh}) &= 0 \qquad \forall (\phi_{kh},\varphi_{kh},\psi_{kh}) \in \tilde{X}_{k,h}^{r,s} \times Q \times \tilde{X}_{k,h}^{r,s}, && (6.64)\\
\tilde{\mathcal{L}}'(u_\sigma,q_\sigma,z_\sigma)(\phi_\sigma,\varphi_\sigma,\psi_\sigma) &= 0 \qquad \forall (\phi_\sigma,\varphi_\sigma,\psi_\sigma) \in \tilde{X}_{k,h}^{r,s} \times Q_d \times \tilde{X}_{k,h}^{r,s}. && (6.65)
\end{aligned}$$

We observe that $\mathcal{L}(u,q,z) = \tilde{\mathcal{L}}(u,q,z)$ due to the continuity of $u \in X$ because the space $W(0,T)$ is continuously embedded into $C(I; L^2(\Omega))$. In order to remain consistency with a posteriori error estimates for stationary problems, we introduce the following notation:

$$\begin{aligned}
\tilde{\rho}(u,q)(\phi) &:= \tilde{\mathcal{L}}'_z(u,q,z)(\phi),\\
\tilde{\rho}^*(u,q,z)(\psi) &:= \tilde{\mathcal{L}}'_u(u,q,z)(\psi),\\
\tilde{\rho}^q(u,q,z)(\varphi) &:= \tilde{\mathcal{L}}'_q(u,q,z)(\varphi).
\end{aligned}$$

With these preparations, we obtain the following result:

PROPOSITION 6.5.1. *Let $\{u,q,z\} \in X \times Q \times X$, $\{u_k,q_k,z_k\} \in \tilde{X}_k^r \times Q \times \tilde{X}_k^r$, and $\{u_{kh},q_{kh},z_{kh}\} \in \tilde{X}_{k,h}^{r,s} \times Q \times \tilde{X}_{k,h}^{r,s}$ be approximations of* (6.62), (6.63), *and* (6.64), *respectively. Furthermore, let $\{\tilde{u}_\sigma,\tilde{q}_\sigma,\tilde{z}_\sigma\} \in \tilde{X}_{k,h}^{r,s} \times Q_d \times \tilde{X}_{k,h}^{r,s}$ be an approximative solution of* (6.65)

obtained by any iterative solver. Then, there hold the following error representations:

$$\begin{aligned} J(u,q) - J(u_k,q_k) &= \frac{1}{2}\tilde{\rho}(u_k,q_k)(z-\psi_k) + \frac{1}{2}\tilde{\rho}^*(u_k,q_k,z_k)(u-\phi_k) \\ &\quad + \frac{1}{2}\tilde{\rho}^q(u_k,q_k,z_k)(q-\varphi_k) + \mathcal{R}_k, \end{aligned} \tag{6.66}$$

$$\begin{aligned} J(u_k,q_k) - J(u_{kh},q_{kh}) &= \frac{1}{2}\tilde{\rho}(u_{kh},q_{kh})(z_k-\psi_{kh}) + \frac{1}{2}\tilde{\rho}^*(u_{kh},q_{kh},z_{kh})(u_k-\phi_{kh}) \\ &\quad + \frac{1}{2}\tilde{\rho}^q(u_{kh},q_{kh},z_{kh})(q_k-\varphi_{kh}) + \mathcal{R}_h, \end{aligned} \tag{6.67}$$

$$\begin{aligned} J(u_{kh},q_{kh}) - J(\tilde{u}_\sigma,\tilde{q}_\sigma) &= \frac{1}{2}\tilde{\rho}(\tilde{u}_\sigma,\tilde{q}_\sigma)(z_{kh}-\tilde{z}_\sigma) + \frac{1}{2}\tilde{\rho}^*(\tilde{u}_\sigma,\tilde{q}_\sigma,\tilde{z}_\sigma)(u_{kh}-\tilde{u}_\sigma) \\ &\quad + \frac{1}{2}\tilde{\rho}^q(\tilde{u}_\sigma,\tilde{q}_\sigma,\tilde{z}_\sigma)(q_{kh}-\tilde{q}_\sigma) + \tilde{\rho}(\tilde{u}_\sigma,\tilde{q}_\sigma)(\tilde{z}_\sigma) + \mathcal{R}_d, \end{aligned} \tag{6.68}$$

with arbitrary $(\phi_k,\varphi_k,\psi_k) \in \tilde{X}_k^r \times Q \times \tilde{X}_k^r$ *and* $(\phi_{kh},\varphi_{kh},\psi_{kh}) \in \tilde{X}_{k,h}^{r,s} \times Q \times \tilde{X}_{k,h}^{r,s}$. *Here, the error due to the approximative solution of* (6.65) *is given by* $\tilde{\rho}(\tilde{u}_\sigma,\tilde{q}_\sigma)(\tilde{z}_\sigma)$. *The remainder terms* $\mathcal{R}_k, \mathcal{R}_h$, *and* $\mathcal{R}_d$ *have the same form as in Lemma 6.5.1.*

PROOF. There holds

$$J(u,q) - J(u_k,q_k) = \tilde{\mathcal{L}}(u,q,z) - \tilde{\mathcal{L}}(u_k,q_k,z_k), \tag{6.69}$$

$$J(u_k,q_k) - J(u_{kh},q_{kh}) = \tilde{\mathcal{L}}(u_k,q_k,z_k) - \tilde{\mathcal{L}}(u_{kh},q_{kh},z_{kh}). \tag{6.70}$$

Thus, the first two identities (6.66) and (6.67) can be shown by applying result (6.60) from Lemma 6.5.1 and using a compactness argument. The details can be found in Meidner [81]. For the error representation involving the approximative solution, we observe

$$J(u_{kh},q_{kh}) - J(\tilde{u}_\sigma,\tilde{q}_\sigma) = \tilde{\mathcal{L}}(u_{kh},q_{kh},z_{kh}) - \tilde{\mathcal{L}}(\tilde{u}_\sigma,\tilde{q}_\sigma,\tilde{z}_\sigma) + \tilde{\mathcal{L}}_z'(\tilde{u}_\sigma,\tilde{q}_\sigma,\tilde{z}_\sigma)(\tilde{z}_\sigma), \tag{6.71}$$

where the last term occurs due to the perturbed Galerkin orthogonality. The assertion follows using the same arguments as in Proposition 6.3.1. □

Since $(\phi_k,\varphi_k,\psi_k) \in \tilde{X}_k^r \times Q \times \tilde{X}_k^r$ and $(\phi_{kh},\varphi_{kh},\psi_{kh}) \in \tilde{X}_{k,h}^{r,s} \times Q \times \tilde{X}_{k,h}^{r,s}$ can be arbitrarily chosen, we follow Meidner [81] and set

$$\hat{q}_k = q \in Q \quad \text{and} \quad \hat{q}_{qh} = q_k \in Q.$$

By these means, we obtain for the error representations:

$$\begin{aligned} J(u,q) - J(u_k,q_k) &\approx \frac{1}{2}\rho^u(u_k,q_k)(z-\hat{z}_k) + \frac{1}{2}\rho^z(u_k,q_k,z_k)(u-\hat{u}_k), \\ J(u_k,q_k) - J(u_{kh},q_{kh}) &\approx \frac{1}{2}\rho^u(u_{kh},q_{kh})(z_k-\hat{z}_{kh}) + \frac{1}{2}\rho^z(u_{kh},q_{kh},z_{kh})(u_k-\hat{u}_{kh}), \\ J(u_{kh},q_{kh}) - J(\tilde{u}_\sigma,\tilde{q}_\sigma) &\approx \frac{1}{2}\rho^u(\tilde{u}_\sigma\tilde{q}_\sigma)(q_{kh}-\tilde{q}_{kh}) + \rho^z(\tilde{u}_\sigma,\tilde{q}_\sigma,\tilde{z}_\sigma)(u_{kh}-\tilde{u}_\sigma) \\ &\quad + \frac{1}{2}\rho^q(\tilde{u}_\sigma,\tilde{q}_\sigma,\tilde{z}_\sigma) + \rho^u(\tilde{u}_\sigma,\tilde{q}_\sigma)(\tilde{z}_\sigma), \end{aligned}$$

where we have neglected the remainder terms $\mathcal{R}_k$, $\mathcal{R}_h$, and $\mathcal{R}_d$.

It is also possible to show the error identity (6.68) with $\tilde{u}_\sigma$ and $\tilde{z}_\sigma$ replaced by arbitrary $\phi_\sigma \in \tilde{X}_{k,h}^{r,s}$ and $\psi_\sigma \in \tilde{X}_{k,h}^{r,s}$, respectively. However, this would change the form of the iteration error estimator and make its evaluation more involved.

Finally, we state the form of the a posteriori error estimates for the cG(r) discretization in time. To this end, we consider the stationary points of the Lagrangian $\mathcal{L}(\cdot,\cdot,\cdot)$ given in (6.52) on different levels of discretization:

$$\begin{aligned}
\mathcal{L}'(u,q,z)(\phi,\varphi,\psi) &= 0 \quad \forall (\phi,\varphi,\psi) \in X \times Q \times X, && (6.72)\\
\mathcal{L}'(u_k,q_k,z_k)(\phi_k,\varphi_k,\psi_k) &= 0 \quad \forall (\phi_k,\varphi_k,\psi_k) \in X_k^r \times Q \times \tilde{X}_k^r, && (6.73)\\
\mathcal{L}'(u_{kh},q_{kh},z_{kh}(\phi_{kh},\varphi_{kh},\psi_{kh}) &= 0 \quad \forall (\phi_{kh},\varphi_{kh},\psi_{kh}) \in X_{k,h}^{r,s} \times Q \times \tilde{X}_{k,h}^{r,s}, && (6.74)\\
\mathcal{L}'(u_\sigma,q_\sigma,z_\sigma)(\phi_\sigma,q_\sigma,z_\sigma) &= 0 \quad \forall (\phi_\sigma,\varphi_\sigma,\psi_\sigma) \in X_{k,h}^{r,s} \times Q_d \times \tilde{X}_{k,h}^{r,s}. && (6.75)
\end{aligned}$$

As previously, we introduce the following notation:

$$\begin{aligned}
\rho(u,q)(\phi) &:= \mathcal{L}_z'(u,q,z)(\phi),\\
\rho^*(u,q,z)(\psi) &:= \mathcal{L}_u'(u,q,z)(\psi),\\
\rho^q(u,q,z)(\varphi) &:= \mathcal{L}_q'(u,q,z)(\varphi).
\end{aligned}$$

With these preparations, we obtain the following result.

PROPOSITION 6.5.2. *Let $\{u,q,z\} \in X \times Q \times X$, $\{u_k,q_k,z_k\} \in X_k^r \times Q \times \tilde{X}_k^r$, and $\{u_{kh},q_{kh},z_{kh}\} \in X_{k,h}^{r,s} \times Q \times \tilde{X}_{k,h}^{r,s}$ be approximations of* (6.72), (6.73), *and* (6.74), *respectively. Furthermore, let $\{\tilde{u}_\sigma,\tilde{q}_\sigma,\tilde{z}_\sigma\} \in X_{k,h}^{r,s} \times Q_d \times \tilde{X}_{k,h}^{r,s}$ be an approximative solution of* (6.75) *obtained by any iterative solver. Then, there hold the following error representations:*

$$\begin{aligned}
J(u,q) - J(u_k,q_k) &= \frac{1}{2}\rho(u_k,q_k)(z-\psi_k) + \frac{1}{2}\rho^*(u_k,q_k,z_k)(u-\phi_k)\\
&\quad + \frac{1}{2}\rho^q(u_k,q_k,z_k)(q-\varphi_k) + \mathcal{R}_k, && (6.76)\\
J(u_k,q_k) - J(u_{kh},q_{kh}) &= \frac{1}{2}\rho(u_{kh},q_{kh})(z_k-\psi_{kh}) + \frac{1}{2}\rho^*(u_{kh},q_{kh},z_{kh})(u_k-\phi_{kh})\\
&\quad + \frac{1}{2}\rho^q(u_{kh},q_{kh},z_{kh})(q_k-\varphi_{kh}) + \mathcal{R}_h, && (6.77)\\
J(u_{kh},q_{kh}) - J(\tilde{u}_\sigma,\tilde{q}_\sigma) &= \frac{1}{2}\rho(\tilde{u}_\sigma,\tilde{q}_\sigma)(z_{kh}-\tilde{z}_\sigma) + \frac{1}{2}\rho^*(\tilde{u}_\sigma,\tilde{q}_\sigma,\tilde{z}_\sigma)(u_{kh}-\tilde{u}_\sigma)\\
&\quad + \frac{1}{2}\rho^q(\tilde{u}_\sigma,\tilde{q}_\sigma,\tilde{z}_\sigma)(q_{kh}-\tilde{q}_\sigma) + \rho(\tilde{u}_\sigma,\tilde{q}_\sigma)(\tilde{z}_\sigma) + \mathcal{R}_d, && (6.78)
\end{aligned}$$

with arbitrary $(\phi_k,\varphi_k,\psi_k) \in X_k^r \times Q \times \tilde{X}_k^r$ and $(\phi_{kh},\varphi_{kh},\psi_{kh}) \in X_{k,h}^{r,s} \times Q \times \tilde{X}_{k,h}^{r,s}$. Here, the error due to the approximative solution of (6.65) *is given by $\tilde{\rho}(\tilde{u}_\sigma,\tilde{q}_\sigma)(\tilde{z}_\sigma)$. The remainder terms $\mathcal{R}_k, \mathcal{R}_h$, and $\mathcal{R}_d$ have the same form as in Lemma 6.5.1.*

PROOF. The proof of the result is obtained using the same arguments as in Proposition 6.5.2. □

6.5.1. Practical realization

The derived error representations involve the unknown errors on different discretization levels. For their approximation, we use the postprocessing of the computed solutions by local higher-order interpolation. Thereby, we proceed as in Meidner & Vexler [83].

We consider the dG(0)-discretization in time. To this end, we introduce the linear operator $\Pi_k := I_k^{(1)} - \mathrm{id}$ with $I_k^{(1)} : \tilde{X}_k^0 \to X_k^1$, which maps the computed solution to the approximations of the corresponding errors,

$$\Pi_k u_k := I_k^{(1)} u_k - u_k, \quad \Pi_k z_k := I_k^{(1)} z_k - z_k.$$

For the interpolation errors in space, we use again as in Section 6.1 the linear operator $\Pi_h = I_{2h}^{(2)} - \mathrm{id}$, where $I_{2h}^{(2)}$ is the operator of patchwise biquadratic (triquadratic) interpolation. In this way, we approximate

$$\Pi_h u_{kh} := I_{2h}^{(2)} u_{kh} - u_{kh}, \quad \Pi_h z_{kh} := I_{2h}^{(2)} z_{kh} - z_{kh}, \quad \Pi_h q_{kh} := I_{2h}^{(2)} q_{kh} - q_{kh},$$

where we have assumed the discretization of the unknown parameter $q \in Q$ by piecewise bilinear (trilinear) functions. For the piecewise constant polynomial discretization, we use the operator $\Pi_d = I_d^{(1)} - \mathrm{id}$ leading to the approximation

$$\Pi_d q_{kh} := I_d^{(1)} q_{kh} - q_{kh}.$$

In all these approximations, we replace the unknown solutions by their fully discrete analogs. This is substantiated by the fact that the caused errors are of a higher order, see Meidner [81].

Finally, we obtain the following computable a posteriori error estimators for the temporal dG(0) discretization:

$$\eta_k := \frac{1}{2}\tilde{\rho}(\tilde{u}_\sigma, \tilde{q}_\sigma)(\Pi_k \tilde{z}_\sigma) + \frac{1}{2}\tilde{\rho}^*(\tilde{u}_\sigma, \tilde{q}_\sigma, \tilde{z}_\sigma)(\Pi_k \tilde{u}_\sigma), \tag{6.79}$$

$$\eta_h := \frac{1}{2}\tilde{\rho}(\tilde{u}_\sigma, \tilde{q}_\sigma)(\Pi_h \tilde{z}_\sigma) + \frac{1}{2}\tilde{\rho}^*(\tilde{u}_\sigma, \tilde{q}_\sigma, \tilde{z}_\sigma)(\Pi_h \tilde{u}_\sigma), \tag{6.80}$$

$$\eta_d := \frac{1}{2}\tilde{\rho}(\tilde{u}_\sigma, \tilde{q}_\sigma)(\Pi_h \tilde{z}_\sigma) + \frac{1}{2}\tilde{\rho}^*(\tilde{u}_\sigma, \tilde{q}_\sigma, \tilde{z}_\sigma)(\Pi_h \tilde{u}_\sigma) + \frac{1}{2}\tilde{\rho}^q(\tilde{u}_\sigma, \tilde{q}_\sigma, \tilde{z}_\sigma)(\Pi_h \tilde{q}_\sigma), \tag{6.81}$$

$$\eta_m := \frac{1}{2}\tilde{\rho}(\tilde{u}_\sigma, \tilde{q}_\sigma)(\tilde{z}_\sigma). \tag{6.82}$$

For a detailed description of the computational procedure of the above residuals, we refer to Meidner & Vexler [83]. We show only the explicit form of the iteration error estimator and the residual term $\rho^q(\cdot,\cdot,\cdot)(\cdot)$. We stabilize the discrete equations by the local projection

method (LPS). Approximating the arising temporal integrals by the box rule and using the abbreviations $\tilde{U}_m := \tilde{u}^-_{\sigma,m}$ and $\tilde{Z}_m := \tilde{z}^-_{\sigma,m}$ the error estimators are given by

$$\begin{aligned}\rho^q(\tilde{u}_\sigma,\tilde{q}_\sigma,\tilde{z}_\sigma)(\Pi_h\tilde{q}_\sigma) &= 2\alpha(\tilde{\mu}_\sigma-\mu^*, I_{2h}^{(2)}\tilde{\mu}_h-\tilde{\mu}_h)+2\alpha(\tilde{\beta}_\sigma-\beta^*, I_{2h}^{(2)}\tilde{\beta}_h-\tilde{\beta}_h)_{\Gamma_G}\\ &\quad+2\alpha(\tilde{\chi}_\sigma-\chi^*, I_{2h}^{(2)}\tilde{\chi}_h-\tilde{\chi}_h)\Big)-\sum_{m=1}^{M}k_m(\tilde{Z}_mE(t_m), I_{2h}^{(2)}\tilde{\mu}_h-\tilde{\mu}_h)\\ &\quad-\sum_{m=1}^{M}k_m(\tilde{Z}_mE_s(t_m), I_{2h}^{(2)}\tilde{\lambda}_h-\tilde{\lambda}_h)_{\Gamma_G}-(\tilde{Z}_0, I_{2h}^{(2)}\tilde{\chi}_h-\tilde{\chi}_h),\\ \rho(\tilde{u}_\sigma,\tilde{q}_\sigma)(\tilde{z}_\sigma) &= \sum_{m=1}^{M}\Big(-k_m\bar{a}(\tilde{U}_m,\tilde{q}_\sigma)(\tilde{Z}_m)-s_h^m(\tilde{U}_m,\tilde{Z}_m)-(\tilde{U}_m-\tilde{U}_{m-1},\tilde{Z}_m)\Big)\\ &\quad-(U_0-\tilde{\chi}_\sigma,\tilde{Z}_0),\end{aligned}$$

where the term $s_h^m(\cdot,\cdot)$ is defined accordingly to (3.10).

The approximation of the a posteriori error estimators for the continuous Galerkin discretization in time with piecewise linear polynomials can be treated in a similar manner. However, in this case for the approximation of the semidiscrete temporal weights, we use the operator $\Pi_k := I_{2k}^{(2)} - \mathrm{id}$ with $I_{2k}^{(2)} : \tilde{X}_k^1 \to X_{2k}^2$, which maps the computed solution to the approximations of the corresponding errors.

For the adaptive refinement the derived a posteriori error estimates must be localized. To this end, the error estimates are first split into their contributions on each subinterval I_m. For the spatial refinement the localization on each of these subintervals procedure is the same as in elliptic case described in Section 6.1. Thus, we obtain the cellwise error indicators for all time steps

$$\eta_h = \sum_{m=0}^{M}\sum_{K\in\mathcal{T}_h}\eta_{h,K}.$$

The localization of the error estimator due to the discretization of the parameter $q \in Q$ is treated analogously. The temporal indicators from the representation

$$\eta_k = \sum_{m=1}^{M}\eta_k^m,$$

can be used directly for the refinement of time intervals. Details on the localization procedure can be found in Meidner [81].

We note that the derived representation of the iteration error is valid for any fixed-point iteration and, consequently, we can employ the Newton-type methods as described in Chapter 5, Section 5.4. Based on the derived error estimators (6.79), (6.80), (6.81), and (6.82), we propose the following adaptive algorithm balancing different error contributions:

Adaptive nonstationary solution algorithm

(1) Choose initial discretizations $\mathcal{T}_{\sigma_0}, \sigma_0 = (k_0, h_0, d_0)$ and set $l = 0$.

(2) Apply one step of the Newton-type method $(q^n_{\sigma_l}, u^n_{\sigma_l}) \to (q^{n+1}_{\sigma_l}, u^{n+1}_{\sigma_l})$.

(3) Evaluate the estimators $\eta^{n+1}_{k_l}, \eta^{n+1}_{h_l}, \eta^{n+1}_{d_l}$, and $\eta^{n+1}_{m_l}$.

(4) If $\eta^{n+1}_{k_l} + \eta^{n+1}_{h_l} + \eta^{n+1}_{d_l} + \eta^{n+1}_{m_l} \leq \mathrm{TOL}$ quit.

(5) If $\eta^{n+1}_{m_l} \geq \kappa \min\{\eta^{n+1}_{k_l}, \eta^{n+1}_{h_l}, \eta^{n+1}_{d_l}\}$ increment n and goto (3).

(6) Determine the discretizations to be refined.

(7) Refine the selected discretizations using error indicators from $\eta^{n+1}_{k_l}, \eta^{n+1}_{h_l}$, and $\eta^{n+1}_{d_l}$.

(8) Increment l and go to (2).

In the proposed method, we use again an equilibration factor $\kappa = 0.1$. This ensures that the local refinement results from the values of the discretization error estimators. On the next finer mesh, we evaluate the discretization error estimators if for the iteration estimator there holds $\eta^{n+1}_{m_{l+1}} \geq \kappa \min\{\eta^{n+1}_{k_{l+1}}, \eta^{n+1}_{h_{l+1}}, \eta^{n+1}_{d_{l+1}}\}$. In step (6) of the algorithm a strategy proposed in Meidner [81] can be used. Here, the error estimators are first sorted in an ascending order. Then, we compute their quotients. If the obtained values exceed some fixed number, the corresponding discretization with a bigger error is refined. We note that for solving problem (6.50,6.51) by the Newton-type methods described in Chapter 5, Section 5.3, the state variable $\tilde{u}_\sigma$ is needed in the whole time interval I. This may be prohibitive with respect to the storage space. The reduction of the required amount of memory can be achieved by applying checkpointing techniques storing the state solution only on selected time points (so-called checkpoints). In this case the storage grows only logarithmic with respect to the number of time intervals. For more details on checkpointing, we refer, e.g., to Griewank [46] or Berggren et al. [18]. Nevertheless, we store the state solution over the whole time interval in all presented nonstationary numerical computations. For two-dimensional applications this can often be done by using the operating memory (RAM). In three spatial dimensions the data must be stored on the hard drive. However, even in this case the time to access the data can be neglected: In order to write a vector with 10^6 "double precision" entries to a solid-state-drive (SSD), we need approximately 0.01632 sec (490 MB/s). For the corresponding read access 0.01568 sec (510 MB/s) are required. This can be assumed to be still much faster than solving several time steps of a possibly nonlinear problem more than once. A further discussion of this topic can be found in Becker et al. [15].

6.6. Numerical example

The example demonstrates the efficiency of the proposed adaptive algorithm for an nonstationary inverse problem. We consider a reaction chain leading to ozone loss discussed in

Chapter 2, Example 1. The aim of the computations is the reconstruction of the unknown initial condition of the system. The inverse problem is regularized using the ordinary Tikhonov regularization with a fixed parameter α. We solve the resulting optimal control problem by the direct Newton method for optimization problems. The equations are discretized using the cG(1)dG(0) method. For the stabilization of the discrete problems, we employ the local projection stabilization (LPS) scheme.

For the convenience of the reader, we state the underlying chemical reaction mechanism again. As before, we denote by $h\nu$ the photolysis, i.e., a process by which molecules are broken down into smaller units through the absorption of light. The chemical reactions are given by:

$$O_2 + h\nu \xrightarrow{k_1} 2\,O \tag{6.83}$$
$$O + O_2 + M \xrightarrow{k_2} O_3 + M \tag{6.84}$$
$$O_3 + h\nu \xrightarrow{k_3} O + O_2 \tag{6.85}$$
$$O + O_3 \xrightarrow{k_4} 2\,O_2 \tag{6.86}$$

Here, $k_i, i = 1, \ldots, 4$, are reaction constants, and M is any nonreactive species stabilizing O_3. Due to the high concentration of oxygen in comparison to the concentrations of the other species, we assume it to be constant over the time. Consequently, we set the respective concentrations to be qual to $[O_2] = [M] = 1$. The unknowns are then denoted by $u_1 = [O]$ and $u_2 = [O_3]$.

Using the Arrhenius law, we drop the dependency of the reaction rates on the temperature and assign fix values $k_1 = 10^{-4}$, $k_2 = 10^{-3}$, $k_3 = 10^{-4}$, and $k_4 = 10^{-5}$. For the numerical computations, we choose the domain $\Omega \subset I\!R^2$ to be $(0,1) \times (0,1)$, fix values for the diffusion coefficients $D_{11} = D_{22} = 10^{-5}$ and for the convection velocity $\beta = (1,1)^T$. The temporal domain is given by $I = [0,1]$. The resulting system of equations reads as follows:

$$\begin{aligned}
\partial_t u_1 - \nabla \cdot (D_1 \nabla u_1) + v \nabla u_1 + f_1(u) &= E_1(t,x) && \text{in } \Omega_T,\\
\partial_t u_2 - \nabla \cdot (D_1 \nabla u_2) + v \nabla u_2 + f_2(u) &= E_2(t,x) && \text{in } \Omega_T,\\
D_1 \partial_n u_1 &= E_{s,1}(t,x) && \text{on } \Sigma,\\
D_2 \partial_n u_2 &= E_{s,2}(t,x) && \text{on } \Sigma,\\
u_1(t_0,x) &= \chi_1(x) && \text{in } \Omega,\\
u_2(t_0,x) &= \chi_2(x) && \text{in } \Omega,
\end{aligned} \tag{6.87}$$

where we have imposed Neumann boundary conditions for the both components of the system. The nonlinear reaction terms $f_i, i = 1, 2$, are modeled according to the mass kinetics described in Chapter 2 and are given in (2.44) and (2.45), respectively. The source terms on the right-hand side $E_i(t,x), i = 1, 2$, are defined in such a way that the exact solution is given by

$$u_i(t,x) = \frac{1}{1 + \gamma_i((x_1 - r(t))^2 + (x_2 - s(t))^2)}, \quad i = 1, 2,$$

with the functions

$$\begin{aligned} r(t) &= \frac{1}{2} + \frac{1}{4}\cos(2\pi t), \\ s(t) &= \frac{1}{2} + \frac{1}{4}\sin(2\pi t). \end{aligned}$$

We prescribe the following values for the parameters of the system, $\gamma_0 = 50$, $\gamma_1 = 200$. The initial concentrations $q(x) := (\chi_1(x), \chi_2(x)) \in Q := L^2(\Omega) \times L^2(\Omega)$ are supposed to be unknown. The overdetermination condition is given by transient measurements integrated over the space. Thus, the corresponding observation operator $\mathcal{C}$ and the measurement space Y are given by

$$\mathcal{C}(u_i) = \int_\Omega u_i(t,x)\,dx \in Y_i, \quad Y_i := L^2(I), \quad i = 1,2.$$

The solution space for the states is given by $X := W(I) \times W(I)$.

The inverse problem is stabilized by the ordinary Tikhonov regularization. Hence, the resulting problem reads as follows:

$$\min_{(u,q)\in X\times Q} J(u,q) := \sum_{i=1}^{2} \|\mathcal{C}(u_i) - g_i\|_{Y_i}^2 + \alpha\|q - q^*\|_Q^2,$$

subject to system (6.87) formulated in a weak sense. We denote the components of the measurement vector by $g_i = \mathcal{C}(u_i)$. As prior knowledge, we set $q^* = (\chi_1^*, \chi_2^*) = (0,0)$.

The unknown initial concentration $q \in Q$ is discretized by the continuous Galerkin finite element method. In order to access a reference value, we solve the problem on finer temporal and spatial meshes. Table 6.16 shows the development of the discretization error and a posteriori error estimators during an adaptive run with local refinement of all types of the discretization. As the stopping criterion for the Newton iteration, we use the first order optimality condition (5.65) with $\mathrm{TOL} = 10^{-10}$.

TABLE 6.16: Example 4, iteration with Alg. $S\,I$ (algebraic stopping criterion).

$\mathrm{N_{tot}}$	$\mathrm{N_{max}}$	M	It	η_{tot}	η_h	η_k	η_m
2 673	243	20	17	5.41e-04	2.78e-04	2.63e-04	1.21e-10
9 447	623	20	16	1.55e-04	1.23e-05	1.43e-04	3.49e-09
9 780	623	24	17	1.29e-04	1.24e-05	1.17e-04	6.09e-10
10 086	623	33	19	5.61e-05	1.24e-05	4.38e-05	7.02e-10
47 340	1505	36	19	3.77e-05	8.11e-06	2.96e-05	2.33e-11
158 484	3659	47	19	2.94e-05	6.23e-06	2.33e-05	8.87e-12
349 704	9329	68	18	5.78e-06	1.22e-06	4.56e-06	6.23e-11

Table 6.17 shows the corresponding values using an adaptive stopping criterion for the Newton method. As we can see, we obtain almost identical values for the discretization

TABLE 6.17: Example 4, iteration with Alg. *S II* (adaptive stopping criterion).

N_{tot}	N_{max}	M	It	η_{tot}	η_h	η_k	η_m
2 673	243	20	9	5.41e-04	2.85e-04	2.63e-04	7.13e-06
9 447	623	20	9	1.55e-04	1.26e-05	1.44e-04	4.56e-07
9 780	623	24	9	1.29e-04	1.29e-05	1.17e-04	5.79e-07
10 086	623	33	10	5.61e-05	1.30e-05	4.40e-05	6.45e-07
47 340	1505	36	10	3.77e-05	8.25e-06	2.93e-05	1.67e-07
158 484	3659	47	9	2.94e-05	6.33e-06	2.33e-05	9.90e-08
349 704	9329	68	9	5.78e-06	1.29e-06	4.57e-06	8.11e-08

errors. However, we observe approximately double work saving by using the adaptive stopping criterion for the Newton method. This shows the reliability and the efficiency of the adaptive algorithm.

In Figure 6.13, we can see the sequence of locally refined meshes from the solution process. The computed initial concentrations $\chi_1(x)$ and $\chi_2(x)$ and the concentrations of O_3 and O at different discrete time points are depicted in Figures 6.14 and 6.15, respectively. We can observe that the meshes are strongly locally refined in regions of high concentrations.

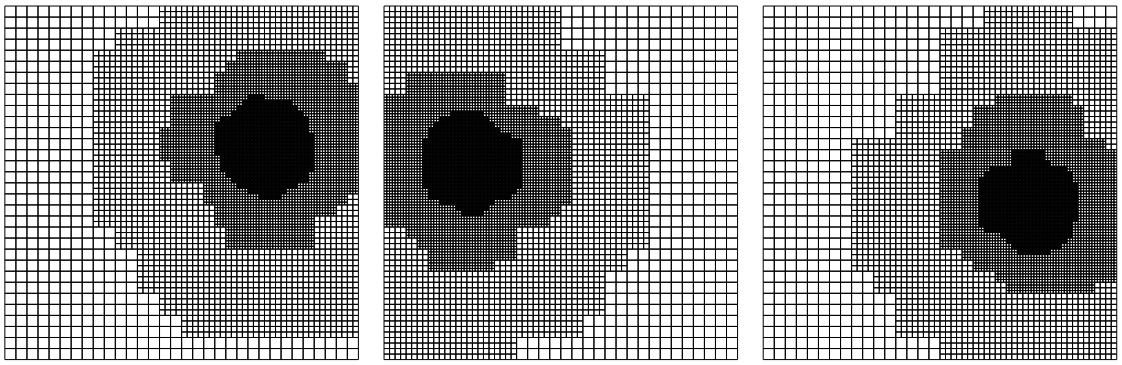

FIGURE 6.13: Example 4, locally refined meshes from solution process at time point $t = 0$ (left), $t = 0.5$ (middle) and $t = 1$ (right).

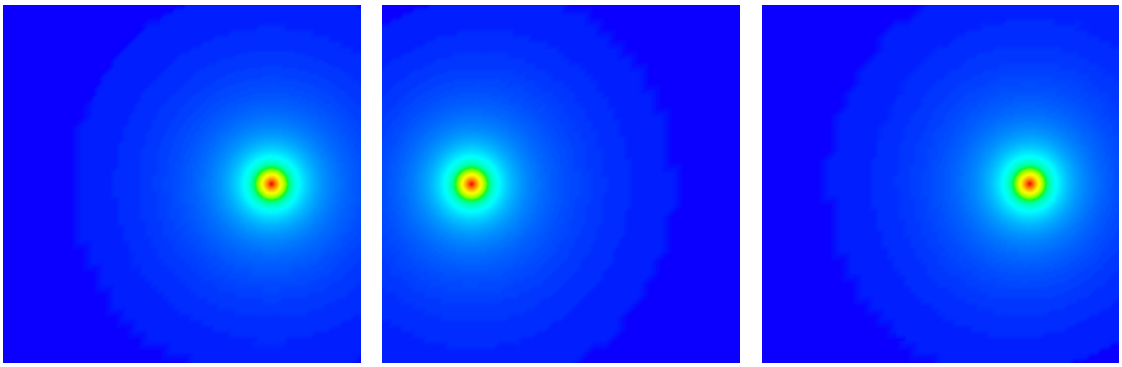

FIGURE 6.14: Example 4, calculated initial condition $\chi_1(x)$ (left) and concentrations of O_3 at time points $t = 0.5$ (middle) and $t = 1$ (right).

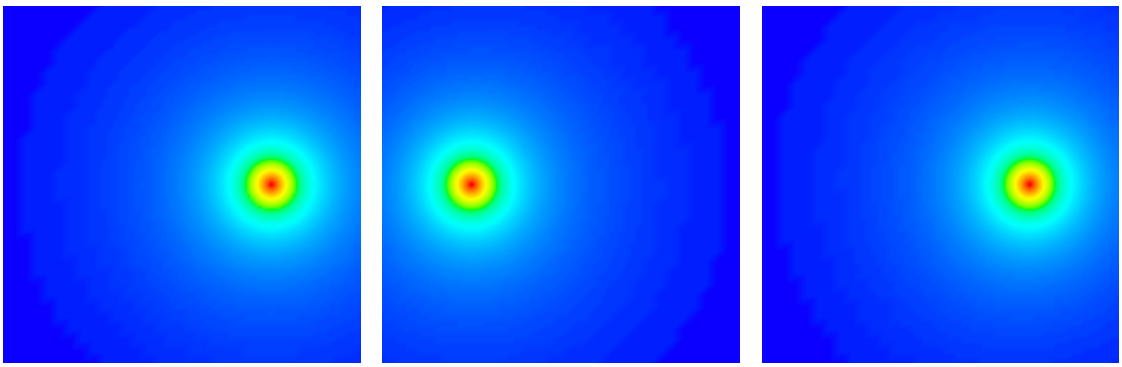

FIGURE 6.15: Example 4, calculated initial condition $\chi_2(x)$ (left) and concentrations of O at time points $t = 0.5$ (middle) and $t = 1$ (right).

CHAPTER 7

Applications

The aim of this chapter is to provide a more detailed description of the parameters of system (2.22) and to present a real world problem for identification of unknown source term in atmospheric transport of bromine oxide (BrO) in a Polar region. Here, we are faced with the situation in which the mechanisms responsible for release or destruction of bromine oxide are not precisely known. However, due to the heavy impact of this trace gas to the ozone loss during the spring time (see, e.g., Simpson et al. [108]) the quantification of the sources is of special importance. Thus, we consider a simplified model given by the following scalar convection-diffusion-reaction equation

$$\begin{aligned} \partial_t u - \nabla \cdot (D\,\nabla u) + \nabla \cdot (vu) &= q(t,x) && \text{in } \Omega_T, \\ u &= u^{\text{in}} && \text{on } \Sigma_I, \\ D\partial_n u &= 0 && \text{on } \Sigma_O, \\ D\partial_n u - wu &= E_s(u,t,x) && \text{on } \Sigma_G, \\ u(t_0) &= u^0 && \text{in } \Omega, \end{aligned} \tag{7.1}$$

where u represent the unknown concentration of BrO, and $q = q(t,x)$ denotes the unknown source term. As overspecification condition, we use integrated observations of bromine oxide. Thus, the observation operator $\mathcal{C} : X \to Y$ and the measurement space Y are given as follows:

$$\mathcal{C}_i(u) = \int_\Omega u(t_i,x)\,dx \in Y_i, \quad Y_i := L^2(0,T),\ i = 1,\dots,M, \tag{7.2}$$

where M stands for the number of discrete time points. Since the given data have a lower dimensionality as the unknown parameters, we further assume distributed observations to be given at a specific time point

$$\mathcal{C}^*(u) = u(t^*,x), \quad (t^*,x) \in \Omega_T, \quad Y^* := L^2(\Omega). \tag{7.3}$$

Nevertheless, the approach still remains heuristic since we cannot show the unique identifiability of the unknown source term. This can be justified if, e.g., the source term can be separated in temporal and spatial parts, see, e.g., Savateev [103] and Young et al. [122]. The numerical results at the end of the chapter show that the obtained recovered concentrations, which are of its own importance, agree with the assimilated observations very well. The computational results and the settings of the problem are taken from Garbe & Vihharev [44].

Equation (7.1) is given in units of the so-called "number density" (mol/m^3). Since the observation are given in units of mole fractions (mol/mol), we rewrite the first equation of

system (7.1) accordingly. To this end, we denote by ρ_a the density of the air and consider the corresponding continuity equation for air

$$\partial_t \rho_a + \nabla \cdot (v \rho_a) = 0. \tag{7.4}$$

In this case the chemical transformations are neglected. We note that air is incompressible. We multiply the continuity equation for the trace gas (7.1) by the air density, combine with the above equation, and obtain after some algebraic transformations the modified continuity equation

$$\begin{aligned} \partial_t u - \frac{1}{\rho_a} \nabla \cdot (\rho_a \, D \nabla u) + v \nabla u &= q(t,x) && \text{in } \Omega_T, \\ u &= u^{\text{in}} && \text{on } \Sigma_I, \\ D \partial_n u &= 0 && \text{on } \Sigma_O, \\ D \partial_n u - w \, u &= E_s(u,t,x) && \text{on } \Sigma_G, \\ u(t_0) &= u^0 && \text{in } \Omega, \end{aligned} \tag{7.5}$$

where $u(t,x)$ now stands for the concentration of bromine oxide expressed in mole fraction.

In the following, we describe the computation of the eddy diffusivity tensor. After that, we rewrite the continuity equation in horizontal spherical coordinates accordingly to the given observations. For the vertical coordinate, we employ the terrain-following sigma-pressure coordinates. We close the chapter by the presentation of the computational results.

7.1. Parametrization of the kinematic turbulent fluxes

In this section, we shortly describe one of the possible parameterizations for the diffusivity tensor introduced in Chapter 2, Section 2.1. The most common approach to parametrizing the diffusion bases on the similarity theory. The form of the diffusion depends on the stability properties of the regions of the atmosphere. Thus, the most turbulent part of the atmosphere is the region between the Earth's surface and $500 - 3000\,\text{m}$ height called the atmospheric boundary layer. The bottom ten percent of the boundary layer is the surface layer. The presented parametrization will be used in the numerical calculations.

In order to parameterize the unknown kinematic fluxes, we use the Monin-Obukhov similarity theory. To this end, we introduce the so-called Monin-Obukhov length L, which describes the stability properties of the atmosphere, and the boundary layer height H. Following the approach of Troen & Marth [117] the vertical diffusion coefficient in boundary layer is modeled by

$$D_{33} = \frac{\kappa \, v_* \, x_3}{\Psi(1 - \tilde{x}_3)},$$

where $\tilde{x}_3$ is the scaled vertical coordinate $\tilde{x}_3 = \frac{x_3}{H}$, κ von Karman's constant taken to be 0.4, v_* the surface friction velocity, and Φ the non-dimensional shear. The friction velocity can be calculated using the surface stress τ_0 and air density ρ_a,

$$v_* = \left(\frac{\tau_0}{\rho_a} \right)^{1/2}.$$

For stable conditions $L > 0$ the shear for the whole boundary layer is given by

$$\Phi_m = 1 + 4.7\, L^{-1}.$$

We set the vertical diffusion coefficient to be constant above the boundary layer

$$D_{33}(x_3) = 0.0013.$$

We use the approach presented in Hess [55] for the modeling of the horizontal diffusion coefficients and set for stable atmospheric conditions

$$D_{11} = D_{22} = 0.143\, H\, u_*\, \tilde{x}_3^{1/2} (1 - \tilde{x}_3)^{1/2}.$$

For unstable conditions $L < 0$, for the surface layer $(0 \leq x_3 \leq 0.1 \cdot H)$ there holds

$$\Phi_m = \left(1 - \frac{7x_3}{L}\right)^{-1/3}.$$

Above the surface layer the vertical diffusion coefficient is given by

$$D_{33}(x_3) = w_s\, H\, \kappa\, \tilde{x}_3\, (1 - \tilde{x}_3)^p,$$

where w_s denotes the velocity scale. The velocity scale can be calculated in terms of convective velocity w_*,

$$w_* = v_* \left(-H\, \kappa^{-1}\, L^{-1}\right)^{1/3}, \quad w_s = 0.65\, w_*.$$

The value of the exponent p varies in the literature, see, e.g., Højstrup [58], however, $p = 2$ is a typical choice in many computations. We use again the approach of Hess [55] for the horizontal diffusion under these atmospheric conditions

$$D_{11} = D_{22} = 0.1\, w_* H.$$

For neutral conditions, $L = 0$, the vertical diffusivity coefficient is expressed as

$$K_3(x_3) = \kappa\, v_*\, x_3\, \exp(-4\, x_3\, H^{-1}).$$

As we can see, the parameters L and H play the central role in calculations of the diffusion coefficients. They are either supplied with the meteorological data or are computed from other quantities. The Monin-Obukhov length can be calculated by the help of the friction velocity v_*, potential temperature Θ_v, and temperature at the surface,

$$L = \frac{v_*^2 \Theta_v}{k\, g\, \Theta}. \tag{7.6}$$

The height of the atmospheric boundary layer can be computed using the definition of the bulk Richardson number. For more details on this issue, we refer to Jacobson [63].

7.2. The continuity equation in spherical terrain-following coordinates

In view of the form of the given observations and meteorological parameters such as wind fields and air density, we rewrite the continuity equation from system (7.5) in spherical horizontal coordinates. So as to account for uneven terrain, we introduce the pressure-sigma coordinates. Finally, we derive the weak form of the continuity equation in new coordinates.

The horizontal spherical coordinates are given by the following transformation

$$T(x_1, x_2) = \begin{pmatrix} R_e \cos(\phi)\lambda \\ R_e \phi \end{pmatrix},$$

where λ denotes the longitude, ϕ the latitude, and $R_e \approx 6371\,\text{km}$ is the Earth's radius.

For the vertical coordinate, we use the terrain-following sigma-pressure coordinates as originally proposed in Phillips [91],

$$\sigma = \frac{p - p_{top}}{p_s - p_{top}},$$

where p denotes the air pressure, p_s and p_{top} stand for the surface and top pressure of the model domain, respectively. Thus, at the surface, we obtain $\sigma = 1$ while at the top of the domain there holds $\sigma = 0$. Then, the species continuity equation in new coordinates is given by

$$\begin{aligned} &\frac{\partial(p_s u)}{\partial t} + \frac{\partial(p_s v_\lambda u)}{\partial \lambda} + \frac{1}{\cos\phi}\frac{\partial(p_s v_\phi \cos\phi u)}{\partial \phi} + p_s \frac{\partial(v_\sigma u)}{\partial \sigma} \\ &= \frac{\partial}{\partial \lambda}\left(p_s D_{\lambda\lambda}\frac{\partial u}{\partial \lambda}\right) + \frac{1}{\cos\phi}\frac{\partial}{\partial \phi}\left(p_s D_{\phi\phi}\cos\phi \frac{\partial u}{\partial \phi}\right) + \frac{G^2}{p_s}\frac{\partial}{\partial \sigma}\left(\rho_a^2 D_{33}\frac{\partial \xi}{\partial \sigma}\right) - p_s q, \end{aligned} \tag{7.7}$$

with the gravitational constant G. Here, the components of the wind in the new coordinates v_λ, v_ϕ, and v_σ are calculated from the cartesian components as follows:

$$v_\lambda = \frac{v_x}{R_e \cos\phi}, \quad v_\phi = \frac{v_y}{R_e}, \quad \text{and} \quad v_\sigma = -\frac{\sigma}{p_s}\left(\frac{\partial p_s}{\partial t} + \frac{\partial p_s}{\partial x}v_x + \frac{\partial p_s}{\partial y}v_y\right) - \frac{\rho_a G}{p_s}v_z$$

The diffusion is calculated accordingly to

$$D_{\lambda\lambda} = \frac{D_{11}}{R_e^2 \cos^2\phi} \quad \text{and} \quad D_{\phi\phi} = \frac{D_{22}}{R_e^2}.$$

In order to rewrite the boundary conditions, we note that for the gradient there holds in the new coordinates

$$\nabla u = \frac{1}{R_e \cos\phi}\frac{\partial u}{\partial \lambda} + \frac{1}{R_e}\frac{\partial u}{\partial \phi} + \frac{-\rho_a\, g}{p_s - p_{top}}\frac{\partial u}{\partial \sigma}.$$

For details on the derivation, we refer, e.g., to Seinfeld & Pandis [107] or Jacobson [63].

7.3. Numerical results

In this section, we present the computational results for the identification of unknown source term and reconstruction of distributed concentrations of bromine oxide. The over-specification is given in terms of integral and terminal conditions given by (7.2) and (7.3), respectively. The parametrization of the turbulent diffusion is performed accordingly to Section 7.1. The wind fields, the initial and boundary conditions are supposed to be provided.

We use the weak form of equation (7.7). The functional spaces used are set accordingly to $X := W(0,T)$ for the state variable u and $Q := L^2(\Omega_T)$ for the unknown source term q. The resulting equations are discretized using the cG(1)dG(0) method as described in Chapter 3. The stabilization of the problem is done by the LPS method introduced in Chapter 3, Section 3.3.

As computational domain Ω, we consider a region in Arctic. The simulation interval $I := [t_0, T]$ is from 4am CET on January 1, 2000 to 4am CET on January 11, 2000. The initial time point is then set as $t_0 = 0$. We use 45 layers for the vertical discretization. The calculation of the corresponding vertical coordinates is done by the procedure described in White [120].

The resulting inverse problem is regularized by the nonstationary iterated Tikhonov method. The Tikhonov functional is given by

$$J(u,q) := \sum_{i=1}^{M} \|\mathcal{C}_i(u) - g_i^{\delta}\|_{Y_i}^2 + \|\mathcal{C}^*(u) - g^{*,\delta}\|_{Y^*}^2 + \alpha\|q - q^*\|_Q^2. \tag{7.8}$$

Since we lack the prior knowledge of the parameter q, we set $q^* = 0$. As stopping criterion for the Tikhonov method, we use the Morozov's discrepancy principle with the noise level of two percent. The initial regularization parameter is set to be equal $\alpha = 10^{-1}$. The resulting optimization problem is solved using the direct Newton method for optimization problems as explained in Chapter 5, Section 5.3.

The qualitative behavior of the calculated solution and the reference values at different time points can be studied in Figure 7.1. Here, we can see that the computed concentrations of bromine oxide resemble the reference values very well. In this case, we require 8 iterations with the last regularization parameter $\alpha = 3.9 \cdot 10^{-3}$ in order to fulfill the discrepancy principle. The corresponding computed source term at different time points is depicted in Figure 7.2. We can observe high BrO production near the surface. The active areas of the source term correspond to the regions of high concentrations of bromine oxide. The obtained results can be further used for parametrization of processes responsible for the release of bromine oxide and analysis of ozone depletion events due to halogen chemistry in Arctic springtime.

Although the presented scalar inverse problem is rather simple from numerical point of view, we need approximately 23 hours for the solution process. In most atmospheric

applications the underlying chemical mechanisms consist of more than one reaction. Thus, e.g., tropospheric ozone depletion events in Arctic surface air associated with elevated bromine are described by 7 chemical reactions involving 10 species (Martinez et al. [80]). The corresponding reaction mechanism with chlorine, which corresponds to an extended reaction chain presented in Chapter 2, Example 1, consists of 8 chemical reactions between 11 species, see, e.g., Solomon [109]. Moreover, applications concerned with the gas exchange between the ocean and the atmosphere require a very fine resolution of source regions, which constitute the goal of the computations, see, e.g., Garbe et al. [42, 43]. Additionally, we have a large amount of data, such as cloud observations and spectral information obtained by remote sensing instruments, needed to be processed. Achieving high accuracy in discretization of the problems is expensive. Hence, the efficient numerical solution requires work reduction, which can be achieved by adaptive discretization and estimation of the algebraic errors as described in Chapter 6. The application of the developed techniques to such large-scale parameter identification problems is a subject of a future work.

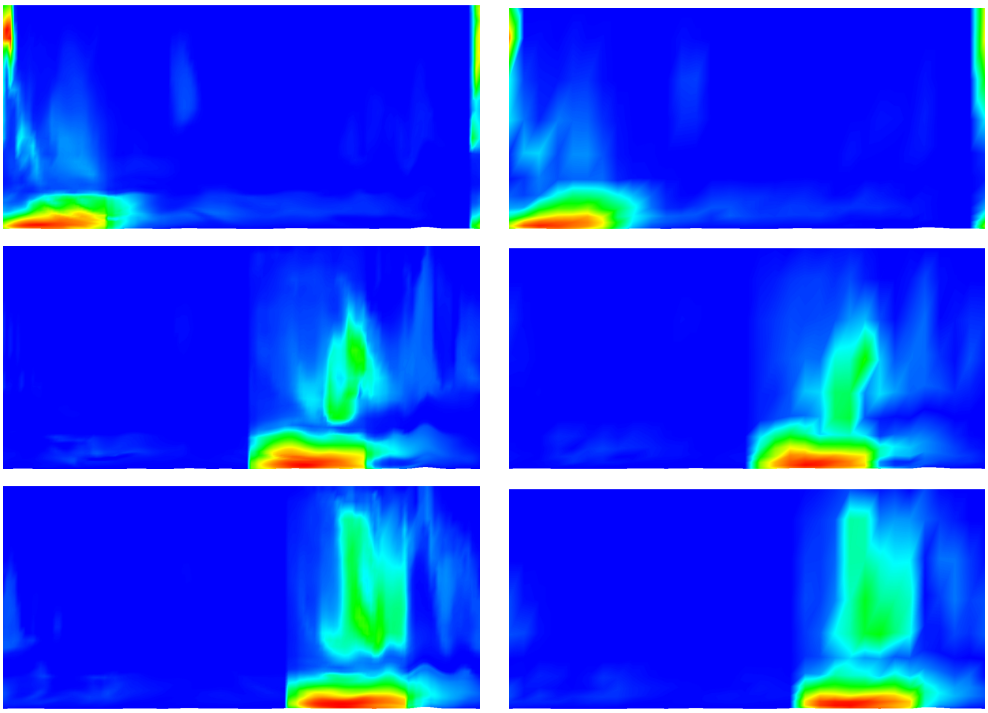

FIGURE 7.1: Assimilated concentrations of bromine oxide at different time points (z-layer) (left column) and the calculated concentrations (right column)

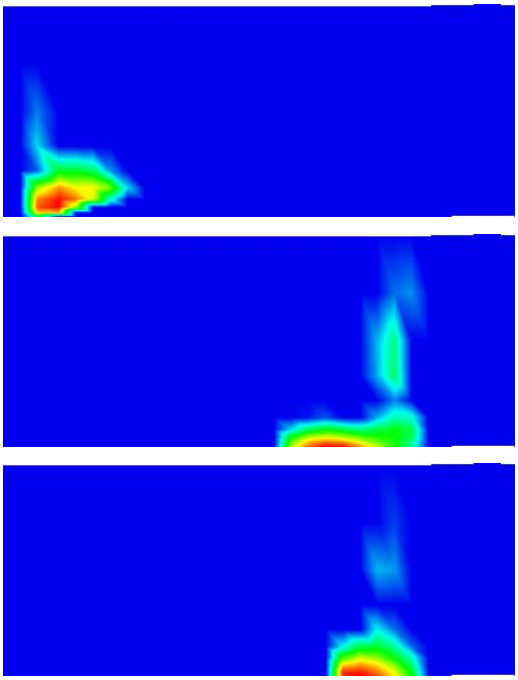

FIGURE 7.2: Computed source term q at different time points (z-layer)

CHAPTER 8

Conclusion and Future Work

This thesis is devoted to analysis and systematic approach for adaptivity for the problems related to the transport of chemical species in the Earth's atmosphere. The problems under consideration involve nonlinear systems of nonstationary parabolic equations, hyperbolic equations given by radiative transfer models, and Euler equations resulting from image segmentation techniques. The arising problems are discretized by the Galerkin finite element method. We provide also the stability analysis for a class of general atmospheric inverse problems including reconstruction of unknown initial concentrations and calibration or identification of parameters.

The main issue of this work is the development of adaptive techniques based on the determination of adaptive discretizations and the control of the algebraic solvers for numerical solution of problems related to the atmospheric transport. However, the presented concept of the adaptivity is rather general and can be applied to a broad class of partial differential equations. Our approach bases on a posteriori error estimation for direct simulations and inverse problems. The presented adaptive methods produce a sequence of locally refined meshes with balanced error contributions due to the discretization and the inexact solution of algebraic systems. The efficiency and reliability of the proposed techniques are confirmed by several example problems involving the cloud segmentation from satellite observations, the calculation of radiative transfer model, and nonlinear parabolic system of partial differential equations. For the problems considered in this thesis the application of the developed adaptive techniques leads to a significant saving of computational time. In numerical tests, we can observe that the use of goal-oriented meshes makes the solution process at least three times faster compared to the method based on uniformly refined meshes. The use of the adaptive stopping criterion for the algebraic solver further reduces the number of iterations and, consequently, the computational time approximately by a factor of two. Balancing of the algebraic errors from the inner and outer iterations in the Newton method leads additionally to double work reduction. In the particular application of cloud segmentation the proposed fully adaptive algorithm outperforms the method based on a heuristic error estimator by a factor of eight in terms of the computational time.

As shown in the thesis, calibration problems describing the transport of atmospheric constituents are generally ill-posed. In this sense, we consider different regularization techniques and put a particular emphasis on Tikhonov-type methods. For this type of regularization, we consider general perturbations of functional using the Morozov's discrepancy principle as a stopping rule. Furthermore, we combine the techniques stemming from the image processing with the numerical methods for analyzing the cloud maps from satellite observations.

All numerical computations are done by the finite element toolkit *Gascoigne*, see Becker & Braack [12], and the optimization toolbox *RoDoBo*, created by Roland Becker, Dominik Meidner, and Boris Vexler [16], both developed in our research group. Therefore, I would like to express my deepest gratitude to everyone involved in the development of the software packages. The visualization of all results is made by the data visualizer MayaVi offering a bride spectrum of capabilities for the representation of the scientific data, see Ramachandran & Varoquaux [94].

In the following, we discuss the possible extensions of the presented work. In this work Newton-types methods are applied to the Tikhonov regularization of inverse problems. The structure of the Lagrange-Newton and DWR methods allows a further refinement and balancing of the error contributions due to the linearization and the iterative solution in the inner iteration. We intent to continue the analysis of the direct Newton method for optimization problems in order to assess the error due to inexact solution of auxiliary equations. Special interest represent nonstationary partial differential equations. Furthermore, we wish to extend the presented adaptivity concepts to the problems with constraints posed on the control variables.

Since chemical species are characterized by their lifetimes, it would be of benefit to consider the change of concentrations of chemical species at different scales. This leads to the construction of tailored discretizations for individual atmospheric constituents and promises a significant reduction of computational effort.

The application of the developed techniques to the parameter identification problems for the real atmospheric transport of chemical species with overspecification given by satellite observations is a subject of a future work. This requires the development of new modules of code for processing of the meteorological data and the grid handling. Especially, the implementation of locally refined meshes for problems posed in terrain-following coordinates consistent with the given measurements represents a technical challenge.

Bibliography

[1] L. El Alaoui, A. Ern, and M. Vohralik. Guaranteed and robust a posteriori error estimates and balancing discretization and linearization errors for monotone nonlinear problems. *Comput. Meth. Appl. Mech. Engrg.*, 200:2782–2795, 2011.

[2] H. W. Alt. *Lineare Funktionalanalysis*. Springer Berlin, 1999.

[3] L. Ambrosio and V. M. Tortorelli. Approximation of functionals depending on jumps by elliptic functionals via Gamma-convergence. *Comm. Pure Appl. Math.*, 43:999–1036, 1990.

[4] I. Babuška and T. Strouboulis. *The Finite Element Method and its Reliability*. Oxford University Press, 2001.

[5] A. B. Bakushinskii. Remarks on choosing a regularization parameter using the quasi-optimality and ratio criterion. *USSR. Comp. Math. and Math. Phys.*, 24(4):181–182, 1984.

[6] G. Bal and K. Ren. Atmospheric concentration profile reconstructions from radiation measurements. *Inverse Problems*, 21:153–168, 2005.

[7] W. Bangerth and R. Rannacher. *Adaptive Finite Element Method for Differential Equations*. Birkhäuser, 2003.

[8] R. E. Bank and T. Dupont. An optimal order process for solving finite element equations. *Math. Comp.*, 36:35–51, 1981.

[9] B. Becker and M. Braack. Multigrid techniques for finite elements on locally refined meshes. *Numer. Lin. Alg. Appl.*, 7(6):363–379, 2000.

[10] R. Becker. An adaptive finite element method for the Stokes equations including control of the iteration error. In *ENUMATH 1997, World Scientific*, pages 609–620, London, 1998.

[11] R. Becker. *Adaptive Finite Element Methods for Optimal Control Problems*. PhD thesis, Fakultät für Mathematik und Informatik, Universität Heidelberg, 2001.

[12] R. Becker and M. Braack. The finite element toolkit GASCOIGNE. Institute of Applied Mathematics, University of Heidelberg, `http://www.gascoigne.uni-heidelberg.de`.

[13] R. Becker and M. Braack. A finite element pressure gradient stabilization for the Stokes equations based on local projections. *Calcolo*, 38(4):173–199, 2001.

[14] R. Becker, C. Johnson, and R. Ranacher. Adaptive error control for multigrid finite element methods. *Computing*, 55(4):271–288, 1995.

[15] R. Becker, D. Meidner, and B. Vexler. Efficient numerical solution of parabolic optimization problems by finite element methods. *Optim. Methods Soft.*, 22(5):813–833, 2007.

[16] R. Becker, M. Meidner, and B. Vexler. RODOBO: A C++ library for optimization with stationary and nonstationary PDEs. Institute of Applied Mathematics, University of Heidelberg, `http://www.rodobo.uni-hd.de`.

[17] R. Becker and R. Rannacher. An optimal control approach to a posteriori error estimation. *Acta Numerica 2001*, 10:1–102, 2001.

[18] M. Berggren, R. Glowinski, and J.-L. Lions. A computational cpproach to controllability issues for flow-related models. (I): Pointwise control of the viscous Burgers equation. *Int. J. of Comp. Fluid Dyn.*, 7(3):237–252, 1996.

[19] F. S. Binkowski and S. J. Roselle. Models-3 Community Multiscale Air Quality (CMAQ) model aerosol component. 1. Model description. *J. of Geophys. Res.*, 108(D6):5719–5727, 2003.

[20] K. W. Bowman, C. D. Rodgers, S. S. Kulawik, J. Worden, E. Sarkissian, G. Osterman, T. Steck, Ming Lou, A. Eldering, M. Shephard, H. Worden, M. Lampel, S. Clough, P. Brown, C. Rinsland, M. Gunson, and R. Beer. Tropospheric emission spectrometer: Retrieval method and error analysis. *IEEE T. Geoscience and Remote Sensing*, 44(5):1297–1307, 2006.

[21] M. Braack, E. Burman, V. John, and G. Lube. Stabilized finite element methods for the generalized Oseen equations. *Comput. Methods Appl. Mech. Engrg.*, 196:853–866, 2007.

[22] J. Bramble. *Multigrid Methods*, volume 294 of *Pitman Research Notes in Mathematics Series*. Longman Scientific, 1993.

[23] V. H. F. Campos, M. R. Moraes, F. M. Ramos, G. A. Degrazia, and D. Anfossi. An automatic methodology for estimating eddy diffusivity from experimental data. *Il Nuovo Cimento C*, 23(1):65–84, 2000.

[24] G. Carmichael, T. Chai, A. Sandu, E. Constantinescu, and D. Daescu. Predicting air quality: Improvements through advanced methods to integrate models and measurements. *J. Comput. Phys.*, 227(7):3540–3571, 2008.

[25] P. G. Ciarlet. *The Finite Element Method for Elliptic Problems*, volume 4 of *Studies in Mathematics and its Applications*. North-Holland Publishing Co., Amsterdam, 1978.

[26] R. Dautray and J. L. Lions. Evolution Problems I. In *Mathematical Analysis and Numerical Methods for Science and Technology*, volume 5. Springer-Verlag, Berlin, 1992.

[27] A. Doicu, T. Trautmann, and F. Schreier. *Numerical Regularization for Atmospheric Inverse Problems*. Springer Verlag, 2010.

[28] H. S. Eggleston, D. Gaudioso, N. Gorissen, R. Joumard, R. C. Rijkeboer, Z. Samaras, and K. H. Zierock. *CORINAIR Working Group on Emission Factors for Calculating 1990 Emissions from Road Traffic: Methodology and Emission Factors*, volume 1. Office for Official Publications of the European Communities, 1993.

[29] L. K. Emmons, G. G. Pfister, D. P. Edwards, J. C. Gille, G. Sachse, D. Blake, S. Wofsy, C. Gerbing, D. Matross, and P. Nédélec. Measurements of pollution in the troposphere (MOPITT) validation exercises during summer 2004 field campaigns over North America. *J. Geophys. Res.*, 106(D24):D12SO2 1–7, 2001.

[30] H. W. Engl, M. Hanke, and A. Neubauer. *Regularization of Inverse Problems*. Mathematics and its Applications. Kluwer Academic Publishers, 2000.

[31] H. W. Engl, K. Kunisch, and A.Neubauer. Convergence rates for Tikhonov regularisation of non-linear ill-posed problems. *Inverse Problems*, 5:523–540, 1989.

[32] H. W. Engl, K. Kunisch, and A. Neubauer. Convergence rates for Tikhonov regularisation of non-linear ill-posed problems. *Inverse Problems*, 5:523–540, 1989.

[33] K. Eriksson and C. Johnson. Adaptive finite element methods for parabolic problems. V: Long-time integration. *SIAM J. Numer. Anal.*, 32(6):1750–1763, 1995.

[34] D. L. Ermak. An analytical model for air pollutant transport and deposition from a point source. *Atmos. Env.*, 11(3):1417–1425, 1977.

[35] A. Ern and M. Vohralík. Adaptive inexact Newton methods for the discretization of nonlinear diffusion PDEs. I. General theory and a posteriori stopping criteria. Technical report, Centre d'Enseignement et de Recherche en Mathématiques et Calcul Scientifique - CERMICS , Laboratoire Jacques-Louis Lions - LJLL, 2012.

[36] A. Ern and M. Vohralík. Adaptive inexact Newton methods for the discretization of nonlinear diffusion PDEs. II. Applications. Technical report, Centre d'Enseignement et de Recherche en Mathématiques et Calcul Scientifique - CERMICS , Laboratoire Jacques-Louis Lions - LJLL, 2012.

[37] L. C. Evans. *Partial Differential Equations*. Graduate Studies in Mathematics Series. American Mathematical Society, 1998.

[38] M. Fischer and D. J. Lary. Lagrangian four-dimensional variational data assimilation of chemical species. *Q. J. R. M. S.*, 121:1681–1704, 1995.

[39] W. E. Fitzgibbon, M. Langais, and J. J. Morgan. A degenerate reaction-diffusion system modeling atmospheric dispersion of pollutants. *J. Math. Anal. Appl.*, 307:415–432, 2005.

[40] L. P. Franca and S. L. Frey. Stabilized finite element methods: II. The incompressible Navier-Stokes equations. *Comput. Methods Appl. Mech. Engrg.*, 99:209–233, 1992.

[41] W. Gao and M. L. Wesely. Modeling gaseous dry deposition over regional scales with satellite observations - I. Model development. *Atmos. Env.*, 29(6):727–737, 1995.

[42] C. S. Garbe, A. Butz, I. Dadou, B. Dewitte, V. Garcon, S. Illig, A. Paulmier, J. Sudre, and H. Yahia. Climatically-active gases in the Eastern Boundary Upwelling (EBU) and Oxygen Minimum Zone (OMZ) systems. In *IGARSS*, pages 6150–6153, 2012.

[43] C. S. Garbe, A. Butz, V. Garçon, J. Vihharev, J. Sudre, H. Yahia, B. Dewitte, A. Paulmier, S. Illig, and I. Dadou. Assessing atmospheric gas concentrations and interfacial fluxes from remote sensing. In *Workshop on "Towards an integrative regional coupling in the Eastern Boundary Upwelling Systems (EBUS)"*, page 14, Lima, Peru, 2012.

[44] C. S. Garbe and J. Vihharev. Modeling of atmospheric transport of chemical species in the polar regions. In *IGARSS*, pages 6047–6050, 2012.

[45] A. Griesbaum, B. Kaltenbacher, and B. Vexler. Efficient computation of the Tikhonov regularization parameter by goal-oriented adaptive discretization. *Inverse Problems*, 24(2):025025, 2008.

[46] A. Griewank. Achieving logarithmic growth of temporal and spatial complexity in reverse automatic differentiation. *Optim. Methods and Soft.*, 1:35–54, 1992.

[47] C. W. Groetsch. Comments on Morozov's discrepancy principle. Improperly posed problems and their numerical treatment, Conf. Oberwolfach, 1983.

[48] A. Guenther, P. Zimmermann, P. Harley, R. Monson, and R. Fall. Isoprene and monoterpene emission rate variability: model evaluation and sensitivity analysis. *J. Geophys. Res.*, 98D(12):12609–12617, 1993.

[49] W. Hackbusch. *Multi-Grid Methods and Applications.* Springer-Verlag, Berlin–Heidelberg–New York, 1985.

[50] A. Hakami, D. Henze, J. H. Seinfeld, K. Singh, A. Sandu, S. Kim, D. Byun, and Q. Li. The adjoint of CMAQ. *Env. Sci. Technol.*, 41:7807–7817, 2007.

[51] F. G. Hall. Introduction to special section: BOREAS III. *J. Geophys. Res.*, 106(D24):33,511–33,516, 2001.

[52] M. Hanke, A. Neubauer, and O. Scherzer. A convergence analysis of the Landweber iteration for nonlinear ill-posed problems. *Numer. Math*, 72:21–37, 1995.

[53] M. Hanke and T. Raus. General heuristic for choosing the regularization parameter in ill-posed problems. *SIAM J. Sci. Comput.*, 17(4):956–972, 1996.

[54] P. C. Hansen. Analysis of discrete ill-posed problems by means of the L-curve. *SIAM Review*, 34(4):561–580, 1992.

[55] G. D. Hess. A photochemical model for air quality assessment: Model description and verification. *Atmos. Env.*, 23(3):643–660, 1989.

[56] V. Heuveline and R. Rannacher. A posteriori error control for finite element approximations of elliptic eigenvalue problems. *Adv. in Comput. Math.*, 15:107–138, 2001.

[57] M. Hinze, M. Köster, and S. Turek. A space-time multigrid method for optimal flow control. In *Constrained Optimization and Optimal Control for Partial Differential Equations*, number 160 in ISNM-Series, pages 147–170. Birkhäuser, 2012.

[58] J. Højstrup. Velocity spectra in the unstable planetary boundary level. *J. Atmos. Sci.*, 39:2239–2248, 1982.

[59] T. Hughes and A. Brooks. The effect of stabilization in finite element methods for the optimal boundary control of the Oseen equations. *Amer. Soc. of Mech. Eng., New York*, 34:19–35, 1979.

[60] P. Hurley. TAPM V4. part 1: Technical description. Tech. report, paper no. 25, CSIRO Marine and Atmospheric Research, Castray Esplanade, Australia, 2008.

[61] K. Ito and K. Kunisch. *Lagrange Multiplier Approach to Variational Problems and Applications*. Advances in Design and Control. SIAM, Philadelphia, 2008.

[62] D. J. Jacob. *Introduction to Atmospheric Chemistry*. Princeton University Press, 1999.

[63] M. Z. Jacobson. *Fundamentals of Atmospheric Modeling*. Cambridge University Press, 2005.

[64] J. Jahn. *Introduction to the Theory of Nonlinear Optimization*. Springer-Verlag, Berlin, 1996.

[65] P. Jiranek, Z. Strakos, and M. Vohralik. A posteriori error estimates including algebraic error and stopping criteria for iterative solvers. *SIAM J. Sci. Comput.*, 32:1567–1590, 2010.

[66] R. Joumard. Methods of estimation of atmospheric emissions from transport: European scientist network and scientific state-of-the art. INRETS - Report LTE 9901, Institut National de Recherche sur les Transports et Leur Sécurité, Bron, France, 1999.

[67] B. Kaltenbacher, A. Kirchner, and B. Vexler. Adaptive discretizations for the choice of a Tikhonov regularization parameter in nonlinear inverse problems. *Inverse Problems*, 27(12):125008, 2011.

[68] B. Kaltenbacher, A. Neubauer, and O. Scherzer. *Iterative Regularization Methods for Nonlinear Ill-Posed Problems*. Springer, 2005.

[69] B. Kaltenbacher, F. Schöpfer, and T. Schuster. Iterative methods for nonlinear ill-posed problems in Banach spaces: convergence and applications to parameter identification problems. *Inverse Problems*, 25:065003, 2009.

[70] G. Kanschat, E. Meinköhn, R. Rannacher, and R. Wehrse. Introduction: The radiation field and its transfer equation. In G. Kanschat, E. Meinköhn, R. Rannacher, and R. Wehrse, editors, *Numerical Methods in Multidimensional Radiative Transfer*, pages 1–19. Springer Verlag, Berlin Heidelberg, 2009.

[71] A. Kirsch. *An Introduction to the Mathematical Theory of Inverse Problems*. Applied Mathematical Sciences. Springer-Verlag New York, Inc., New York, NY, USA, 2011.

[72] W. Kirstine, I. Galbally, Y. Ye, and M. Hooper. Emissions of volatile organic compounds (primary oxygenated species) from pasture. *J. Geophys. Res.*, 103:10605–10619, 1998.

[73] C. Kravaris and J. H. Seinfeld. Inentification of parameters in distributed parameter systems by regularization. *SIAM J. Control and Optim.*, 23(2):217–241, 1985.

[74] K. Kunisch and J. Zou. Iterative choices of regularization parameters in linear inverse problems. *Inverse Problems*, 14(5):1247–1264, 1998.

[75] B. Lamb, D. Gay, H. Westberg, and T. Pierce. A biogenic hydrocarbon emission inventory for the U.S.A. using a simple forest canopy model. *Atmos. Env. Part A. General Topics*, 27(11):1673–1690, 1993.

[76] R. G. Lamb. Note on the application of K-theory to diffusion problems involving nonlinear chemical reactions. *Atmos. Env.*, 7(3):257–263, 1973.

[77] H. Lu and Y. Shao. Toward qunatitative prediction of dust storms: an integrated wind erosion modeling system and its application. *Env. Modeling & Soft.*, 16:233–249, 2001.

[78] O. Manley, M. Marion, and R. Temam. Equations of combustion in the presence of complex chemistry. *Indiana Univ. Math. J.*, 42(3):941–967, 1993.

[79] G. I. Marchuk. Construction of adjoint operators in non-linear problems of mathematical physics. *Sbornik: Mathematics*, 189(10):1505–1516, 1998.

[80] M. Martinez and T. Arnoldand D. Perner. The role of bromine and chlorine chemistry for arctic ozone depletion events in Ny-Ålesund and comparison with model calculations. *Ann. Geophysicae*, 17:941–956, 1999.

[81] D. Meidner. *Adaptive Space-Time Finite Element Methods for Optimization Problems Governed by Nonlinear Parabolic Systems*. PhD thesis, Fakultät für Mathematik und Informatik, Universität Heidelberg, 2008.

[82] D. Meidner, R. Rannacher, and J. Vihharev. Goal-oriented error control of the iterative solution of finite element equations. *J. Numer. Math.*, 17:143–172, 2009.

[83] D. Meidner and B. Vexler. Adaptive space-time finite element methods for parabolic optimization problems. *SIAM J. Control Optim.*, 46:116–142, 2007.

[84] E. Meinköhn, G. Kanschat, R. Rannacher, and R. Wehrse. Numerical methods for multidimensional radiative transfer. In W. Jäger, R. Rannacher, and J. Warnatz, editors, *Reactive Flows, Diffusion and Transport*, pages 1–42. Springer Verlag, Berlin Heidelberg, 2006.

[85] I. Neizel and B. Vexler. A priori error estimates for space-time finite element discretization of semilinear parabolic optimal control problems. *Numer. Math.*, 120(2):345–386, 2011.

[86] A. Neubauer and O. Scherzer. Finite-dimensional approximation of Tikhonov regularized solutions of non-linear ill-posed problems. *Numer. Func. Anal. and Optim.*, 11:85–99, 1990.

[87] R. N. Nochetto. L^∞-error estimates for semilinear elliptic problems with free boundaries. *Numer. Math.*, 54:243–255, 1988.

[88] S. Noël, J. P. Burrows, J. Frerick, K. V. Chance, A. P. H. Goede, and C. Muller. Atmospheric trace gas sounding with SCIAMACHY. *Adv. Space. Res.*, 26(12):1949–1954, 2000.

[89] D. E. Norman. Chemically reacting fluid flows: weak solutions and global attractors. *J. of Diff. Eq.*, 152(1):75–135, 1999.

[90] J. M. Norman. Simulation of microclimates. In J. L. Hatfield and I. J. Thomason, editors, *Biometeorology in Integrated Pest Management: Proceedings of a Conference on Biometeorology and Integrated Pest Management Held at the University of California, Davis, July 15-17, 1980*, Biometeorology in Integrated Pest Management, pages 65–69. Academic Press, New York, 1982.

[91] N. A. Phillips. A coordinate system having some special advantages for numerical forecasting. *J. Meteor.*, 14:184–185, 1957.

[92] M. Pierre. Global existence in reaction-diffusion systems with control of mass: a survey. *Milan J. Math.*, 78:417–455, 2010.

[93] M. Pierre and R. Texier-Picard. Global existence for degenerate quadratic reaction-diffusion systems. *Annales de l'Institut Henri Poincare (C) Non Linear Analysis*, 26:1553–1568, 2009.

[94] P. Ramachandran and G. Varoquaux. Mayavi: Making 3D data visualization reusable. In Varoquaux, Gaël and Vaught, Travis and Millman, Jarrod, editor, *Proceedings of the 7th Python in Science Conference*, pages 51–56, Pasadena, CA USA, 2008.

[95] R. Ramlau. Morozov's discrepancy principle for Tikhonov regularization of non-linear operators. *J. Num. Func. Anal. and Opt.*, 23:147–172, 2002.

[96] R. Rannacher. Finite element solution of diffusion problems with irregular data. *Numer. Math*, 43:309–327, 1984.

[97] R. Rannacher and J. Vihharev. Adaptive finite element analysis of nonlinear problems: balancing of discretization and iteration errors. *J. Numer. Math.*, 2013. To appear.

[98] R. Rannacher and J. Vihharev. Balancing discretization and iteration error in finite element a posteriori error analysis. In S. Repin, T. Tiihonen, and T. Tuovinen, editors, *Numerical Method for Differential Equations, Optimization and Technological Problems*, volume 27 of *Computational Methods in Applied Sciences*, pages 109–132. Springer Netherlands, Dordrecht, 2013.

[99] R. Rannacher, A. Westenberger, and W. Wollner. Adaptive finite element analysis of elliptic eigenvalue problems: balancing of discretization and iteration error. *J. Numer. Math.*, 18:303–327, 2010.

[100] F. Rocadenbosch, I. Mattis, A. Ansmann, U. Wandinger, C. Bockmann, G. Pappalardo, A. Amodeo, J. Bosenberg, L. Alados-Arboledas, A. Apituley, D. Balis, A. Chaikovsky, A. Comeron, C. Munoz, M. Sicard, V. Freudenthaler, M. Wiegner, O. Gustafsson, G. Hansen, R.-E. Mamouri, A. Papayannis, V. Mitev, D. Nicolae, C. Perez, M. R. Perrone M.R., A. Pietruczuk, M. Pujadas, J.-R. Putaud, F. Ravetta, V. Rizi, V. Simeonov, N. Spinelli, D. Stoyanov, and T. Trickl. The European Aerosol Research Lidar Network (EARLINET): An overview. In *Geoscience and Remote Sensing IEEE International Symposium*, pages 410–413, 2008.

[101] A. Rösch. Fréchet differentiability of the solution of the heat equation with respect to a nonlinear boundary condition. *Z. Anal. Anw.*, 15:603–618, 1996.

[102] Y. Saad. *Iterative Methods for Sparse Linear Systems*. SIAM, Philadelphia, 2003.

[103] E. G. Savateev. On problems of determining the source function in a parabolic equation. *J. Inv. Ill-Posed Problems*, 3(1):83–102, 1995.

[104] O. Scherzer. Convergence rate of iterated Tikhonov solutions of nonlinear ill-posed problems. *Numer. Math.*, 66:259–279, 1995.

[105] A. Schiela. Barrier methods for optimal control problems with state constraints. *SIAM J. on Optim.*, 20(2):1002–1031, 2009.

[106] E. Schock. Approximate solution of ill-posed equations: arbitrarily slow convergence vs. superconvergence. In G. Hämmerlin and K. H. Hoffmann, editors, *Constructive Methods for the Practical Treatment of Integral Equations*, volume 73 of *International Series of Numerical Mathematics*, pages 234–243. Birkhäuser, Basel, 1985.

[107] J. H. Seinfeld and S. N. Pandis. *Atmospheric Chemistry and Physics: From Air Pollution to Climate Change*. J. Wiley-Interscience, 2006.

[108] W. R. Simpson, R. von Glasow, K. Riedel, P. Anderson, P. Ariya, J. Bottenheim, J. Burrows, L. J. Carpenter, U. Frieß, M. E. Goodsite, D. Heard, M. Hutterli, H. W. Jacobi, L. Kaleschke, B. Neff, J. Plane, U. Platt, A. Richter, H. Roscoe, R. Sander, P. Shepson, J. Sodeau, A. Steffen, T. Wagner, and E. Wolff. Halogens and their role in polar boundary-layer ozone depletion. *Atmos. Chem. Phys.*, 7:4375–4418, 2007.

[109] S. Solomon. Stratospheric ozone depletion: A review of concepts and history. *Reviews of Geoph.*, 37(3):275–316, 1999.

[110] B. Sportisse and L. Bois. Numerical and theoretical investigation of a simplified model for the parameterization of below-cloud scavenging by falling raindrops. *Atmos. Env.*, 36:5719–5727, 2002.

[111] R. B. Storch, L. C. G. Pimentel, and H. R.B. Orlande. Identification of atmospheric boundary layer parameters by inverse problem. *Atmos. Env.*, 41:1417–1425, 2007.

[112] Z. Su, W. J. Timmermans, C. van der Tol, R. Dost, R. Bianchi, J. A. Gómez, , A. House, I. Hajnsek, M. Menenti, V. Magliulo, M. Esposito, R. Haarbrink, F. Bosveld, R. Rothe, H. K. Baltink, Z. Vekerdy, J. A. Sobrino, J. Timmermans, P. van Laake, S. Salama, H. van der Kwast, E. Claassen, A. Stolk, L. Jia, E. Moors, O. Hartogensis, and A. Gillespie. EAGLE 2006 - Multi-purpose, multi-angle and multi-sensor in-situ and airborne campaigns over grassland and forest. *Hydrol. Earth. Syst. Sci.*, 13:833–845, 2009.

[113] U. Tautenhahn and Q. Jin. Tikhonov regularization and a posteriori rules for solving nonlinear ill-posed problems. *Inverse Problems*, 19(1):1–21, 2003.

[114] R. Temam. *Navier-Stokes Equations. Theory and Numerical Analysis*. North-Holland Publishing Co., Amsterdam, 1984.

[115] A. M. Thompson, J. C. Witte, R. D. McPeters, S. J. Oltmans, F. J. Schmidlin, J. A. Logan, M. Fujiwara, V. W. J. H. Kirchhoff, F. Posny, G. J. R. Coetzee, B. Hoegger, S. Kawakami, T. Ogawa, B. J. Johnson, H. Vömel, and G. Labow. Southern Hemisphere Additional Ozonesondes (SHADOZ) 1998-2000 tropical ozone climatology 1. Comparison with Total Ozone Mapping Spectrometer (TOMS) and ground-based measurements. *J. Geophys. Research (Atmosphere)*, 108:PEM 10–1, 2003.

[116] A. N. Tikhonov and V. Y. Arsenin. *Solutions of Ill-Posed Problems*. V. H. Winston & Sons, Washington, D. C.: John Wiley & Sons, New York, 1977.

[117] I. Troen and L. Mahrt. A simple model of the atmospheric boundary layer; sensitivity to surface evaporation. *Bound.-Layer Meteor.*, 37:129–148, 1986.

[118] F. Tröltzsch. *Optimale Steuerung Partieller Differentialgleichungen*. Vieweg+Teubner, Wiesbaden, 2009.

[119] R. Verfürth. *A Review of A Posteriori Error Estimation and Adaptive Mesh-Refinement Techniques*. Wiley/Teubner, 1996.

[120] P. W. White. Part III: Dynamics and numerical procedures (CY25R1). IFS Documentation, ECMWF, 2002.

[121] J. Xie and J. Zou. An improved model function method for choosing regularization parameters in linear inverse problems. *Inverse Problems*, 18(3):631–643, 2002.

[122] L. Yang, J.-N.-Yu, G.-W.-Luo, and Z.-C.-Deng. Reconstruction of a space and time dependent heat source from finite measurements data. *Int. J. of Heat and Mass Transf.*, 55:6573–6581, 2012.

[123] W. Zdunkowski, T. Trautmann, and A. Bott. *Radiation in the Atmosphere. A Course in Theoretical Meteorology*. Cambridge University Press, 2007.

[124] L. Zhang and A. Sandu. Data Assimilation in Multiscale Chemical Transport Model. In Y. Shi, G. D. Albada, J. Dongarra, and P. M. A. Sloot, editors, *Computational Science - ICCS 2007*, volume 4487 of *Lecture Notes in Computer Science*, pages 1026–1033. Springer, Berlin, Heidelberg, 2007.